

INFORMATION TO USERS

This manuscript has been reproduced from the microfilm master. UMI films the text directly from the original or copy submitted. Thus, some thesis and dissertation copies are in typewriter face, while others may be from any type of computer printer.

The quality of this reproduction is dependent upon the quality of the copy submitted. Broken or indistinct print, colored or poor quality illustrations and photographs, print bleedthrough, substandard margins, and improper alignment can adversely affect reproduction.

In the unlikely event that the author did not send UMI a complete manuscript and there are missing pages, these will be noted. Also, if unauthorized copyright material had to be removed, a note will indicate the deletion.

Oversize materials (e.g., maps, drawings, charts) are reproduced by sectioning the original, beginning at the upper left-hand corner and continuing from left to right in equal sections with small overlaps.

ProQuest Information and Learning
300 North Zeeb Road, Ann Arbor, MI 48106-1346 USA
800-521-0600

UMI[®]



**The Nature and Origins of Caldera Structure and Morphology, using
Results from Analogue Modeling**

By

Ben Kennedy

A thesis submitted to the Faculty of
Graduate Studies and Research in partial
fulfillment of the requirements
for the degree of Master of Science

Department of Earth and Planetary Sciences
McGill University, Montreal

© Ben Kennedy, 2000



**National Library
of Canada**

**Acquisitions and
Bibliographic Services**

**385 Wellington Street
Ottawa ON K1A 0N4
Canada**

**Bibliothèque nationale
du Canada**

**Acquisitions et
services bibliographiques**

**385, rue Wellington
Ottawa ON K1A 0N4
Canada**

Your file Votre référence

Our file Notre référence

The author has granted a non-exclusive licence allowing the National Library of Canada to reproduce, loan, distribute or sell copies of this thesis in microform, paper or electronic formats.

The author retains ownership of the copyright in this thesis. Neither the thesis nor substantial extracts from it may be printed or otherwise reproduced without the author's permission.

L'auteur a accordé une licence non exclusive permettant à la Bibliothèque nationale du Canada de reproduire, prêter, distribuer ou vendre des copies de cette thèse sous la forme de microfiche/film, de reproduction sur papier ou sur format électronique.

L'auteur conserve la propriété du droit d'auteur qui protège cette thèse. Ni la thèse ni des extraits substantiels de celle-ci ne doivent être imprimés ou autrement reproduits sans son autorisation.

0-612-70723-7

Canada

FRONTISPIECE

View of Ilopango caldera lake, El Salvador, with San Vicente volcano in the distance:
photo taken looking east from the city of San Salvador.

ABSTRACT

Calderas illustrate a variety of different styles which are controlled by their internal structure and morphology. The internal structure of many calderas is not exposed; as a result, the calderas frequently are interpreted as simple pistons. The results and examples from this thesis indicate that caldera structure is often more complex than this and that caldera formation consists of several stages controlled by complex interactions of many variables. Internal processes and parameters include rock properties (shear strength, planes of weakness, vertical and horizontal variations), dimensions and internal pressure of the associated magma chamber, styles of tumescence and resurgence, and the size of the eruption. External processes and parameters are also important, such as the regional stress regime (e.g., extensional and pull-apart basins), pre-existing topography, and pre-existing structures (e.g., regional faults, basement grain).

Scaled physical models of caldera formation were carried out to investigate the effects of some of these variables on the temporal development of calderas. Dry sand contained in a 1 m-diameter cylinder was used as an analogue of crustal rocks, and a water-filled 60 cm-diameter rubber bladder was used as an analogue for a magma chamber. Scaling parameters used were a length ratio (L^*) of 2.5×10^{-5} and a stress ratio (σ^*) of 2.0×10^{-5} . The collapse process was initiated by withdrawing water from the bladder at a rate of $1600 \text{ cm}^3 \text{ min}^{-1}$. The depth of the rubber bladder then was varied from 6.0 to 24 cm to simulate different magma chamber depths (2.4-9.6 km). The pressure within the bladder also was varied by changing the initial volume of water in the bladder from 40 to 45 liters before evacuation. The effects of different surface topography prior to collapse also were investigated by building scaled ridges, mountain ranges, and stratocone volcanoes, and positioning them in different positions and orientations above the bladder. Experiments also were carried out with the rubber bladder tilted to promote asymmetric collapse.

Generally, deformation began with broad sagging, then an arcuate or linear outward dipping fault formed on one side of the caldera. This fault propagated laterally

around the caldera in both directions and sometimes joined up with other faults, forming a polygonal caldera. As subsidence continued, the caldera grew incrementally outwards, progressively forming a series of concentric subsidence-controlling faults. Lastly, a peripheral zone of downsagging would develop, bounded by an inward dipping outer fault related to extension. As the depth of the bladder was increased, (1) the volume of the caldera decreased, (2) the area of faulting decreased, (3) the symmetry of the caldera was affected and (4) the coherence of the subsiding block decreased. With greater topographic relief, (1) the volume of the resultant caldera increased, (2) single ring fractures became larger and more coherent, and (3) the caldera was more prone to slumping. The location of the topographic relief in relation to the bladder did not appear to affect the symmetry of subsidence. As the initial volume and internal pressure of the bladder was decreased, (1) the resultant caldera had a larger volume, and (2) faults were initiated earlier. When the bladder was tilted, subsidence was highly asymmetric: faults formed first where the bladder was shallowest. Subsidence then shifted rapidly to where the bladder was deepest, producing an elongate trapdoor caldera which was deepest where the bladder was deepest.

RESUME

Les calderas démontrent une variété de styles différents qui sont contrôlés par leur structure ainsi que leur morphologie internes. La structure interne de plusieurs calderas n'est pas exposée; par conséquent, les calderas sont fréquemment interprétées comme de simples pistons. Les résultats et les exemples de cette thèse indiquent que la structure d'une caldera est souvent plus complexe qu'un simple modèle de piston et que sa formation consiste en plusieurs étapes contrôlées par des interactions complexes entre de nombreuses variables.

Les processus internes incluent des paramètres comme les propriétés de la roche (force de cisaillement, plans de faiblesse, variations verticales et horizontales), les dimensions et la pression interne de la chambre magmatique, les styles de bombement et de résurgence, et l'ampleur de l'éruption. Les processus externes, également importants, comprennent les paramètres suivants: le régime de stress régional (par exemple, les bassins d'extension et de transtension), la topographie pré-existante, et la structure pré-existante (par exemple, les failles régionales et la structure du socle).

Des modèles physiques à l'échelle de la formation d'une caldera sont ici proposés pour investiguer les effets de certaines variables sur le développement temporel des calderas. Du sable sec contenu dans un cylindre de 1 mètre de diamètre a été utilisé comme analogue de la roche de la croûte terrestre, et un ballon de caoutchouc de 60 centimètres de diamètre rempli d'eau tenait le rôle d'une chambre magmatique.

Les paramètres de calibration utilisés étaient un rapport de longueur (L^*) de $2.5 \cdot 10^{-5}$ et un rapport de cisaillement (σ^*) de $2.0 \cdot 10^{-5}$. L'effondrement était initié par l'évacuation de l'eau du ballon à un taux de $1600 \text{ cm}^3 \text{ min}^{-1}$.

Par la suite, la profondeur à laquelle le ballon était situé était variée de 6.0 à 24 cm pour simuler la profondeur de différentes chambres magmatiques (2.4-9.6 km). La pression à l'intérieur du ballon était également contrôlée en changeant le volume initial d'eau dans le ballon de 40 à 45 litres avant l'évacuation.

Les effets de différentes topographies de surface précédant l'effondrement ont aussi été étudiés en construisant des crêtes à l'échelle, des chaînes de montagnes, et des stratovolcans, et en les positionnant dans différentes positions et orientations au-dessus du ballon. Certaines expériences ont été réalisées avec le ballon incliné pour promouvoir un effondrement asymétrique.

Généralement, la déformation commençait par un large affaissement, ensuite une faille avec un pendage vers l'extérieur soit en arc soit linéaire se formait sur un des côtés de la caldera. Cette faille se prolongeait latéralement autour de la caldera dans les deux directions et parfois se joignait avec d'autres failles, formant une caldera polygonale. Au fur et à mesure que l'effondrement se poursuivait, la caldera s'agrandissait vers l'extérieur, formant progressivement une série de failles concentriques contrôlant l'affaissement. Finalement, une zone périphérique d'affaissement se développait, délimitée par une faille à pendage vers l'intérieur reliée à l'extension.

Lorsque la profondeur du ballon était augmentée, (1) le volume de la caldera diminuait, (2) l'aire de failles diminuait, (3) la symétrie de la caldera était affectée et (4) la cohérence du bloc affaisant se réduisait. Avec un relief topographique plus prononcé, (1) le volume de la caldera augmentait, (2) de simples fractures en anneaux devenaient plus larges et plus cohérentes, et (3) la caldera avait plus tendance à s'effondrer.

La disposition du relief topographique par rapport au ballon ne semblait pas affecter la symétrie de l'affaissement. Lorsque le volume initial et la pression interne du ballon étaient augmentés, (1) la caldera résultante avait un volume plus grand, et (2) des failles se formaient plus tôt. Quand le ballon était incliné, l'affaissement était grandement asymétrique, et les failles se formaient d'abord où le ballon était enfoui le moins creux. L'affaissement se déplaçait ensuite rapidement où le ballon était enfoui le plus profondément, produisant une caldera allongée en style de trappe qui était plus profonde où le ballon était plus profond.

ACKNOWLEDGMENTS

Firstly and most importantly I would like to thank my supervisor, Dr. John Stix, for his constant support, assistance and enthusiasm during the experiments, fieldwork and writing of the thesis. I would also like to thank Dr. James Vallance and Dr. Andrew Hynes for useful advice, discussions and helpful criticism; Dr. Ronald Doig for the use of his laboratory and his continued interest and help throughout the experimental work; Yan Lavallée for his dedication and enthusiasm during long weeks in the laboratory and the field; Dr. A. E. Williams-Jones (Willy) and his research group for giving me a place to work and for constant help with the computers; Mathieu Richer and Oliver Schatz for help in the panic of putting together this thesis; Michel Demidoff for his assistance with the figures in Chapter 1.

Financial support for this work was provided to me by funds from the Department of Earth and Planetary Sciences, McGill University, and from GEOTOP, Université du Québec à Montréal, and by a research grant to J. Stix from the Natural Sciences and Engineering Research Council of Canada.

TABLE OF CONTENTS

FRONTISPIECE.....	ii
ABSTRACT.....	iii
RESUMÉ.....	v
ACKNOWLEDGMENTS.....	viii
TABLE OF CONTENTS.....	ix
LIST OF FIGURES AND TABLES.....	xii
PREFACE.....	xviii
CHAPTER 1. INTRODUCTION TO CALDERA FORMATION.....	1
General Statement.....	1
Previous Work.....	4
Theoretical studies of caldera formation.....	4
Analogue models of subsidence.....	11
A Descriptive Outline of Caldera Types.....	16
Simple piston.....	17
Inward dipping piston.....	17
Outward dipping piston.....	19
Polygonal piston.....	19
Downsag calderas.....	21
Trapdoor calderas.....	23
Concentric step-down calderas.....	23
Chaotic calderas.....	25
Rifted calderas.....	29
Pull-apart calderas.....	29
Piecemeal/ regional fault-controlled calderas.....	30
Stages in the Temporal Evolution of Calderas.....	33
Stage 1. Magma chamber intrusion.....	33
Stage 2. Initial eruption and chamber evacuation.....	40
Stage 3. Downsagging and the onset of subsidence.....	42
Stage 4. Main subsidence and eruption phase.....	45
Stage 5. Eruption quiescence and peripheral extension.....	49
Stage 6. Continued eruption, subsidence and change in eruptive style.....	51
Stage 7. Resurgence and dome and flow extrusion.....	54

CHAPTER 2. AN EXPERIMENTAL STUDY OF CALDERA FORMATION.....	59
General Statement.....	59
Methodology.....	59
Experimental setup.....	59
Scaling of variables.....	64
Relevance and Limitations.....	66
Results.....	68
Depth.....	68
Topography.....	76
Pressure.....	79
Tilted chamber.....	81
General observations of experimental calderas.....	82
Interpretation of Results.....	83
Temporal caldera development in plan view.....	83
Temporal fault development in cross-section.....	86
Downsagging and peripheral extension.....	88
Controls on caldera morphology.....	92
Discussion.....	108
The nature and origin of caldera faults.....	108
Downsagging.....	114
Resurgence.....	117
Implications for styles of caldera collapse.....	117
Conclusions.....	119
References.....	125

LIST OF FIGURES AND TABLES

- Figure 1. Smith and Bailey's (1968) classic model of resurgent cauldrons.....5
- Figure 2. Caldera types actual and inferred (Walker, 1984): a) downsagged, b) normal faults with downsagging, c) Anderson-type ring fault subsidence, d) vertical ring fault, e) collapse into a cored-out explosive vent for small calderas, f) downsagged graben.....5
- Figure 3. Three-dimensional block diagram of piston collapse along vertical ring faults, with a back-eroded topographic margin.....18
- Figure 4. a) Three-dimensional block diagram of piston collapse along inward dipping faults; two concentric ring faults can be seen. b) An example from Suswa volcano, Gregory rift valley, Kenya (Skilling, 1993).....18
- Figure 5. a) Three-dimensional block diagram of outward dipping piston collapse with a peripheral area of normal faulting. b) An example of earthquakes marking the ring fault, 1983-1985, from Rabaul caldera, Papua New Guinea (Mori and McKee, 1987).20
- Figure 6. a) Three-dimensional block diagram of polygonal piston collapse, with linear subsidence-controlling faults. b) An example from the Ossipee cauldron, New Hampshire (Kingsley, 1931).....20
- Figure 7. Temporal evolution of Ishizuchi cauldron, Japan (Yoshida, 1984). This structure shows a combination of different styles of piston collapse, including subsidence along both inward and outward dipping faults and a polygonal-shaped subsiding block.22
- Figure 8. a) A model of a caldera formed by downsagging (Lipman, 1997), with examples from b) Taupo caldera, New Zealand, and c) Rotorua caldera, New Zealand (Walker, 1984).....22
- Figure 9. a) A model of a trapdoor-style caldera (Lipman, 1997). b) An example from Kumano caldera, southwest Honshu, Japan (Miura, 1999).....24
- Figure 10. a) Three-dimensional block diagram of step-down concentric collapse, showing a small central piston and concentric nested faults. b) An example from Guayabo caldera, Costa Rica (Hallinan, 1993).....24
- Figure 11. a) Cross-sectional diagram of chaotic collapse, showing no clear ring faults at the surface and a disrupted caldera floor. b) An example from a hypothetical cross-section through Aira caldera, southern Kyushu, Japan (Aramaki, 1984). The internal structure of this caldera is poorly constrained; a funnel-shaped gravity anomaly was interpreted as an inward dipping ring fault. However, an alternative explanation is a funnel-shaped subsurface structure controlled by outward dipping faults.....26

- Figure 12. a) High aspect ratio collapse, showing nested cones; b) low aspect ratio collapse, showing a simpler piston (Roche et al., 2000).....26
- Figure 13. a) High aspect ratio magma chamber at Mount Pinatubo, Philippines, as illustrated by post-climactic eruption seismicity, 29 June-16 August 1991 (Mori et al., 1996). b) Low aspect ratio magma chamber at Rabaul caldera, Papua New Guinea, based on seismicity between late 1983 and mid 1985 (Mori and McKee, 1987).....28
- Figure 14. a) Three-dimensional block diagram of a rifted caldera. b) An example from Toba caldera, northern Sumatra (Chesner and Rose, 1990).....28
- Figure 15. a) Three-dimensional block diagram of a piano-key caldera. b) An example from Snowdon caldera, Wales (Branney and Kokelaar, 1999).....31
- Figure 16. Diagram showing formation of a pull-apart caldera, Vulcano Island, Italy (Ventura, 1994).....31
- Figure 17. a) A model of a piecemeal-style caldera (Lipman, 1997). b) An example from Glencoe, Scotland (Moore and Kokelaar, 1998).....32
- Figure 18. Doming experiments inducing collapse (Komuro, 1984).....36
- Figure 19. Principle stress trajectories at a recently intruded and overpressured, shallow sill-like magma chamber. These trajectories run orthogonal to the free surfaces, which are represented by the magma chamber and the surface. Faults will form where these principal stress trajectories are closest together, above the margins of the magma chamber (Gudmundsson, 1997). These principal stress trajectories cause tension at the surface and form a conjugate shear set which can produce either inward or outward dipping faults at depth.....36
- Figure 20. Cone sheets, ring dykes and radial dykes. a) Gran Canaria, Canary Islands (Schirnack et al., 1999). b) Volcan Alcedo, Galapagos Islands (Geist et al., 1994). c) Volcan Fernandina, Galapagos Islands (Chadwick and Howard, 1991).....38
- Figure 21. Possible scenarios after magma chamber intrusion but prior to eruption. a) Doming with radial and concentric fractures. b) Block faulting uplift. c) Rifting.....39
- Figure 22. Possible scenarios for the initial plinian stage of a caldera-forming eruption. a) Central vent eruption. b) Regional fissure eruption. c) Rift-related eruption.....41
- Figure 23. A schematic view of downsagging. New shear faults begin to form at depth, and sagging at the surface causes extension at the hinges of the depression. The sagging also rotates inward dipping faults towards a vertical position.....44
- Figure 24. Initially asymmetric subsidence along an outward dipping fault, maintaining an open conduit.....44

Figure 25. Possible scenarios for the style of initial subsidence a) Downsagging-controlled subsidence. b) Trapdoor subsidence. c) Ring fault subsidence	46
Figure 26. Fault development and propagation as a function of stress trajectories between the surface and the magma chamber.....	48
Figure 27. Early fault development as illustrated by scaled experimental studies (Roche et al., 2000).	48
Figure 28. A simple down-slope gravity slide showing normal fault, thrust fault and crevasse formation (Branney and Kokelaar, 1999).....	50
Figure 29. Graben structures in the Whorneyside phreatomagmatic tuff; the graben formed peripheral to a subsiding basin, Scafell caldera, England (Branney and Kokelaar, 1999).....	50
Figure 30. Late-stage peripheral downsagging, continued normal faulting, megabreccia and crevasse formation.....	52
Figure 31. Pre-resurgence lava effusion along ring fractures and other conduits.....	56
Figure 32. Comparison between experimental doming and resurgence. a) Timber Mountain caldera resurgent dome (Smith and Bailey, 1968). b) Valles caldera resurgent dome (Smith and Bailey, 1968). c) Experimental doming without extension (Withjack and Scheiner, 1982). d) Experimental doming with extension (Withjack and Scheiner, 1982).....	56
Figure 33. Location of post-collapse domes at Valles caldera, New Mexico (Walker, 1984).....	58
Figure 34. Structural resurgence of a caldera, forming a broad central dome. Magma chamber stoping and shallow intrusion may produce localized uplift and graben formation. The ring faults also may be re-activated during resurgence, which may cause peripheral uplift.....	58
Figure 35. Experimental setup, with camera mounted on ladder above cylinder containing sand.....	62
Figure 36. Verification of surface and magma chamber morphology using a dipstick and grid.....	62
Figure 37. Type experiment for shallow magma chambers (6.0 cm, scaled to 2.5 km), showing temporal evolution of faults at the surface.....	71
Figure 38. Type experiment for shallow-medium depth magma chambers (9.5 cm, scaled to 3.8 km), showing temporal evolution of faults at the surface.....	71

- Figure 39. Type experiment for medium depth magma chambers (11.6 cm, scaled to 4.6 km), showing temporal evolution of faults at the surface.....73
- Figure 40. Type experiment for medium depth magma chambers (13.9 cm, scaled to 5.5 km), showing temporal evolution of faults at the surface.....73
- Figure 41. Type experiment for medium-deep depth magma chambers (17 cm, scaled to 6.8 km), showing temporal evolution of faults at the surface.....75
- Figure 42. Type experiment for deep magma chambers (24 cm, scaled to 9.6 km), showing temporal evolution of faults at the surface.....75
- Figure 43. Type experiment for a 1 kg stratocone (magma chamber depth 11.6 cm, scaled to 4.6 km) showing temporal evolution of faults at the surface.....78
- Figure 44. Type experiment for a 1 kg sand ridge (magma chamber depth 11.2 cm, scaled to 4.5km), showing temporal evolution of faults at the surface.....78
- Figure 45. Type experiment for a 5.7 kg sand range (magma chamber depth 11.3 cm, scaled to 4.5 km), showing temporal evolution of faults at the surface.....80
- Figure 46. Type experiment for a low pressure 40 liter bladder (magma chamber depth 14 cm scaled to 5.6 km), showing temporal evolution of faults at the surface.....80
- Figure 47. Type Experiment for tilted bladder chamber depth (high in northeast, minimum depth 10.4 cm, scaled to 4.2 km), showing temporal evolution of faults at the surface.....84
- Figure 48. Subsidence controlled by both sagging and faulting. a) Faulting develops first in the south where downsagging is greatest. Downsagging is shown by the change in angle of the red laser line. b) The laser line distinguishes two styles of subsidence: the gradual curve of the laser showing downwarping-controlled downsagging, and the sharp notches in the laser line where faulting controls the subsidence.....84
- Figure 49. a) Fault propagation laterally from the area of maximum subsidence, indicated by arrows. b) Faults joining up to form polygonal ring faults, but still propagating away from the side of maximum subsidence.....85
- Figure 50. a) Due to the convex nature of the upper surface of the magma chamber, as magma is progressively removed from the chamber, the position of ring faults shifts progressively outward, producing an incrementally-growing caldera. b) A flat-topped chamber will not cause this effect.....85
- Figure 51. In the blue box marked A in experiment 14B, a terrace is observed between two inner subsidence-controlling faults; this terrace shows very little downsagging. In the

green box marked B, comparatively large amounts of downsagging are seen between an inner subsidence-controlling fault and a peripheral extension-related outer fault.....87

Figure 52. Peripheral extension outside the subsidence-controlling fault in the southwest region of experiment 14B.....87

Figure 53. Outward dipping faults which are curved and steepen with depth. a) Experimental models (Sanford, 1959). b) Ice-melt collapse pits (Branney, 1995). c) Experimental model from Odonne et al. (1999); this diagram also shows horizontal terraces between parallel, outward dipping faults. d) Experimental model from Roche et al. (2000); this figure also shows peripheral inward tilting (downsagging) between inner and outer faults.....89

Figure 54. Inferred cross-sectional structure as it varies with depth and aspect ratio of the magma chamber.....90

Figure 55. Peripheral downsagging caused by differential displacement on an outward dipping inner fault and an inward dipping outer fault.....91

Figure 56. Slumping causing an inward dipping surface. The red square shows how a slump deposit results in a previously horizontal area of the caldera dipping inwards. This will cause pyroclastic rocks laid down on this deposit to dip inwards, and so producing the apparent downsag93

Figure 57. Caldera volume versus chamber depth.....93

Figure 58. Maximum radius of faulting versus chamber depth.....95

Figure 59. Summary of experimental caldera styles for different chamber depths.....95

Figure 60. The diameter of faulting decreases with depth due to the outward dipping nature of the subsidence-controlling faults.....97

Figure 61. a) The principal stress trajectories associated with a shallow magma chamber. These stress trajectories run orthogonal to the free surfaces, which are the convex chamber roof and the horizontal surface. b) The principal stress trajectories associated with a deep chamber. The increased depth of the chamber does not significantly alter the orientations of the trajectories. However, the increased lithostatic load causes these stress trajectories to be concentrated. The closer the spacing of the trajectories, the more likely faulting is to occur.....97

Figure 62. Summary of experimental caldera styles for different masses and styles of pre-existing topography.99

Figure 63. Cross-sectional changes in symmetry as a function of topography.....99

Figure 64. Caldera volume versus changes in topography.....	100
Figure 65. Additional topography increases the lithostatic load without increasing the depth of the chamber, therefore maintaining the diameter of the caldera.	100
Figure 66. Changing the position and the orientation of the topography has little effect on the final caldera morphology.....	101
Figure 67. Topography promotes slumping; only a small amount of collapse asymmetry is required to cause failure.....	103
Figure 68. Summary of experimental caldera styles for chambers of different volume..	103
Figure 69. Caldera volume versus chamber pressure (40 liters = low pressure. 45 liters = high pressure).....	104
Figure 70. a) For experiment 22, subsidence in cross-section is greatest where the chamber is deepest. b) In Lipman's (1997) conceptual model, subsidence is greatest where the chamber is shallowest.....	106
Figure 71. Summary of experimental caldera styles for a horizontal magma chamber and for a tilted chamber.....	106
Figure 72. a) The way in which the magma chamber deforms is affected by the subsiding block, causing lateral movement of magma within the chamber. The inverted listric nature of the subsidence-controlling faults promotes lateral motion at the surface, as observed during the experiments. b) Graben development is a product of extrados-type extension in the hinge area of the caldera, similar to the extension seen on the upper surfaces of anticlinal folds.....	107
Figure 73 a) Sande cauldron, Oslo region, Norway (Ofstedahl, 1953). b) Ishizuchi cauldron, Japan (Yoshida, 1984). c) Liruei ring complex, Nigeria (Jacobson et al., 1958). d) Ossipee cauldron, New Hampshire (Kingsley, 1931).....	109
Figure 74. Crossing faults in experiment 23B.....	109
Figure 75. Subsidence on a ring fault that dips inward on one side and outward on the other produces oblique slip motions.....	112
Figure 76. The surface expression of subsidence-controlling faults is inward of their actual position. From Roche et al. (2000).....	112
Figure 77. As deposition and faulting is synchronous and as ignimbrites pond in depressions, thickness variations will occur across subsidence-controlling faults. This will result in progressively less displacement upon the faults upward in the sequence, as seen for growth faults in subsiding sedimentary basins.....	113

Figure 78. a) Experiment 33A showing lateral fault propagation from the area of maximum subsidence. b) Experiment 22B showing initial faults formed in the area of minimum subsidence. c) Vent evolution at Long Valley caldera, California, showing propagation of the ring fault towards the area of maximum subsidence (Wilson and Hildreth, 1997).....	113
Figure 79. a) Megabreccias causing inward dipping caldera-fill deposits (Lipman, 1997). b) Downsagging in experiments from Roche et al. (2000).....	116
Figure 80. The displacement of the red laser line indicates the effects of downsagging. a) In experiment 11B, the effects of downsagging extend beyond the topographic boundary of the caldera by an amount equal to the diameter of the fault-bounded part of the caldera. b) Inward dips extending well beyond the topographic margin of Taupo caldera, New Zealand (Cole et al., 1998).....	116
Figure 81. a) Gravity map of Long Valley caldera, California (Jachens and Roberts, 1985), where the steepest gravity gradients are in the east. b) Surface fault map of Long Valley (Bailey, 1989); the major subsidence-controlling faults also occur in the east ...	118
Figure 82. Resurgence "push ups". a) Theoretical cross-sections. b) Plan view in experiment 22B.....	118
Table 1. Summary of the experimental results.....	70

PREFACE

This thesis consists of two chapters, both of which are intended for submission to refereed journals. I wrote the entire thesis. My thesis supervisor, Dr. J. Stix, and Dr. J. Vallance, of the Department of Civil Engineering and Applied Mechanics, are the second and third authors of the intended manuscripts. Their roles in the preparation of the manuscripts consisted of critical evaluation of data and interpretations, as well as editorial suggestions regarding the organization of the text.

This study is based on experiments which I undertook in the Earth and Planetary Sciences Department, McGill University, in 1999-2000. I designed, planned and ran all experiments, assisted by Yan Lavallée. Some ideas and concepts discussed in the thesis are based on fieldwork which I undertook at calderas in the Lake District, Snowdonia, and Glencoe areas, Great Britain, as well as at calderas in Ecuador, El Salvador and California, U.S.A.

CHAPTER 1

INTRODUCTION TO CALDERA FORMATION

General Statement

Calderas or cauldrons have been recognized in the geological record since Fouqué's ideas on the origin of Santorini, Greece, in (1879) and Clough's work on Glencoe caldera, Scotland, in 1909. Following this work, a vast amount of material has been published describing and interpreting calderas, and the nature of the caldera-forming process has remained the subject of heated debate since this time. Williams (1941) described a caldera as "a large volcanic depression, more or less circular or cirquelike in form". Recently, this definition has been broadened to include ancient volcanic subsidence structures defined primarily by paleotopography (Branney and Kokelaar, 1999). The term cauldron often is used as "the exhumed internal structure of an inferred former caldera following erosion" (Branney and Kokelaar, 1999). To clarify the difference between the two terms, cauldron has been recently defined as "a deeper level subsidence structure defined by fault displacements"; this structure may not be clearly defined by paleotopography (Branney and Kokelaar, 1999).

Hundreds of calderas have been identified on Earth and other planets ranging from two to more than a hundred kilometers in diameter. These volcanic depressions vary widely in morphology but also in terms of formation. Many authors have attempted to theoretically or physically model caldera formation. However, no model has yet provided a comprehensive explanation. Perhaps it is a mistake to attempt to explain caldera formation in this fashion. Recent years have seen the development and classification of

calderas into caldera types and more recently combinations of types (Walker, 1984; Lipman 1997, 2000). However, these different types are oversimplified and lack detail and explanation. There are a large number of variables that control caldera type and morphology. These variables can interact in a variety of ways, giving rise to a complex intrusion and collapse history.

A major problem involved in the interpretation of caldera formation is that the process rarely has been observed. Very few major silicic caldera-forming eruptions have occurred in historic times, and the eruptions are far too violent to observe directly. Subsidence at basaltic caldera systems may be a less violent process, as was observed at Fernandina volcano in the Galapagos Islands in June 1968. This collapse event resulted in up to 300 meters of asymmetric subsidence, possibly caused by magma withdrawal from beneath the chamber, since eruptive products were only of a relatively small volume (Simkin and Howard, 1970; Munro and Rowland, 1995). Basaltic systems may represent a different collapse mechanism and appear to require a strong regional or local extensional component.

Most of the published material on calderas is in the form of case studies from individual calderas. This material provides detailed caldera stratigraphy and allows eruption sequences to be established. However, in the case of many young calderas (i.e., <2 Ma), there is commonly little exposure inside the caldera's topographic rim. The internal structure of the caldera is often buried beneath hundreds to thousands of meters of intracaldera ignimbrite. The internal structure then is inferred using the following

techniques: distribution of post-caldera vents, drilling data, seismic and gravity surveys and any available intracaldera outcrop. These limited data are then often fitted to one of the available conceptual models. However, if there are no drilling data available, evidence for the existence of subsidence-controlling faults is limited to the presence of post-caldera domes. This approach may be incorrect and lead to an oversimplified idea of the collapse history and to the classification of many young calderas as piston types.

Older deeply eroded calderas, where intracaldera deposits are well exposed, often reveal a complex pattern of faulting, leading to complicated interpretations and collapse histories that are specific to the individual caldera. Such histories may include multiple collapse episodes, periods of tumescence or resurgence and the effects of regional structural systems unrelated to the caldera. Calderas may form during one episode of collapse that takes place over a period of days or weeks, or from a series of separate events that take place over hundreds of thousands of years.

The calderas that will be examined in this thesis are those of large silicic systems, involving large volumes of erupted pyroclastic material, with subsidence occurring as a result of removal of material from the magma chamber. Observations of large silicic calderas will have implications for other calderas of different scales and chemistries.

Firstly, this thesis aims to summarize current knowledge of the process of caldera formation. This will be done by examining previous experimental and theoretical models, providing an-up-to date classification scheme for calderas and outlining some of the

stages involved in caldera formation. Secondly, the thesis presents the results and interpretations of scaled experimental models investigating some of the controls on caldera formation.

Previous Work

Theoretical studies of caldera formation

Smith and Bailey (1968) produced the classic cyclic resurgent caldera model. The model consisted of six stages: (1) regional tumescence and the creation of ring fractures: (2) caldera-forming eruptions: (3) piston-style caldera collapse: (4) pre-resurgence volcanism and sedimentation: (5) resurgent doming: (6) major ring fracture volcanism: (7) terminal solfatara and hot spring activity (Fig. 1). This model was widely accepted and applied to many large resurgent calderas. However, it has many shortcomings that have been illustrated in many of the recent theoretical papers. These problems are largely associated with the formation of ring fractures and the style of collapse.

G. Walker (1984) started to readdress some of the principles behind caldera collapse by introducing the important sentence, "No single structural or genetic model applies to all calderas, and the fact of subsidence may be the only common feature". Walker's ideas were based on re-evaluation of many maps and further fieldwork. He noted the importance of downsagging, which is the inward tilting of strata caused by collapse. He also further investigated the distribution of post-caldera vents, concluding that post-caldera magmas rarely use ring faults, or that clear ring faults rarely exist. He also noted that cauldrons (piston-style collapse blocks) are related to larger calderas.

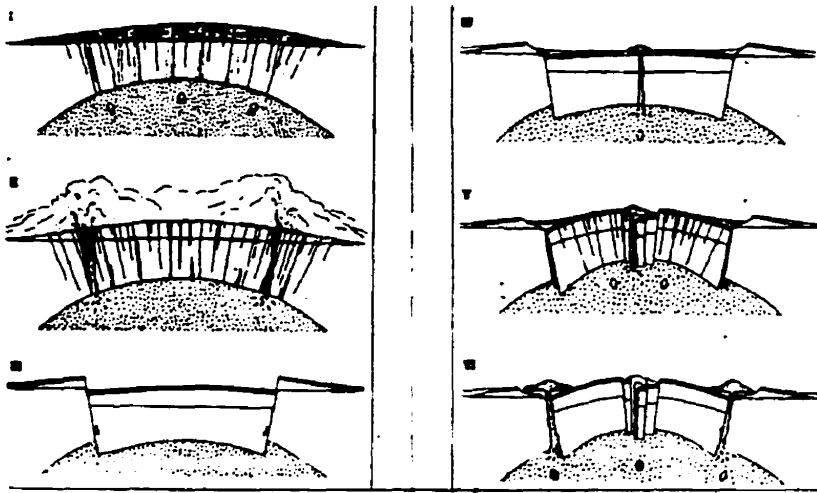


Figure 1. Smith and Bailey's (1968) classic model of resurgent cauldrons.

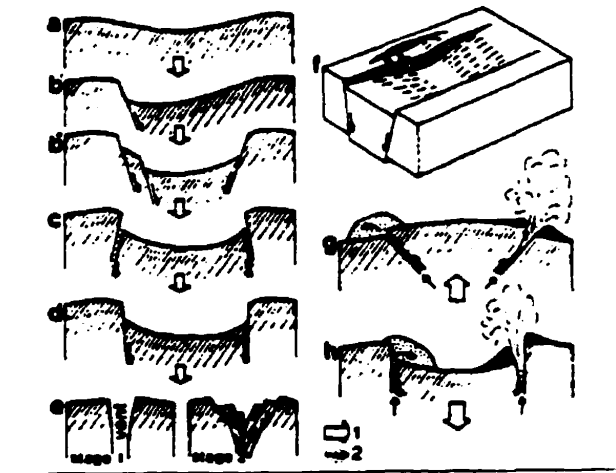


Figure 2. Caldera types actual and inferred (Walker, 1984): a) downsagging, b) normal faults with downsagging, c) Anderson-type ring fault subsidence, d) vertical ring fault, e) collapse into a cored-out explosive vent for small calderas, f) downsagging graben.

Walker also proposed that crustal strength may be important when considering the style of collapse. Walker's main contribution was to propose a variety of caldera types (Fig. 2).

T.H. Druitt and R.S. Sparks (1984) developed a two-stage model of caldera collapse, based on pressure variations within the chamber. The initial stage is an overpressured magma chamber propagating fractures to the surface, allowing eruption. This initial eruption occurs as a plinian eruption which reduces the pressure within the chamber by evacuating material. The decreased volume of magma and the reduction of pressure below lithostatic within the chamber causes its roof to fail and subsidence to occur. Subsidence attempts to reestablish lithostatic pressure within the chamber. Eruptions continue as the conduits are kept open, with a pressure gradient existing between the vesiculating magma in the conduit and the magma in the chamber. Large volumes therefore can be erupted at this second stage. By contrast, calculations showed that at the initial overpressured stage, large volumes cannot be erupted.

The model is elegant and appears to fit observed data from eruption sequences. However, there is a major problem with the model. The model is dependent on underpressure (pressure lower than lithostatic within the chamber), and this can only be achieved if conduits remain open. This situation seems unlikely, as a chamber pressure of less than lithostatic would promote the closure of conduits. Yet the model does provide a very interesting way of looking at the caldera problem, as it is important to address the crucial issue of magma chamber pressure during caldera formation. Such a model is not specific to any collapse style and is thus relevant to calderas of different types.

Gudmundsson (1988, 1997, 1998) attempted to explain the formation of collapse calderas by looking at stress fields associated with magma chambers. By using a boundary element computer program, he produced stress fields for different shaped magma chambers subjected to different stress regimes. He explained that the intrusion and growth of a shallow sill-like magma chamber will promote the concentration of tensile stresses suitable for ring fracture formation. In the 1998 paper, Gudmundsson took his ideas further by using a series of equations to explain the development of the principal caldera faults, uplift amounts and eruption volumes. Gudmundsson made many assumptions in both his stress field models and his equations, leaving his explanation applicable to very few caldera types. In addition, the data he chose to use for his equations were not relevant to the type of caldera he was describing for his uplift stress field model. This is because he was applying data from large complex silicic systems to his model, which only may be relevant to smaller simple, normal fault piston calderas. However, the focusing and concentration of regional stress by a shallow sill-like magma chamber may be relevant for ring fault formation at normal fault calderas. His conclusions on the shape and depth of the magma chamber were consistent with other authors' ideas on this type of caldera.

R. Scandone (1990) discussed the chaotic collapse of calderas. He used data compiled by Spera and Crisp (1981), as well as mining subsidence structures and gravimetric profiles from different calderas. He used these lines of evidence to dismiss an explosive decapitation origin for Krakatoan-type calderas. The paper provides interesting insights into calderas of small diameter and provides a clearer explanation than Escher's

(1926) cored-out explosive vent model, which was included in Walker's (1984) caldera types. However, there are several problems with Scandone's chaotic collapse model as pointed out by Yokoyama and De La Cruz-Reyna (1991). They demonstrate that many explanations are possible for a given gravity anomaly, including low-density magma chambers and coarse caldera fill. Furthermore, the application of mining subsidence structures has certain scaling problems involving rock tensile strengths. Yokoyama and De La Cruz-Reyna present some of their own ideas by introducing restrictions to the existence of maximum sizes and depths of cavities within the crust. However, these restrictions were made assuming spherical and cylindrical cavities with no pre-existing fractures, making their application limited.

M.J. Branney (1995) added important detail to theoretical structural studies of collapse calderas. Branney developed his ideas from detailed field studies of ancient eroded calderas where the internal structure is exposed. He also used evidence from collapse geometries from ice melt and mining subsidence structures. His main contributions to the process of caldera collapse focussed on the orientation of ring faults and the importance of peripheral extension to collapse structures. Branney clearly showed that pure subsidence results in a specific structure related to central compression and peripheral extension. This implies that the subsidence-controlling ring faults may be outward dipping and peripheral faults inward dipping. The faults and downsagging related to this stress system can be seen at many large calderas. Branney's ideas of peripheral extension explain some of the structures seen at calderas: (1) arcuate crevasses, normal faults and graben observed near the margins of many calderas: (2)

peripheral inward-tilted pyroclastic sequences; (3) the large difference in diameter between the topographic boundary of a caldera and the position of the ring fault; (4) funnel-shaped gravimetric anomalies observed at some Japanese calderas.

The papers of P.W. Lipman (1984, 1997, 2000) show an interesting evolution of ideas. The 1984 paper proposes a simple Smith and Bailey-style origin for many North American calderas, with piston subsidence occurring along steeply inward dipping fractures. The 1997 paper acts as a synthesis of ideas regarding caldera formation and presents different caldera types in a way similar to Walker (1984). He discusses these different types and suggests possible origins for them. The paper also examines geometric relationships regarding the topographic rim, the collapse collar and the structural caldera; these are discussed with a bias towards the piston model. Perhaps the most important insight in this paper is the origin of landslide breccias and their temporal relationship with collapse and eruption. By 2000, Lipman illustrates subsidence occurring along outward dipping ring faults and shows an evolution of ring fault orientation during caldera formation. He also classifies calderas and introduces the idea that some calderas may be composite in type (a combination of more than one model).

P. McLeod (1999) produced a theoretical paper which attempted to explain magma chamber pressure variation during caldera formation. The specific problem that McLeod tried to address is that of producing underpressure necessary for collapse, since underpressure is crucial to the caldera forming process. McLeod attempted to use magma buoyancy to explain this concept. There appear to be some problems in the details of

some of the equations in the paper, but the idea of buoyancy can produce a mechanism for pressure variation within the chamber. The initial eruption can be stopped if overpressure falls to zero at the top of the chamber, while allowing underpressures lower in the chamber. Buoyancy ultimately may prove to be insignificant in caldera formation, but the attainment and magnitude of underpressure required for collapse needs to be addressed.

A detailed thermomechanical study of large ash flow calderas by Burov and Guillou-Frottier (1999) has produced a new approach to the caldera problem. The study uses analytical and numerical models to account for both the elastic-plastic rheology and the physical properties of the caldera rocks. Unlike previous models, this approach includes the effect of ignimbrite ponding above the magma chamber as the eruption proceeds. Treating caldera formation in this manner, both brittle and ductile deformation occur. Faults are initiated at the surface above the margins of the chamber, as this is where maximum bending occurs, either from subsidence or uplift and extension: the normal load from the ponded ignimbrite sheets aids the subsidence-related bending. The brittle rock strength is also lowest at the surface, promoting fault initiation here rather than at depth. Interesting fault geometries are proposed for different aspect ratio magma chambers. The general fault geometry is a coherent piston bounded by inward dipping faults initiated at the surface and subvertical faults that are initiated at depth. Fault orientation is dependent on the geometry of the brittle-ductile transition layer. The effect of a superimposed extensional regime on the system causes the center of the subsiding block to rift apart. As in any theoretical model, some of the assumptions may cause some inaccuracies in the results. For example, pressure in the chamber is kept constant, the

magma chamber has an unrealistic geometrical shape, and structures formed from the emplacement of the magma chamber are not considered. However, these assumptions may not affect the general patterns observed. This approach to the caldera problem has contributed very interesting and possibly very significant ideas regarding caldera formation and the effects of brittle and ductile behavior of the crust.

Analogue models of subsidence

Scaled physical models have been used to investigate the various ideas behind caldera formation. Physical models are a necessary approach to the caldera problem. Scaling allows the process to be reproduced accurately at an understandable and manageable scale. These models reveal structural details of collapse evolving in a temporal manner. In nature, these structural details are obscured by eruptions and further complicated by resurgence and post-collapse magmatism.

Komuro et al. (1984) investigated the formation of collapse basins during the Green Tuff orogenesis in Japan. In this paper Komuro proposed an origin for collapse basins: these structures could be termed calderas. Komuro's experiments showed that collapse basins could be produced by simple doming and that chamber evacuation was not necessary. His results showed structures dominated by radial cracks and an irregular, polygonal-shaped depression. Komuro formed these structures by intruding a rigid globe through dry sand and powdered clay. The relevance of this technique for caldera formation is perhaps dubious due to the apparent absence of radial fractures at calderas. This forceful intrusion mechanism and simulation also may be considered unrealistic, as

a more passive model of magma chamber intrusion is preferred for these shallow magma chambers.

Further experiments were performed by Komuro (1987), in which an evaporating ball of dry ice was used to simulate the contraction of a magma body after eruption. Results showed outward dipping ring faults delimiting a bell jar-shaped subsiding block. This block does not appear coherent, although this is not discussed in his paper. The total evaporation of a circular ball of dry ice represents complete evacuation of a magma chamber, which may be unrealistic. Yet the experiments did show outward dipping ring fractures and peripheral extensional fractures: these features have been identified at many calderas and in subsequent work. Komuro's initial work also tested the idea that calderas may form as a combined result of fractures created by doming, followed by fractures created by chamber evacuation.

J. Marti et al. (1994) used a spherical inflating and deflating air-filled balloon in a medium of fine uncompacted fused alumina powder to simulate the caldera system. Although unclear, it appears that the balloons were entirely emptied and filled. The experiments thus appear unrealistic in three ways. (1) A spherical chamber was used, which does not accurately represent the sill-like nature of most high-level silicic reservoirs. (2) Total filling or evacuation of a reservoir is unlikely to occur. (3) A reservoir is unlikely to deform purely by expansion or contraction. Some experiments were done with oblate balloons, which is a more realistic magma chamber shape, but little useful information was recorded. Magma chamber deformation is likely to occur in

the form of both contraction as well as flattening and failure of a convex roof by faulting. Despite these problems, inner outward dipping ring fractures and outer inward dipping ring fractures were seen; this pattern has been observed in most subsequent experimental caldera models. Furthermore, when the depth of the balloon was increased, the area of the caldera was seen to decrease. The depressions that formed rarely showed coherent floors, and the aspect ratio of chamber depth to chamber diameter was high for large silicic systems. For this reason, these experiments may have more relevance to funnel-type calderas.

Marti et al. also modeled the effect of precursory tumescence and post-collapse resurgence. The nature of the tumescence, as represented by the gradual inflation of an initially emptied balloon, may not be relevant to the complex process of intrusion. For these reasons, the details of fault patterns observed in the experiments may have limited application to real calderas. However, the experiments do introduce a source of extension and formation of normal faults; both features are commonly observed at calderas. Depressions which experienced previous doming had characteristics different from those that formed as a result of simple balloon evacuation. Important ideas from this work are those of fault reactivation and changes in the sense of movement of faults. Smaller-area calderas were produced by calderas that were previously inflated. However, this may be a function of compaction of the powder, rather than a factor that can be applied to natural calderas.

F. Odonne et al. (1999) used analogue models to investigate fault formation above a depleting oil reservoir. This process is essentially the same seen in simple caldera formation. Odonne et al. used two techniques: (1) a deflating latex balloon in a layered sand box; (2) a reduction in pressure of an air-tight space contained within a silicone layer. Both techniques produced similar results, the subsidence being controlled by cone-shaped outward dipping faults. When the reservoirs depths exceeded 12 cm, these cone-shaped faults did not cut the surface.

O. Roche et al. (2000) modeled caldera collapse in these last experiments using a cylinder of silicone putty to represent a magma chamber. They therefore avoided problems associated with a balloon, since the elastic rubber interface of the balloon does not exist around magma chambers. The silicone putty was contained in dry sand and was connected via a tube to the open air; this allowed subsidence to occur as a result of the weight of the overlying sand. This system provided detailed results in both two and three dimensions (plan view and cross section). It enabled a clear understanding of the temporal development of classic piston-type collapse. They observed that an outward dipping inner fault develops and propagates around from the side of maximum subsidence, followed by an inward dipping fault that develops initially on the side of minimum subsidence and propagates in the other direction. The paper also provides insights into funnel-type calderas and the causes for a less coherent subsiding block. Reverse faults clearly could be seen developing cone-like structures in the lower parts of the subsiding block, breaking up lower parts of the block. These cone structures allow the lower parts of the block to subside independently. The change from piston-type calderas

to funnel-type is clearly explained in terms of chamber roof aspect ratio. Shallow, large-diameter chambers produce piston-type calderas, whereas deep, small-diameter calderas produce funnel-type calderas. The paper clearly illustrated how areas of extension and compression occur simultaneously at calderas, and how normal and reverse faults form respectively in these areas.

It should be noted that the style of caldera collapse is a direct result of their experimental set up. The silicone putty has a very high viscosity, which is not scaled; this means that the cylinder of putty subsides as a coherent piston. This high viscosity prevents the putty from being displaced by subsiding blocks and subdues asymmetry. As a result, the calderas formed are normally coherent pistons, with well-developed circular ring faults. Whether this represents the way a magma chamber subsides is debatable; this subsidence style appears to be an artifact of the experimental methodology.

Analogue modeling also was used to investigate the formation of calderas on fast spreading ocean ridges (Lagabrielle and Garel, 2000). These experiments used silicone putty to represent rocks in the brittle-ductile transition within oceanic crust. The magma chamber was represented by an elongate water-filled balloon that could be deflated to represent caldera formation. This representation of a magma chamber was developed based on thermal models of spreading ridges. Two experiments were carried out, simple extension without evacuation of the balloon, and evacuation of the balloon at the same time as extension. Motor-driven mobile walls which were displaced at a controlled rate allowed extension. A domed area also was built up to represent the morphology of the

ridge. Evacuation of the chamber resulted in outward dipping reverse faults. The extension exaggerates the normal faults observed by Roche et al. (2000), and full graben are seen to form. When there is only extension, a deep central graben is seen, and no outward dipping faults or lateral graben form.

In conclusion, these recent scaled physical analogue models all show the same basic collapse patterns, irrespective of their experimental techniques: an inner ring fault that is outward dipping and becomes steeper with depth. Outer ring faults that dip inward also develop in response to the inner ring fault, and these can be seen best when the evacuated source is shallow.

A Descriptive Outline of Caldera Types

The caldera types proposed by Walker (1984) and Lipman (1997) provide a simplified view of the different calderas which may exist in nature. A combination of descriptive and interpretative definitions has been used, causing some confusion in the literature when describing and discussing examples. For example, Lipman (2000) points out the confusion that has arisen over funnel-type calderas. Piecemeal-type calderas and chaotic-type calderas also appear to be confused in some of the literature, as they both represent non-coherent collapse, but at completely different styles and scales. Therefore, this section attempts to establish a more comprehensive and realistic definition of the different caldera types that can be applied to specific calderas. These types are purely a structural description and do not imply anything about the manner of formation. One caldera type can form from a variety of intrusion, eruption, collapse and resurgence

histories, which are dependent on a great many variables. It is important to note that there is a gradation between all the caldera types, and most calderas will show some features of several types.

Simple piston

This is the classic model of a coherent subsiding block, bounded by a circular ring fault which controls the subsidence. The caldera will appear roughly symmetrical in plan view and in terms of subsidence. The caldera topographic boundary is an expression of the back-eroded ring fault scarp (Fig. 3). Very few calderas are, in fact, as simple as this: perhaps the only example of a completely coherent piston is Hwasan caldera in Korea (M. Branney, personal communication, 1999). However, piston-type calderas with a more or less coherent piston have been identified, e.g., Bachelor, Stillwater range in the U.S., (Lipman, 2000) and many calderas in northern Honshu, Japan, e.g., Ishizuchi (Yoshida, 1984). The dip direction of the ring fault has been a subject of heated debate, and it appears that the ring fault is generally near-vertical (Lipman, 1997). However, piston-type calderas with an inward dipping or an outward dipping ring fault also exist (Branney, 1995).

Inward dipping piston

There is a space problem with a simple inward dipping ring fault caldera, as subsidence along inward dipping fractures requires a horizontal length increase (this is not a problem in areas of extension). In areas of rifting such as Iceland and the East



Figure 3. Three-dimensional block diagram of piston collapse along vertical ring faults, with a back-eroded topographic margin.

a)

b)

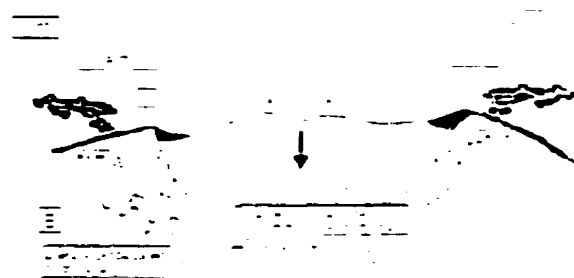


Figure 4. a) Three-dimensional block diagram of piston collapse along inward dipping faults: two concentric ring faults can be seen. b) An example from Suswa volcano, Gregory rift valley, Kenya (Skilling, 1993).

Africa rift, this caldera type may be common (Gudmundsson, 1998). Piston calderas with an inward dipping ring fault may be associated with a series of concentric down-stepping normal faults outside of the main coherent piston, producing nested structures with benches or terraces between ring faults. The Hawaiian calderas may be of this type (Francis, 1993). At Suswa volcano, Gregory Rift Valley, Kenya, repeated collapses occurred producing nested, inward dipping pistons (Skilling, 1993) (Fig. 4b).

Outward dipping piston

Subsidence along an outward dipping ring fault has no space problem and is the favored geometry of a purely subsidence-related structure. These faults will promote failure of the caldera walls and megabreccia formation. Also associated with an outward dipping ring fault will be features of peripheral extension outside the coherent piston, such as inward dipping stratigraphy and arcuate normal faulting and crevasses (Fig. 5a). Rabaul caldera, Papua New Guinea, is an example of a piston caldera with outward dipping ring faults (Mori and McKee, 1987) (Fig. 5b).

Polygonal piston

Another type of piston caldera is one that appears polygonal in plan view instead of circular. The caldera still subsides as a coherent block, but the block is bounded by a series of connected near-linear faults (Fig. 6a). It may be difficult to recognize these calderas from their surface morphology, as erosion will round corners, making the caldera appear circular in plan. Older eroded calderas where the ring fault is clearly defined often show polygonal outlines. Cone sheets or ring dykes are exposed at many

a)



b)



Figure 5. a) Three-dimensional block diagram of outward dipping piston collapse with a peripheral area of normal faulting. b) An example of earthquakes marking the ring fault, 1983-1985, from Rabaul caldera, Papua New Guinea (Mori and McKee, 1987).

a)



b)

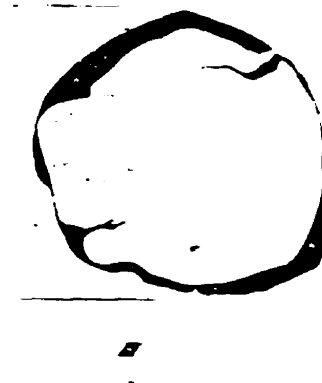


Figure 6. a) Three-dimensional block diagram of polygonal piston collapse, with linear subsidence-controlling faults. b) An example from the Ossipee cauldron, New Hampshire (Kingsley, 1931).

intrusions: although previously described as circular, they actually show a clear polygonal shape. Excellent examples of this feature are seen in the cauldrons of the White Mountain Igneous Province, New Hampshire, including the classic structure of Ossipee cauldron (Fig. 6b).

Ishizuchi cauldron, Japan, shows aspects of all four types of piston caldera: it has two concentric faults in the north dipping inward, while in the south only a single ring fault dips outward with evidence for inward tilted stratigraphy (downsagging). The ring fault even shows a polygonal form (Fig. 7). Nested outward dipping cones also can be seen beginning to form.

Downsag calderas

This type of caldera will show inward tilting of pre-caldera stratigraphy that was originally horizontal (Figs. 2, 8). There also will be an absence of tangential subsidence-controlling fault scarps (Walker, 1984). This type of caldera will allow ignimbrite sheets to pond in a depression that is not bounded by significant tangential faults, implying that ignimbrite thicknesses will increase gradually towards the center of the depression, rather than abruptly across syn-subsidence faults. Previously-erupted ignimbrite sheets will be back-tilted by the subsidence. Examples of this type of caldera are Rotorua and Taupo, New Zealand (Walker, 1984) (Fig. 8b). It should be pointed out that downsag calderas may exhibit faults, but they are not concentric to the depression and are usually tectonic in origin, without large displacements across them. It may be rare to find purely downsagged calderas, as most calderas have an element of arcuate concentric faulting.

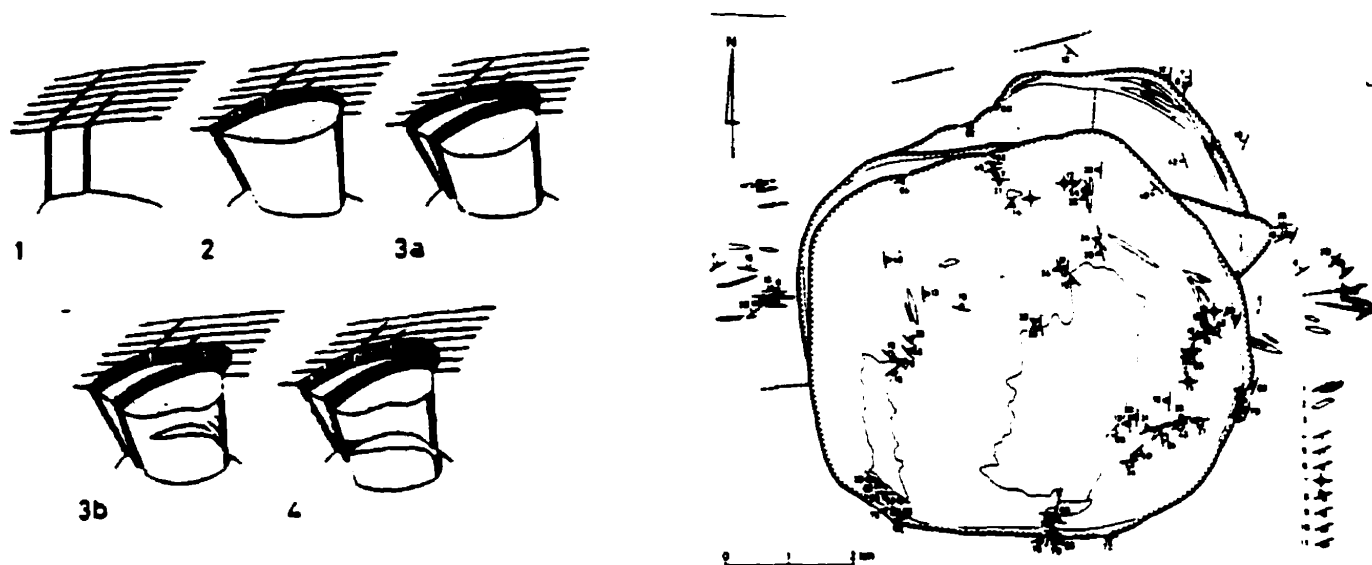
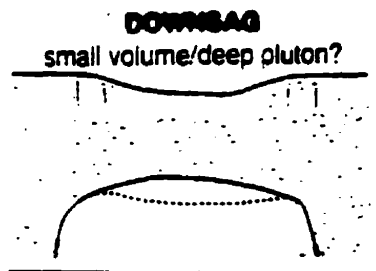


Figure 7. Temporal evolution of Ishizuchi cauldron, Japan (Yoshida, 1984). This structure shows a combination of different styles of piston collapse, including subsidence along both inward and outward dipping faults and a polygonal-shaped subsiding block.

a)



b)



c)

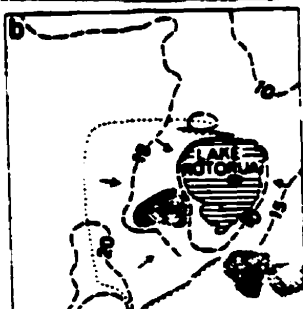


Figure 8. a) A model of a caldera formed by downsagging (Lipman, 1997), with examples from b) Taupo caldera, New Zealand, and c) Rotorua caldera, New Zealand (Walker, 1984).

However, downsagging is an important element of many caldera types, as a high percentage of calderas show inward tilting of stratigraphy, particularly associated with areas that are peripheral to the subsidence-controlling faults (Branney, 1995).

Trapdoor calderas

This type of caldera is produced when subsidence is highly asymmetric. A subsidence-controlling fault with large displacement should exist only on one side of the caldera (Fig. 2, 9). The subsidence on the other side of the caldera is controlled largely by downsagging (Walker, 1984). The downsagged side of the caldera acts as a flexural hinge and may be associated with small-scale arcuate normal faults, graben and crevasse formation. Such asymmetric subsidence causes significant variations in the thickness of the ignimbrite sheet inside the caldera margins. Although it is not a defining characteristic, these calderas also often show asymmetry in plan view. Examples include Silverton, Organ Mountains, Eagle Mountain, Big John, Whitehorse and Tuscan Mountain calderas in the U.S., Bolsena in Central Italy, Sakugi in southwest Japan (Lipman, 1999) and Kumano caldera, southwest Honshu, Japan (Miura, 1999).

Concentric step-down calderas

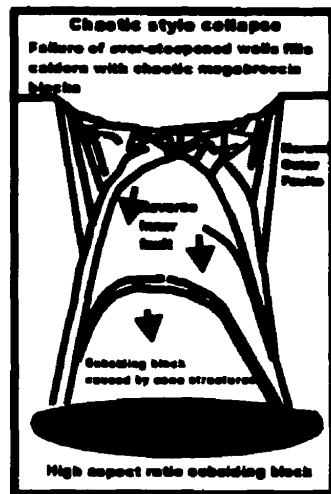
These calderas consist of a series of concentric rings and arcuate faults. Collapse occurs along these faults, each with small displacement. These faults generally have increasing displacements towards the center, although subsidence is not necessarily symmetric. A small central piston may exist, but its area will be less than half of the caldera area (Fig. 10a). The caldera may grow incrementally outward during subsidence.

increasing its overall area (Hallinan, 1993). This type of caldera also will be associated with a V-shaped (funnel-shaped) gravity anomaly. Guayabo caldera, Costa Rica, is a classic example of this type of caldera, showing all of the above-mentioned features (Hallinan, 1993) (Fig. 10b). A concentric pattern of faults exists at Dorobu caldera, northeastern Honshu, Japan; this was interpreted as representing a series of collapses moving sequentially toward the caldera center, the opposite case to Guayabo caldera (Miura and Tamai, 1997). Drilling at Valles caldera, New Mexico, originally interpreted as the classic piston example, has revealed that the caldera has some characteristics of these step-down calderas (Nielson and Hulen, 1984). Latera caldera, Italy, also has been interpreted as this type of caldera, with its formation linked to multiple collapse episodes (Barberi et al., 1984).

Chaotic calderas

These calderas tend to be of smaller scale (<15 km diameter) than many of the other types. The caldera floor is disrupted, without clear subsidence-controlling faults (Fig. 11a). Faults located lower within the subsiding block may produce multiple nested cones (Roche et al., 2000) (Fig. 12). The topographic wall of the caldera represents the slide surfaces of foundering blocks, not a ring fault. This type of collapse is often associated with the collapse of a volcanic edifice that previously has been hydrothermally weakened. Slide blocks and faults blocks will become mixed and form the caldera floor. This low-density brecciated material that forms the caldera floor produces a V-shaped gravity low. These calderas have been termed funnel calderas in some reviews; this leads

a)



b)

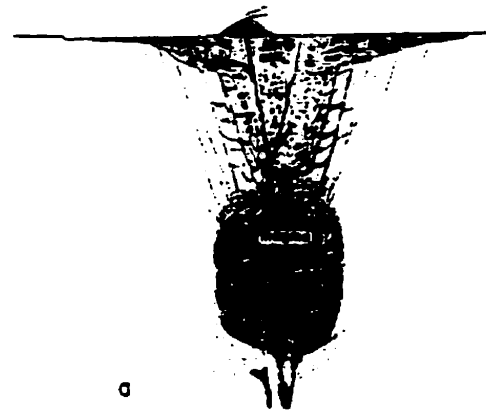
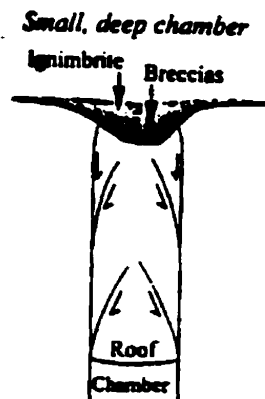


Figure 11. a) Cross-sectional diagram of chaotic collapse, showing no clear ring faults at the surface and a disrupted caldera floor. b) An example from a hypothetical cross-section through Aira caldera, southern Kyushu, Japan (Aramaki, 1984). The internal structure of this caldera is poorly constrained; a funnel-shaped gravity anomaly was interpreted as an inward dipping ring fault. However, an alternative explanation is a funnel-shaped subsurface structure controlled by outward dipping faults.

a)



b)

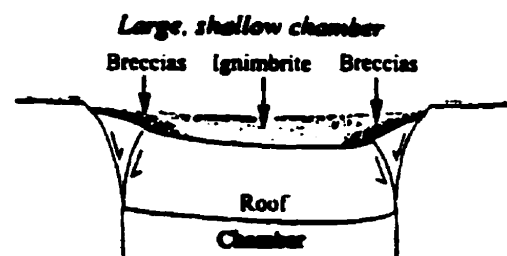


Figure 12. a) High aspect ratio collapse, showing nested cones: b) low aspect ratio collapse, showing a simpler piston (Roche et al., 2000).

to confusion, however, as calderas of many types show a funnel-shaped gravity profile (Lipman, 2000).

The 1883 caldera-forming eruption of Krakatau could be interpreted as this type of caldera (Scandone 1990). It is possible that the 1991 caldera-forming eruption of Mount Pinatubo, Philippines, also formed this type of caldera. Large amounts of hydrothermal alteration occurred in the edifice before the eruption, and no evidence of ring structures was observed in fissures or vents before the eruption. Post-climactic eruption seismicity during the eruptions reveal the beginning of an outward dipping ring fault up to 14 km beneath the volcano (Mori et al., 1996); however, this structure never was used and was of a much larger scale than the caldera which formed. The chamber roof is 14 km deep and 10 km in diameter, giving a high aspect ratio of 1.4 (Mori et al., 1996). The coalescence of the seismicity at 0-4 km suggests the beginnings of a cone structure (Fig. 13a). High aspect ratios of the chamber roof may promote this type of caldera. By contrast, the ring structure at Rabaul caldera depicts a coherent piston at the surface, with an underlying chamber 4 km deep, 6 km in diameter, so having an aspect ratio of 0.67. (Mori et al., 1987) (Fig. 13b).

Chaotic collapse also has been proposed to explain some of the Japanese funnel (V-shaped gravity anomaly) calderas. Aira caldera, southern Kyushu, Japan, was interpreted as having a central chaotic area of subsidence which becomes more coherent near its margins (Aramaki, 1984) (Fig. 12b). This is an example of a combination of a concentric step-down type caldera and a chaotic collapse-type caldera. Shishimuta caldera, Japan, also appears to be of this type (Kamata, 1989).

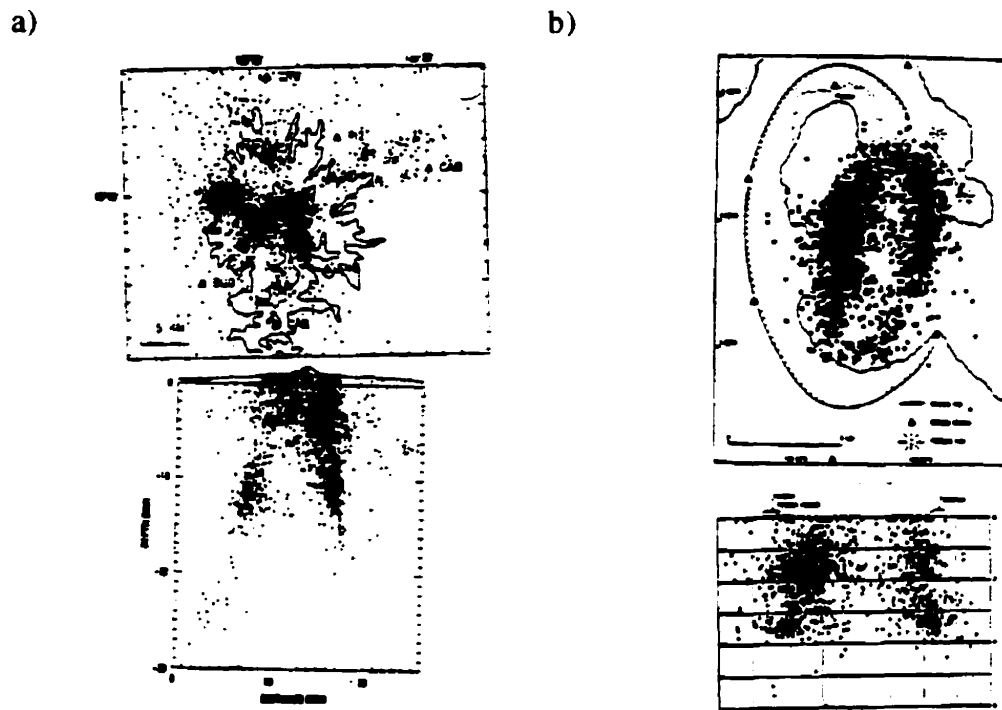


Figure 13. a) High aspect ratio magma chamber at Mount Pinatubo, Philippines, as illustrated by post-climactic eruption seismicity, 29 June-16 August 1991 (Mori et al., 1996). b) Low aspect ratio magma chamber at Rabaul caldera, Papua New Guinea, based on seismicity between late 1983 and mid 1985 (Mori and McKee, 1987).

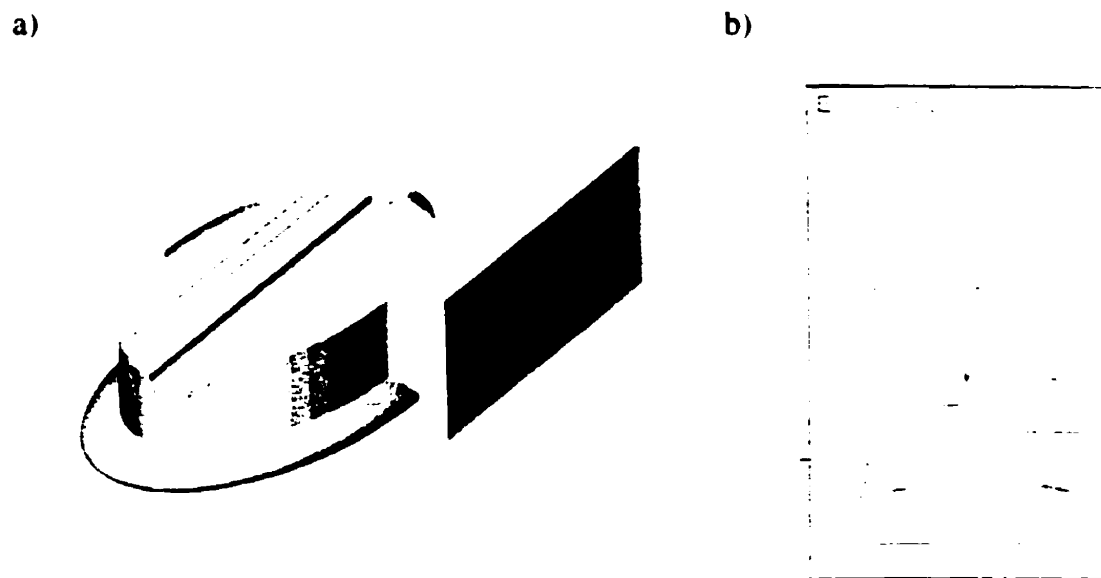


Figure 14. a) Three-dimensional block diagram of a rifted caldera. b) An example from Toba caldera, northern Sumatra (Chesner and Rose, 1990).

Rifted calderas

This type of caldera has not been discussed previously in the literature as an individual type. These calderas have a significant amount of subsidence controlled by a linear graben. The rest of the caldera subsidence is controlled by either arcuate faulting or by downsagging (Fig. 14a). An example is Toba caldera in Northern Sumatra, which is elongate along the orientation of the Latung Graben (Fig. 14b). This graben clearly was reactivated during subsidence and resurgence (Chesner and Rose, 1990). Emory cauldron, New Mexico, is highly elongate parallel to the regional rifting axis and also fits this caldera type (Elston, 1984). Calderas which form on the sea floor associated with spreading ridges of the East Pacific Rise also are being recognized and interpreted as this type of caldera (E. Garel, personal communication, 1999). Snowdon caldera, North Wales, is also a rifted-type caldera in a northeast-southwest cross sectional view: this caldera also has a large component of asymmetry and is also a trapdoor-type caldera. The term "piano key" caldera has been applied to this structure (P. Kokelaar, personal communication, 1999) (Fig. 15). Rifting also results in significant amounts of subsidence in some piecemeal calderas (see below).

Pull-apart calderas

These calderas appear asymmetric in plan view and are associated with strike-slip induced extension. The calderas are frequently elongate parallel to the regional strike-slip faults. Caldera faults parallel with the regional strike-slip system should be near vertical, and normal faults will control subsidence on the other edges (Fig. 16). A central rifted area also may be present. The classic example of this type is seen on Vulcano Island.

Italy (Ventura, 1994). The island shows clear pull-apart basin morphology (Fig. 16). It is important to note that calderas commonly form in transtensional tectonic regimes. The Negra Muerta caldera, northwest Argentina, shows evidence of strike-slip-controlled collapse (Riller et al., in review). The New Zealand calderas also form in a transtensional regime and may show some of these characteristics.

Piecemeal/ regional fault-controlled calderas

Piecemeal calderas consist of a series of blocks which subside at different rates. This type of caldera may show aspects of all caldera types mentioned above. However, there is no large piston that controls the subsidence (Fig. 17a). Some areas of the caldera may be subsiding along pre-existing linear graben structures, strike-slip faults or even thrust faults. Other subsidence-related faults may form during collapse and will be curved and either inward or outward dipping. Downsagging and peripheral extension are likely to control significant amounts of subsidence. Different blocks may subside at different times, associated with separate eruptions. This causes significant stratigraphic thickness variations, particularly in ponded ignimbrite sheets, from one fault block to the next. The irregular patterns of faulting associated with these caldera types means that there is significant asymmetry in both cross-sectional and plan views. These calderas also may be polygonal in plan view. Scafell caldera, England, is well exposed in three dimensions and can be seen to be of this type (Branney and Kokelaar, 1994). Glencoe, Scotland, was previously thought to be a classic piston-type caldera; further study has revealed a piecemeal-type morphology and collapse history (Moore and Kokelaar, 1998) (Fig. 17b).

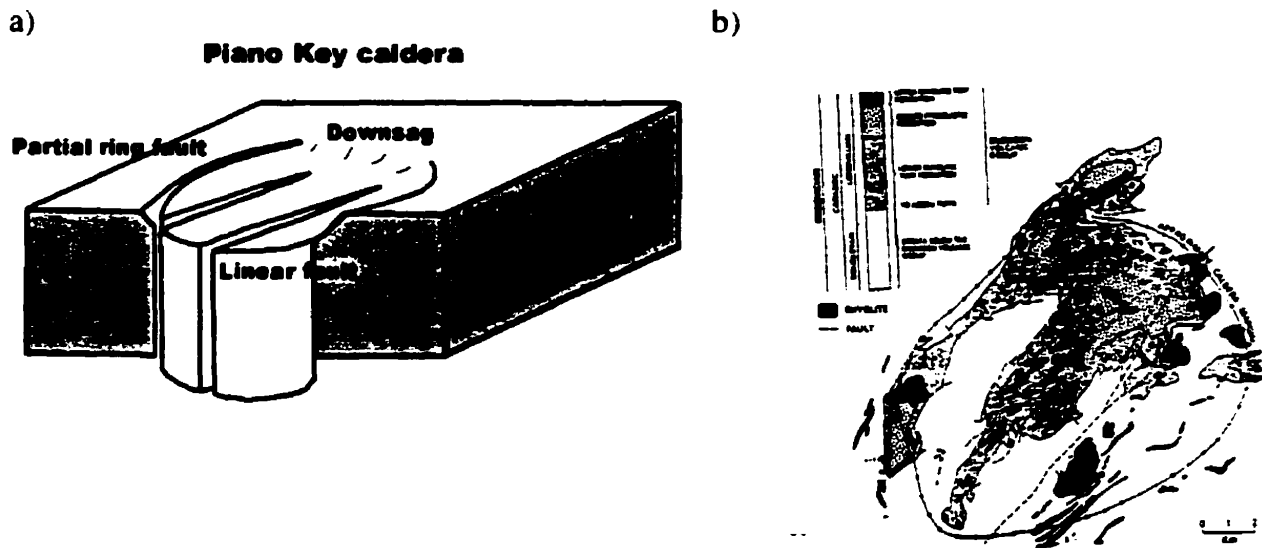


Figure 15. a) Three-dimensional block diagram of a piano-key caldera. b) An example from Snowdon caldera, Wales (Branney and Kokelaar, 1999).

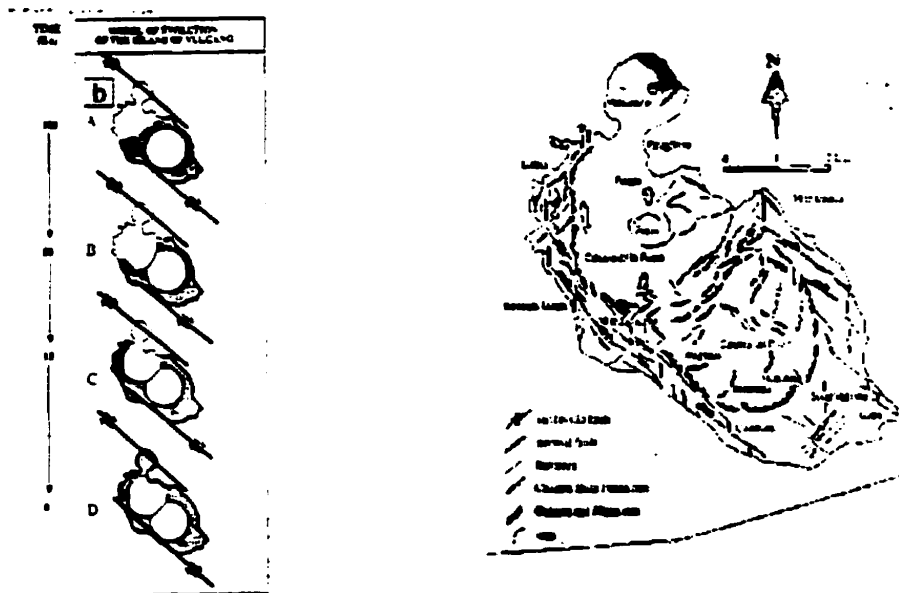


Figure 16. Diagram showing formation of a pull-apart caldera, Vulcano Island, Italy (Ventura, 1994).

Stages in the Temporal Evolution of Calderas

This section will attempt to illustrate some of the different stages that are often involved in formation of a caldera. Little is known about the early stages in caldera formation, and they are often neglected in the literature: because the base of the subsiding block is rarely well-preserved. A largely conceptual approach to the temporal development of calderas therefore has been adopted. At each stage there are a number of different scenarios that will interact to eventually form a caldera. This section aims to illustrate some of the processes that are responsible for the formation of the different caldera types. While this approach is similar in some respects to that of Smith and Bailey (1968), it is fundamentally different in other respects by attempting to view caldera development as a series of structural events which are related in a spatial and temporal sense.

Stage 1. Magma chamber intrusion

Large, shallow (2-10 km), sill-like magma chambers are associated with calderas (Gudmundsson, 1988, 1997, 1998; Lipman, 1997, 2000). For the intrusion of such magma chambers, certain tectonic conditions are needed. Some degree of upper crustal extension is required to create the space necessary for the intrusion. If this upper crustal extension is not sufficient, doming of the surface may result. This doming may be the result of (1) faults formed by forceful intrusion; (2) upper crustal volume changes caused by thermal expansion; (3) elastic plate bending caused by magma pressure (Withjack and Scheiner, 1982); and (4) faulting and structural uplift caused by overpressure. The latter is local and of low magnitude, producing small structures which may not be significant to

collapse. A combination of these effects is likely to result from an intrusion capable of forming a caldera.

Doming may comprise an area which is larger than the caldera. This is seen in the "Green Tuff beds" along the inner Japan arc where doming of a 80 km-diameter area preceded a 5 km-diameter collapse (Komuro et al., 1984), and the ignimbrite-related regressive cycles of volcano-sedimentary Silurian strata in southwest Ireland (Marti et al., 1994). There is evidence at Grizzly Peak caldera, Colorado, for precursory doming, as the area was a topographic high with some of the subsidence-controlling faults existing prior to collapse (Fridrich et al., 1991). Many cone sheets and radial dykes were emplaced related to this doming. Such doming is likely due to thermal expansion, which creates radial, arcuate or polygonal fractures. Fractures during this stage are likely to be tensional and may evolve into normal faults (Marti et al., 1994). The greater the uplift, the more likely normal faults are to form. Sufficient doming can produce some subsidence at this stage due to the development of polygonal concentric normal faults (Komuro, 1984, 1987) (Fig. 18a). However, there is rarely sufficient evidence to support the magnitudes of doming required for this kind of subsidence. Experimental studies of dome formation show that if preferentially-oriented extension is applied at the same rate as uplift, normal faults may form which are perpendicular to the direction of extension on the crests of the domes. On the flanks of the domes, normal faults will be oblique to this direction. If extension is double the uplift rate, normal faulting will be dominantly perpendicular to the extension direction, and peripheral strike-slip faults also may form (Withjack and Scheiner, 1982).

At Kakeya caldera, southwest Japan, collapse was preceded by more than 350 m uplift of the basement by block faulting (Sawada, 1984). Precursory uplift by block faulting may be related to forceful intrusion of a magma chamber, but it is not commonly observed before collapse.

After intrusion, the magma chamber will become overpressured, and principle stress trajectories will be oriented perpendicular to the surface of the earth and to the upper surface of the magma chamber. These principle stress trajectories are likely to promote tensional failure at the surface and shear failure at depth (Fig. 19). Extension at the surface is caused by bending and extrados-type extension. Extrados-type extension is caused by the length increase that occurs on the outside of a fold (Fig. 19). The increased lithostatic pressure at depth prevents tensional fractures from penetrating beyond 130-800 m in most volcanic fields (Gudmundsson, 1998), but it will promote shear failure and normal fault formation at these depths.

Structural evidence for precursory tumescence consists of radial and ring fractures or dykes (Fig. 21a). An external stress field acting on a shallow sill-like chamber may promote cone sheet formation as opposed to radial fractures during tumescence (Gudmundsson, 1998). Many examples of radial and concentric dykes can be observed at calderas; these dykes exposed at the surface are usually post-collapse features, however, since older pre-collapse structures will have been buried. Radial dykes are seen at Las Canadas caldera, Tenerife, and radial fissures also are seen on the flanks of calderas on

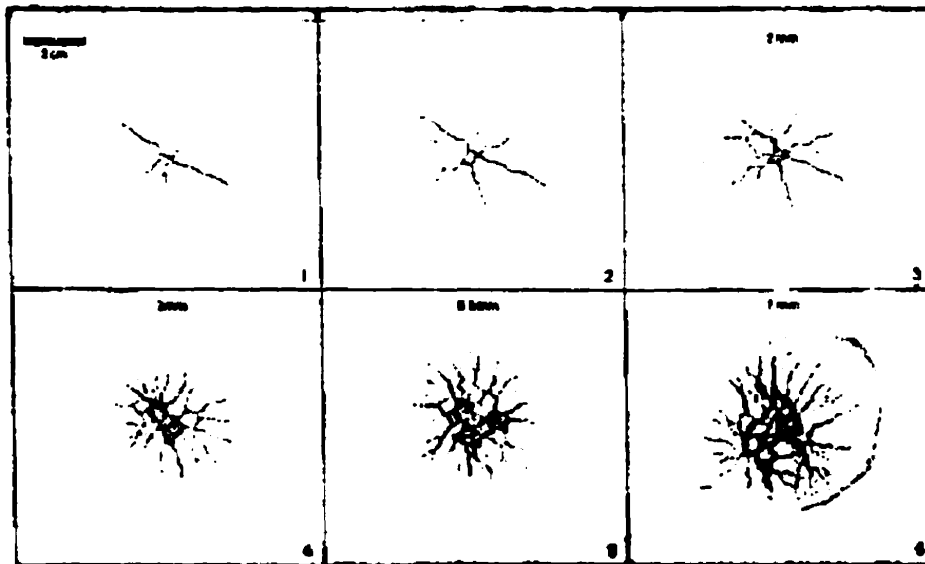


Figure 18. Doming experiments inducing collapse (Komuro, 1984).

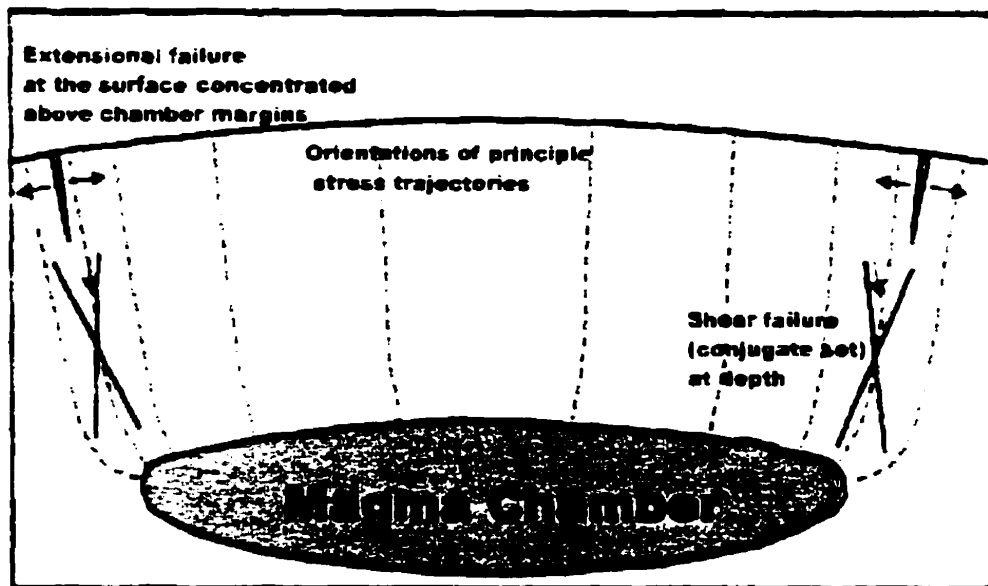


Figure 19. Principle stress trajectories at a recently intruded and overpressured, shallow sill-like magma chamber. These trajectories run orthogonal to the free surfaces, which are represented by the magma chamber and the surface. Faults will form where these principal stress trajectories are closest together, which is situated above the margins of the magma chamber (Gudmundsson, 1997). These principal stress trajectories cause tension at the surface and form a conjugate shear set which can produce either inward or outward dipping faults at depth.

Fernandina and Isabella calderas. Galapagos Islands (Chadwick and Dieterich, 1995) (Fig. 20a). Cone sheets are beautifully preserved in Gran Canaria, Canary Islands (Schirnack et al., 1999) (Fig. 20b) and Volcan Alcedo, Galapagos Islands (Fig. 20c). Cone sheets also are common at eroded igneous ring complexes as seen in many of the Tertiary Northwest Scottish intrusions. The radial fissures and the cone sheets and /or vertical ring dykes seen on the Galapagos volcanoes may be due to magma pressure from a flat-topped magma chamber which is not necessarily the result of precursory tumescence but instead a general feature of magma pressure (Anderson, 1936; Chadwick and Dieterich, 1995).

Very rapid extension may result in classic graben formation (Fig. 21c) with less doming. Evidence for this is illustrated by the rifts seen at Toba and Snowdon (P. Kokelaar, personal communication, 1999; C. Chesner, personal communication, 2000) (Figs. 14, 15). In the case of a strong transtensional system which is often associated with caldera-forming environments, the beginnings of pull-apart basin structures may form oblique to strike-slip systems. Vulcano Island, Italy, illustrates this tectonic regime (Ventura, 1994) (Fig. 16).

Structural evidence for precursory doming is often absent at calderas (Lipman, 1997); this implies that a passive intrusion may be common, or that precursory tumescence evidence is lost due to later deformation episodes. Passive intrusion of the pluton will result in only limited thermal doming, without substantial fracturing of the surface; stratigraphy may dip away from the center of the intrusion. The only evidence for this would be in the uplift and erosional history of the area. From the sedimentary

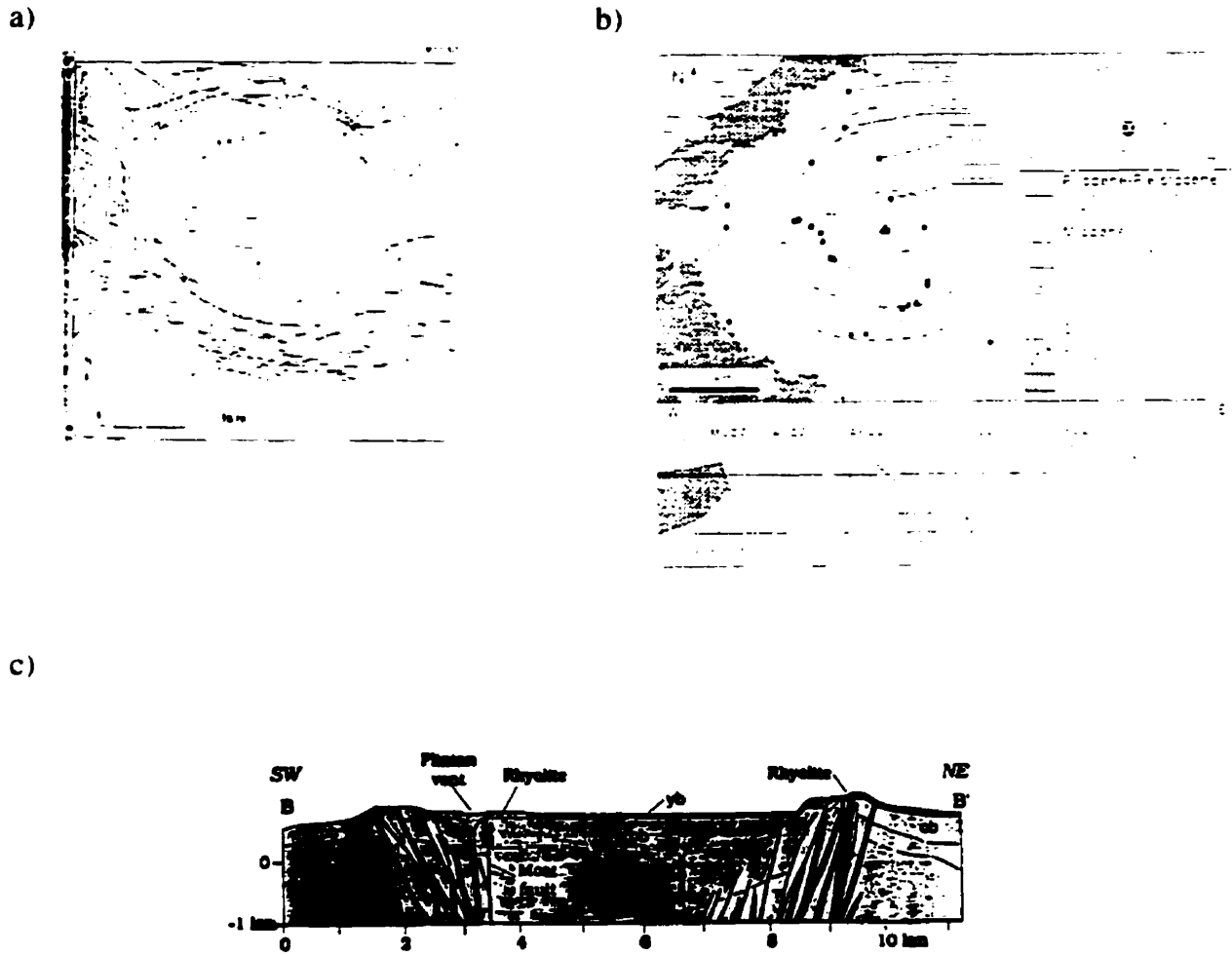
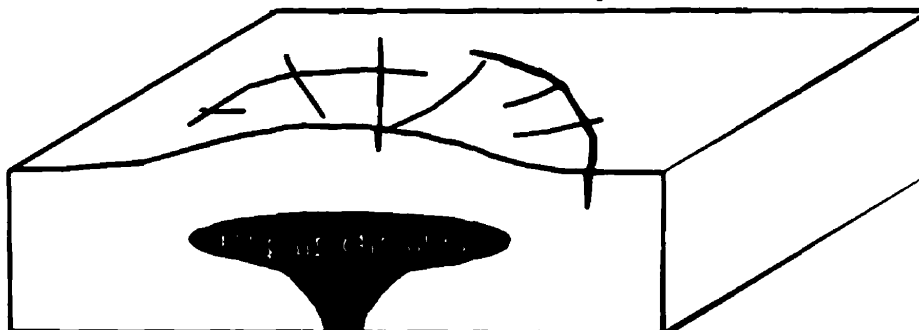


Figure 20. Cone sheets, ring dykes and radial dykes. a) Volcan Fernandina, Galapagos Islands (Chadwick and Howard, 1991). b) Gran Canaria, Canary Islands (Schirnack et al., 1999). c) Volcan Alcedo, Galapagos Islands (Geist et al., 1994).

a)

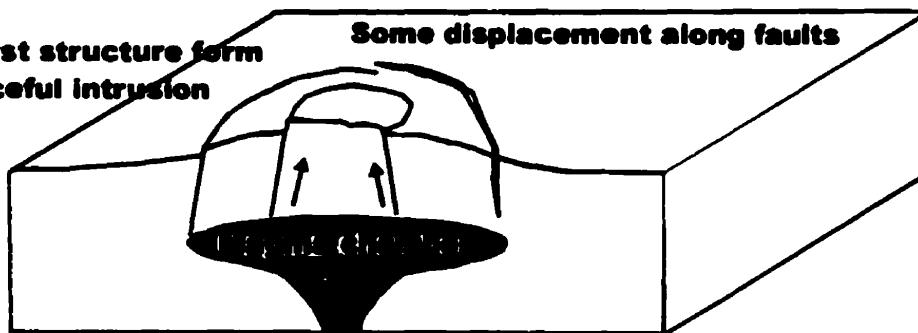
Radial and concentric fractures no fault displacement



b)

Horst structure form forceful intrusion

Some displacement along faults



c)

Rifting with curvi-linear normal faults

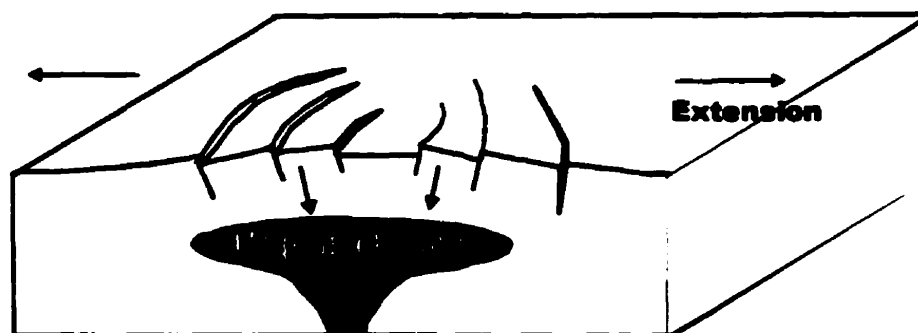


Figure 21. Possible scenarios after magma chamber intrusion but prior to eruption. a) Doming with radial and concentric fractures. b) Block faulting uplift. c) Rifting.

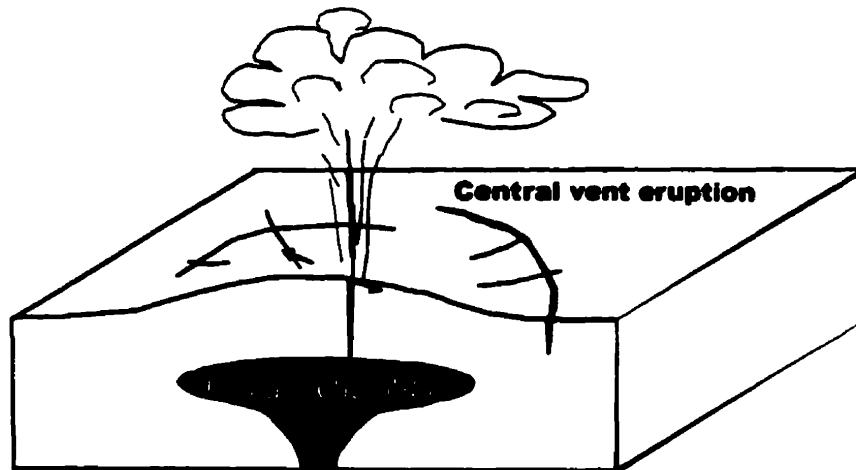
record unconformities could reveal details of uplift and erosion; sedimentation rates also can be used to determine uplift and erosion rates.

Stage 2. Initial eruption and chamber evacuation.

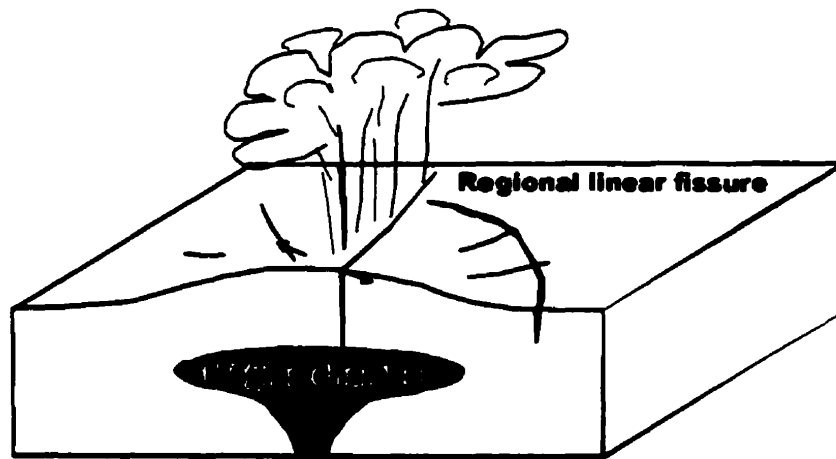
Maximum overpressure is reached within the chamber before the initial eruption. If fractures produced during intrusion penetrate from the surface down to the magma chamber, they will be used for the initial eruption. If overpressures exceed the tensile strength of the rock, new fractures can be created which will propagate up from the edges of the magma chamber. These initial fractures will form as a result of the orientation and concentration of the principal stresses (Fig. 19). Overpressures within the chamber are likely to exploit preferentially-oriented weaknesses or fractures in the crust, forming a conduit that runs from the magma chamber to the surface (Fig. 22). Initial eruptions from Ishizuchi cauldron, Japan, occurred along fissures parallel to the principal regional compressional stress (Yoshida, 1984) (Fig. 7). At Crater Lake, Cascades, U.S.A. there is evidence for a single vent phase before a ring vent eruption phase (Bacon, 1983).

The initial eruption is likely to continue only so long as conduits are kept open by magma pressure. Once pressure is reduced to lithostatic at the top of the chamber, conduits will close and eruptions will stop (McLeod, 1999). Therefore, only limited eruption volumes appear to be possible at this overpressured stage (Druitt and Sparks, 1984; Gudmundsson, 1998). Several calderas show evidence for an initial small-volume plinian eruption before large-volume pyroclastic flow eruptions occur. The caldera forming events at Valles caldera show the plinian fallout unit from the Lower Bandelier Tuff has a volume of only 20 km^3 (Dense Rock Equivalent, DRE) compared to 400 km^3

a)



b)



c)

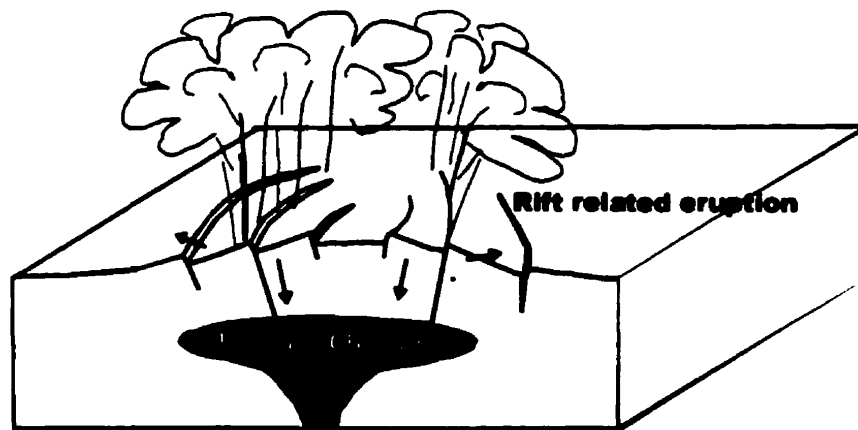


Figure 22. Possible scenarios for the initial plinian stage of a caldera-forming eruption.
a) Central vent eruption. b) Regional fissure eruption. c) Rift-related eruption.

DRE of pyroclastic flows. The upper Bandelier Tuff consists of 15 km³ DRE of plinian fall and 250 km³ DRE of pyroclastic flows (Self and Lipman, 1989).

This initial plinian stage may not occur if magma viscosities are low, as in the case of most basaltic calderas, or if vent geometries are not appropriate. If the magma in the chamber is allowed to degas, then high overpressures may never develop, and this initial plinian stage may not occur. An initial plinian phase was not seen at the relatively small caldera-forming event at Mount Pinatubo, Philippines, in 1991 (Gerlach and Westrich, 1992).

Stage 3. Downsagging and the onset of subsidence

Unless there was substantial extension during the early stages, faults will not have developed sufficiently for instantaneous failure. A period of bending and sagging of the caldera roof will help propagate tensional fractures downward and shear fractures upward (Fig. 23). This early stage of surface downsagging is clearly seen in experimental models (Marti et al., 1994; Roche et al., 2000; this thesis). An initial period of downsagging-dominated subsidence was seen before ring faults became active at Grizzly Peak caldera, Colorado (Fridrich et al., 1991). Many calderas show inward-tilted beds, especially at early stages, which are a direct result of downsagging (Walker, 1984). If these fracture sets never fully develop, a downsag-style caldera develops. Taupo caldera, New Zealand, has been interpreted as such a downsag caldera (Walker, 1984) (Fig. 8b). Scaled models show that a ring fault will develop on one side first, producing initially asymmetric subsidence; some magma chamber roof aspect ratios will promote this more than others

(Burov and Guillou-Frottier, 1999; Roche et al., 2000; this thesis). This initial asymmetric subsidence will be exaggerated by any heterogeneities in magma chamber geometry or crustal strength. If the initial conduit is near to vertical and located close to the chamber margins, it also may be used for subsidence at this stage. This is seen at Ishizuchi cauldron, Japan, where sections of the initial eruptive fissures were interpreted to control the initial period of subsidence (Yoshida, 1984) (Fig. 7).

This bending period also will result in the rotation of tensional fractures or normal faults formed by tumescence. The sags at the surface and at the chamber roof also will change the orientation of the principal stress trajectories (Fig. 23). Rotation will cause inward dipping fracture to be rotated towards the vertical, which is a more favourable orientation for subsidence (Fig. 23). Depending on the amount of rotation caused by sagging and the original orientation of the fractures, some features produced by tumescence could be re-used during the various stages of subsidence.

The orientation of the initial fault, which controls subsidence, will depend on the presence or absence of a superimposed stress regime. In the absence of a superimposed stress regime, the fault is likely to be outward dipping (Roche et al., 2000). This fault will allow further eruption, since the geometry of this fault favors large volumes to be erupted at this stage. For example, the motion of the subsiding block will keep this fault or conduit open even when the pressure in the magma chamber drops below lithostatic (Fig. 24).

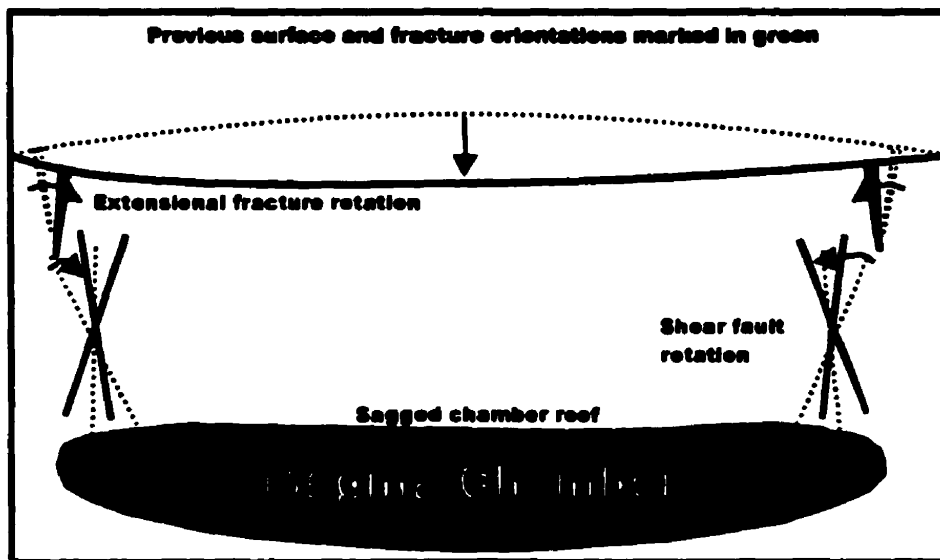


Figure 23. A schematic view of downsagging. New shear faults begin to form at depth, and sagging at the surface causes extension at the hinges of the depression. The sagging also rotates inward dipping faults towards a vertical position.

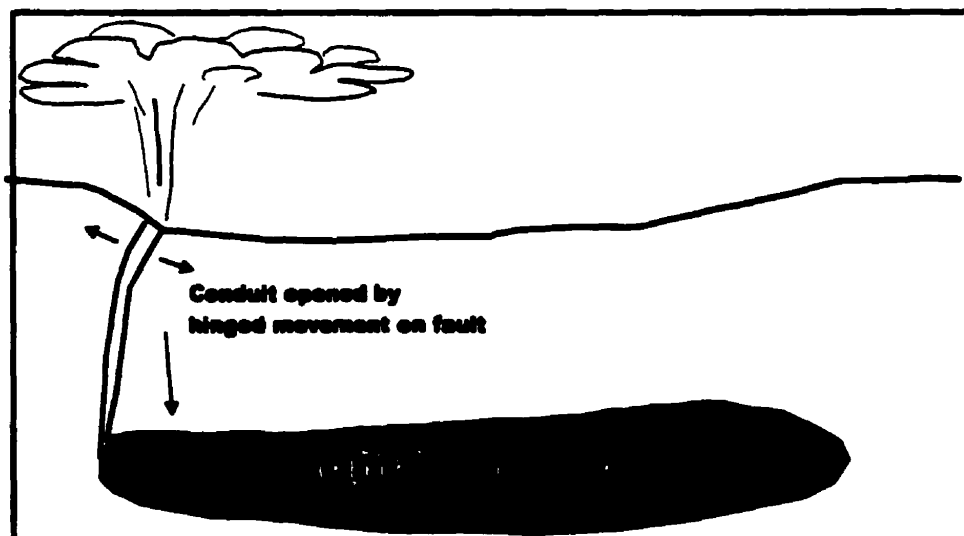


Figure 24. Initially asymmetric subsidence along an outward dipping fault, maintaining an open conduit.

If ring faults were partially formed by earlier stages of extension and intrusion, fault-controlled subsidence is possible at this early stage (Fig. 25). In this case, subsidence will be extension-controlled rather than eruption-controlled due to the space problem created by inward dipping fractures. This results in an inward dipping piston-type caldera, e.g., Kilauea caldera, Hawaii. If well developed regional faults suitable for subsidence exist, they also can be used at this stage without the need for sagging. Use of such faults can be seen in the early stages in the development of Glencoe caldera, Scotland, which is a tectonically-controlled piecemeal caldera (Moore and Kokelaar, 1998).

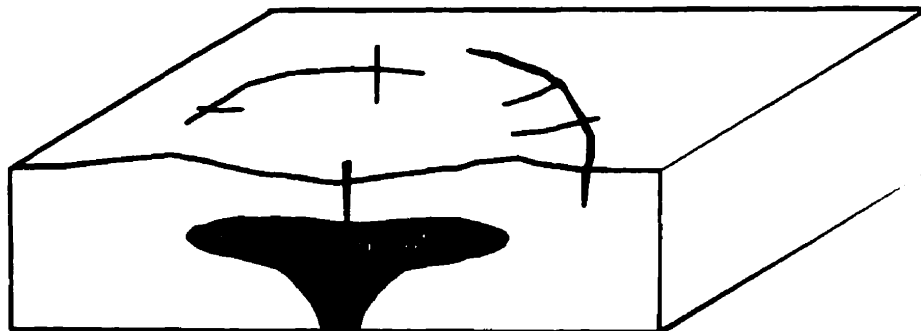
Stage 4. Main subsidence and eruption phase.

The initial subsidence-controlling fault and the nature of the movement upon this structure is likely to significantly alter the stress field associated with the chamber. Movement on this fault will increase the bending on the opposite side of the caldera, promoting tensional failures and normal faulting (Fig. 26). Experimental studies support this idea (Odonne et al., 1999; Roche et al., 2000; this thesis) (Fig. 26). Initial subsidence upon an inward dipping fault, without sufficient extension, may result in a outward dipping fault forming on the opposite side, as seen at Ishizuchi cauldron, Japan (Yoshida, 1984).

As subsidence continues, the initial fault will propagate laterally from the side of maximum subsidence (Roche et al., 2000; this thesis). This fault may never propagate fully to the other side, resulting in a trapdoor-style caldera (Fig.9), e.g., Silverton, Organ Mountains, Eagle Mountain, Big John, Whitehorse and Tuscan mountain calderas in the U.S., Bolsena in Central Italy and Sakugi in southwestern Japan (Lipman, 2000). In the

a)

Initial downsag from downwarping

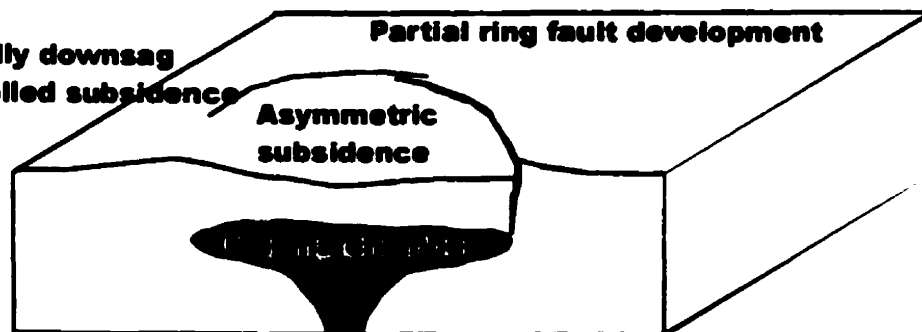


b)

Partially downsag controlled subsidence

Partial ring fault development

Asymmetric subsidence



c)

Subsidence along ring faults



Figure 25. Possible scenarios for the style of initial subsidence.

a) Downsagging-controlled subsidence. b) Trapdoor subsidence. c) Ring fault subsidence.

case of Snowdon caldera, a trapdoor-style collapse was complicated by linear rift related faults producing a piano key-style caldera (P. Kokelaar, personal communication, 1999) (Fig. 15). Subsidence occurred along both the rift-related faults and a trapdoor-style partial ring fault.

Faults may have begun developing on the opposite side of the caldera due to the asymmetric subsidence. These faults may eventually join up to produce a coherent piston, e.g., Grizzly Peak, Bachelor, Stillwater range in the U.S. (Lipman, 2000) and many calderas in northern Honshu, Japan, e.g., Ishizuchi cauldron (Yoshida, 1984) (Fig. 7).

The orientation of these faults and the way in which they propagate and join up will depend mainly on the following factors. (1) The external stress field can control the transition from inward dipping piston-style collapse to outward dipping piston-style collapse or the development of pull-apart basin-type calderas, e.g., Vulcano Island, Italy (Ventura, 1994) (Fig. 16). (2) The depth and diameter of the magma chamber (aspect ratio of the roof) can control the transition from outward dipping piston collapse to chaotic-type collapse (Figs. 11-13). (3) The three-dimensional symmetry of the magma chamber or brittle-ductile transition associated with the magma chamber (Burov and Guillou-Frottier, 1999; Lipman, 2000; Roche et al., 2000) may control the symmetry of collapse and could cause trapdoor-style subsidence. A magma chamber with an irregular upper surface could result in a complex piecemeal-style caldera (Fig. 17). Other factors that are likely to affect the details of how these faults develop are (1) pre-existing structures, faults, folds, metamorphic grain and topography; (2) lateral and vertical

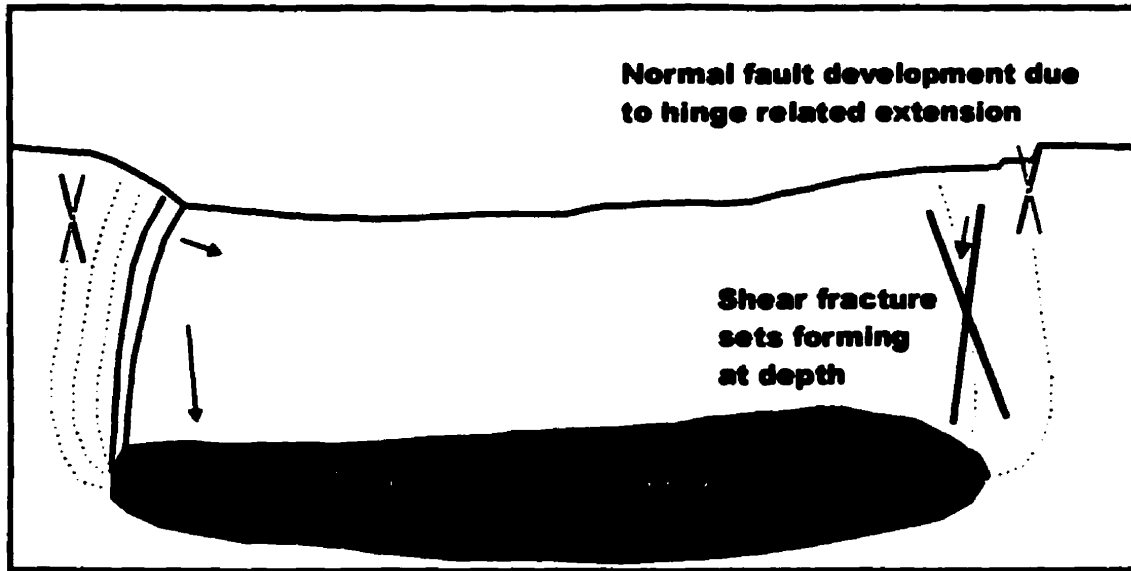


Figure 26. Fault development and propagation according to stress trajectories

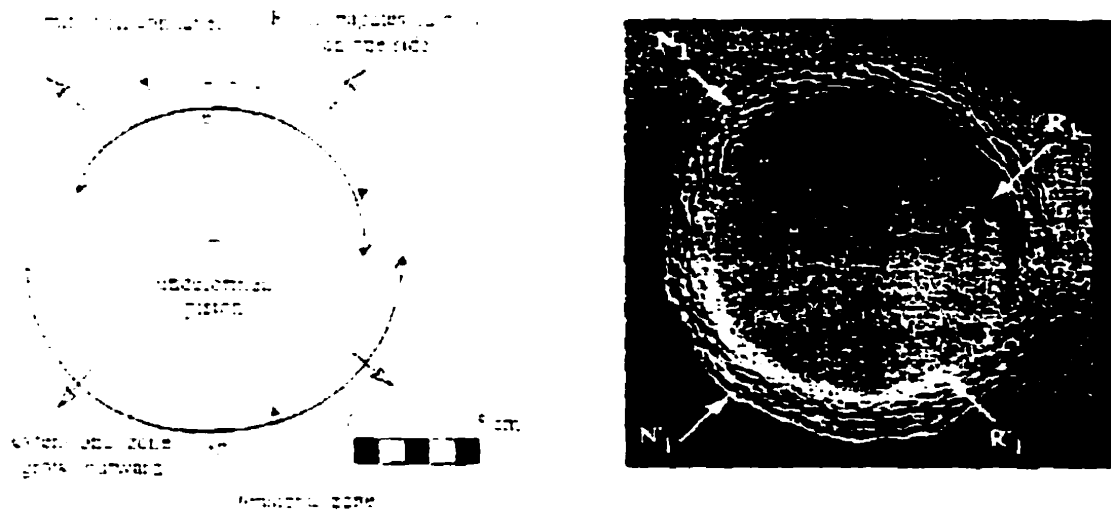


Figure 27. Early fault development as illustrated by scaled experimental studies (Roche et al., 2000).

variations in the tensile strength of the rocks that comprise the subsiding block. e.g., hydrothermally-weakened areas which are common in volcanic terrains; (3) the position of the erupted ignimbrite sheets within the caldera, which add load to the subsiding block. These factors will promote deviation from the classic model, and interactions of many of these factors will result in a complex mix of caldera types. Caldera faults may develop as a series of linear faults which connect to form distinct corners, as in the polygonal style (Fig. 6), rather than a continuous ring as in the piston styles (Figs. 3-5).

Stage 5. Eruption quiescence and peripheral extension.

As the main subsidence-controlling faults develop, outer faults also grow which are related to extension caused by the subsidence (Walker, 1984; Branney, 1995; Roche et al., 2000; this thesis). These faults are thus a response to the main caldera faults located in more central regions of the caldera. The faults may form along tensional fractures that were created during bending from either tumescence or downsagging. The steep fault scarps produced by the main subsidence phase will be subject to failure. These fault scarps will be further steepened by peripheral downsagging and extension. Large megabreccia blocks may slide into the caldera at this stage (Lipman, 1997). The same forces that are responsible for these slide blocks also will produce peripheral normal faulting in the region outside the main subsidence area (Fig. 28). Arcuate crevasses also may form related to slide blocks (Branney, 1995). Peripheral graben and normal faulting may form in areas where no clear subsidence-controlling fault has formed, and bending is at a maximum (Fig. 29). These structures are well exposed at Scafell caldera, England, and Snowdon caldera, Wales (Branney, 1995; Kokelaar and Branney, 1999).

28.

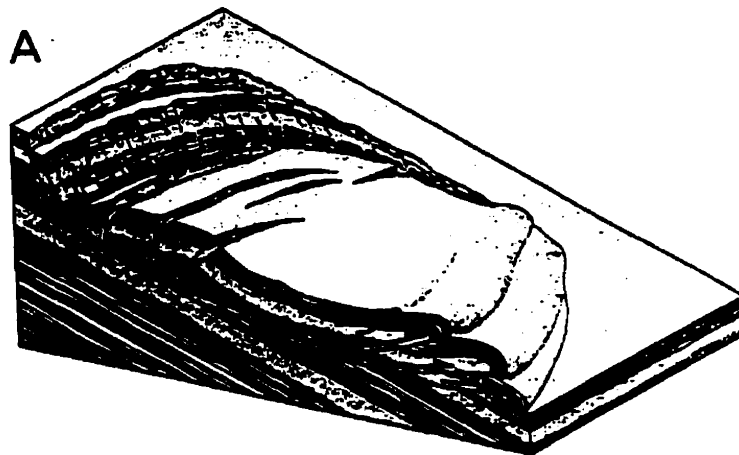


Figure 28. A simple down-slope gravity slide showing normal fault, thrust fault and crevasse formation (Branney and Kokelaar, 1999).

29.

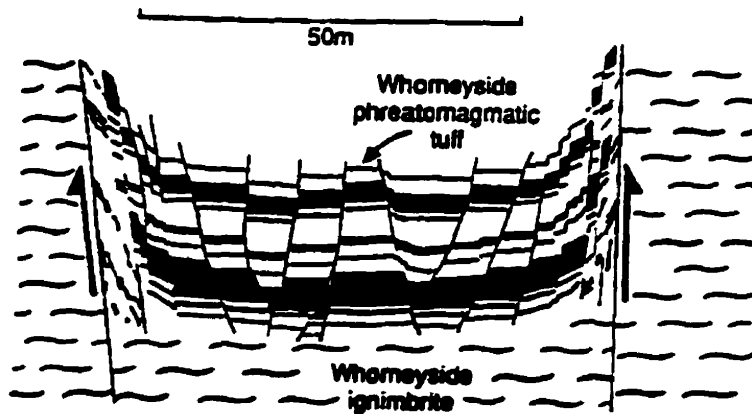


Figure 29. Graben structures in Whomeyside phreatomagmatic tuff: the graben formed peripheral to a subsiding basin, Scafell caldera, England, (Branney and Kokelaar, 1999).

At Suswa volcano, Gregory Rift, Kenya, both inner and outer ring fractures are seen (Skilling, 1993). Collapse occurred on the inner ring fault, whilst eruptions proceeded on the outer ring fractures. However, both the outer and inner ring faults at Suswa are inward dipping (Skilling, 1993). A coupled relationship may exist between the inner subsidence-controlling faults and the outer extensional faults. The faults may form as a result of a conjugate shear set related to subsidence (Fig. 26). Movement on the outer faults may push and close any conduits that are still open on the inner faults (Fig. 30). This process may promote eruptions from outer faults; alternatively a pressure buildup would be required to reopen the inner eruption conduit and prolong the eruption.

Stage 6. Continued eruption, subsidence and change of eruptive style.

Many calderas show multiple collapse and eruption episodes within a single caldera forming cycle, e.g., the British calderas Scafell, Glencoe and Snowdon. This could be due to a post-collapse increase in chamber pressure that further drives eruptions and allows continued collapse. A possible mechanism for increasing pressure within the chamber above lithostatic is by exsolution of volatiles. After collapse the magma chamber is likely to be still underpressured (less than lithostatic) due to the buoyancy effects of magma (McLeod, 1999). Due to this underpressure, the magma will be rapidly vesiculating, and the gas produced by the bubbles will exert a pressure. A suitably oversaturated magma may be able to produce bubbles sufficiently fast to overpressure the chamber, reopen conduits and drive further eruptions. Continued removal of material from the chamber also will cause continued collapse of the caldera.

30.

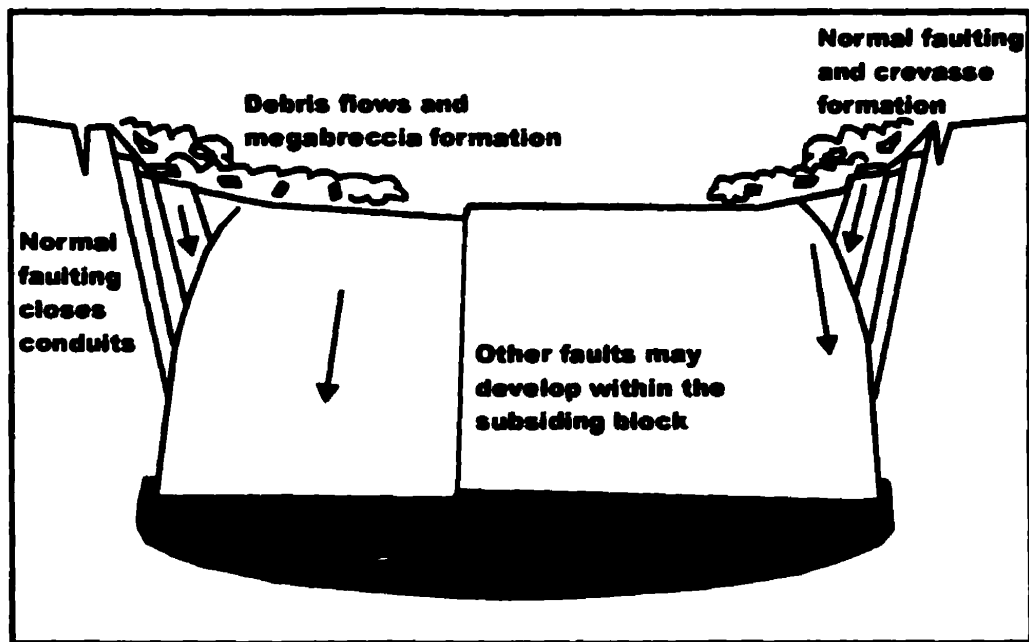


Figure 30. Late-stage peripheral downsagging, continued normal faulting, megabreccia and crevasse formation.

Further eruptions could be driven by magma interactions with groundwater or water in a caldera lake. This may have occurred at Ilopango caldera, El Salvador (J. Vallance, personal communication, 2000). Alternatively, renewed influxes of magma into the chamber and magma mixing may promote continued eruption. In these cases, it is likely that the subsidence-controlling faults will reactivate, and peripheral extension features will continue to form. Eruptions again will cease when the conduit closes, and the pressure at the top of the chamber returns to lithostatic. Collapse also can be continued by magma withdrawal away from the chamber, with little solid material erupted, e.g., Fernandina, Galapagos (Chadwick and Dieterich, 1995). Loading from intrusions and cumulates may have caused progressive collapse of the Hawaiian calderas (Walker, 1988).

The eruption-collapse sequence may repeat itself several times if gas concentrations in the magma remain sufficiently high after a second pulse of eruption and collapse. Vesiculation will again increase the pressure in the magma chamber. Overpressures can therefore be developed that further drive eruptions and result in further subsidence events. Longer periods of time will exist between these eruption and subsidence events as the magma becomes progressively degassed. As dissolved gas concentrations decrease in the magma, it will become progressively more difficult to diffuse gas from magma into bubbles, since diffusion times increase significantly as magma is dewatered (Watson, 1994).

Eruption events also may become progressively less explosive due to magma degassing, and the eruptive style can shift from explosive to effusive. This shift is observed at many calderas; for example, lava domes and lava flows were extruded soon after the main pyroclastic phase of eruption at many caldera-forming eruptions. At Long Valley caldera, California, large volumes of rhyolite lava flows were erupted within 100,000 years of collapse (Bailey, 1976). These vents are likely the same as those used for the pyroclastic eruptions. A similar shift is observed after the most recent caldera collapse event at Yellowstone caldera, where large volumes of rhyolite lavas were erupted after ignimbrite eruptions (Christansen, 1984). The accumulation of these lava flows often will produce a topographic high within the caldera that should not be confused with the resurgent dome (Fig. 31).

Stage 7. Resurgence and dome and flow extrusion.

Smith and Bailey (1968) proposed that resurgence is a critical part of the caldera-forming process and that it could be attributed to a renewed rise of magma beneath the subsiding block, regional detumescence, magmatic rebound, or magmatic convection and vesiculation. Marsh (1984) indicates that the timescale of magmatic rebound is too short to be relevant to resurgence and prefers regional detumescence as the main mechanism for resurgence.

Resurgent domes have different characteristics; they may form a broad structural dome (Smith and Bailey, 1968), re-activate subsidence or regional faults (Acocella and Funicello, 1999), produce new structures such as radial faults and central horst and

graben structures (McConnell et al., 1995) or a combination of these. When resurgence occurs, the block above the magma chamber has been broken up by faults related to collapse. These faults may be used as conduits to allow smaller, shallow intrusions to form above the main magma chamber; associated with these intrusions will be faulting, structural uplift and extension. This renewed influx does not usually reactivate subsidence-controlling faults, as might be expected and as experimental models would predict (Marti, 1994). However, it is unlikely that resurgence is a simple re-inflation of the magma chamber, but rather an upward intrusion and stoping of particular areas of the chamber. At Okueyama volcano-plutonic center, southwest Japan, resurgence as a result of stoping caused volcanic rocks to be intruded by the resurgent batholith, with no evidence for lateral pushing (Takahashi, 1986). Basement rock xenoliths are also common in the upper parts of the pluton and represent evidence for engulfment. At Long Valley caldera, the intrusion of 300 m of sills above the main magma chamber in early post-caldera time has been proposed to explain the resurgent uplift (McConnell et al., 1995).

New sets of extensional faults appear to form at the surface, often with a preferred linear orientation related to a regional stress field as seen at Long Valley caldera, California, Toba caldera, Northern Sumatra, and Valles caldera, New Mexico. Radial patterns also are seen at Timber Mountain caldera, Nevada (Smith and Bailey, 1968) (Fig. 32a), and to some extent at Valles (Fig. 32b); these patterns have similarities to doming experiments under an external extensional stress field (Withjack and Scheiner 1982) (Fig. 32d). At Toba caldera, northern Sumatra, precursory rift structures appear to be reactivated. Perhaps one reason that subsidence structures are rarely reactivated by

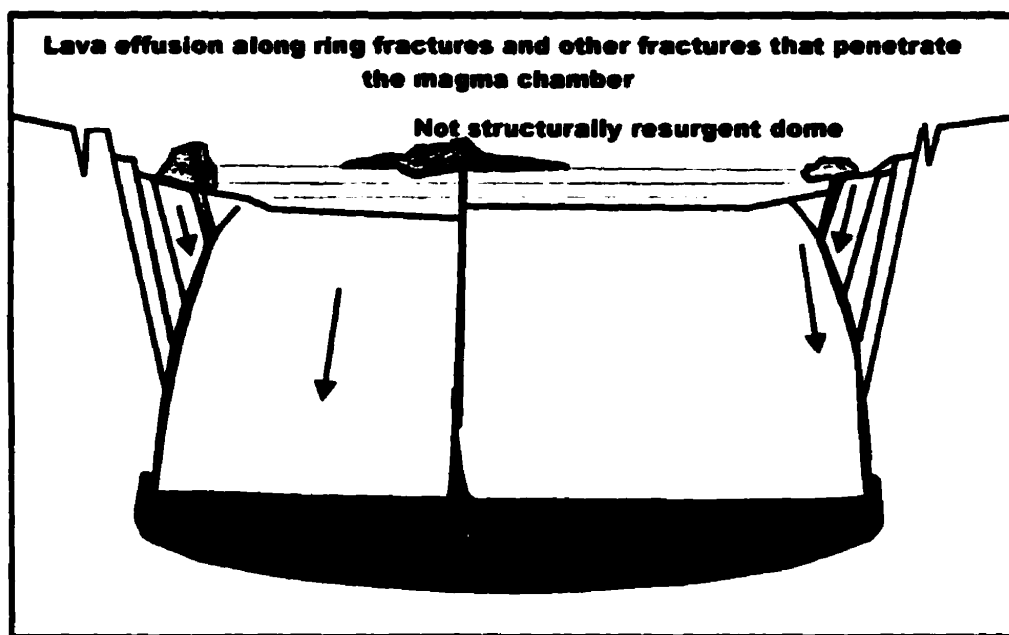


Figure 31. Pre-resurgence lava effusion along ring fractures and other conduits.

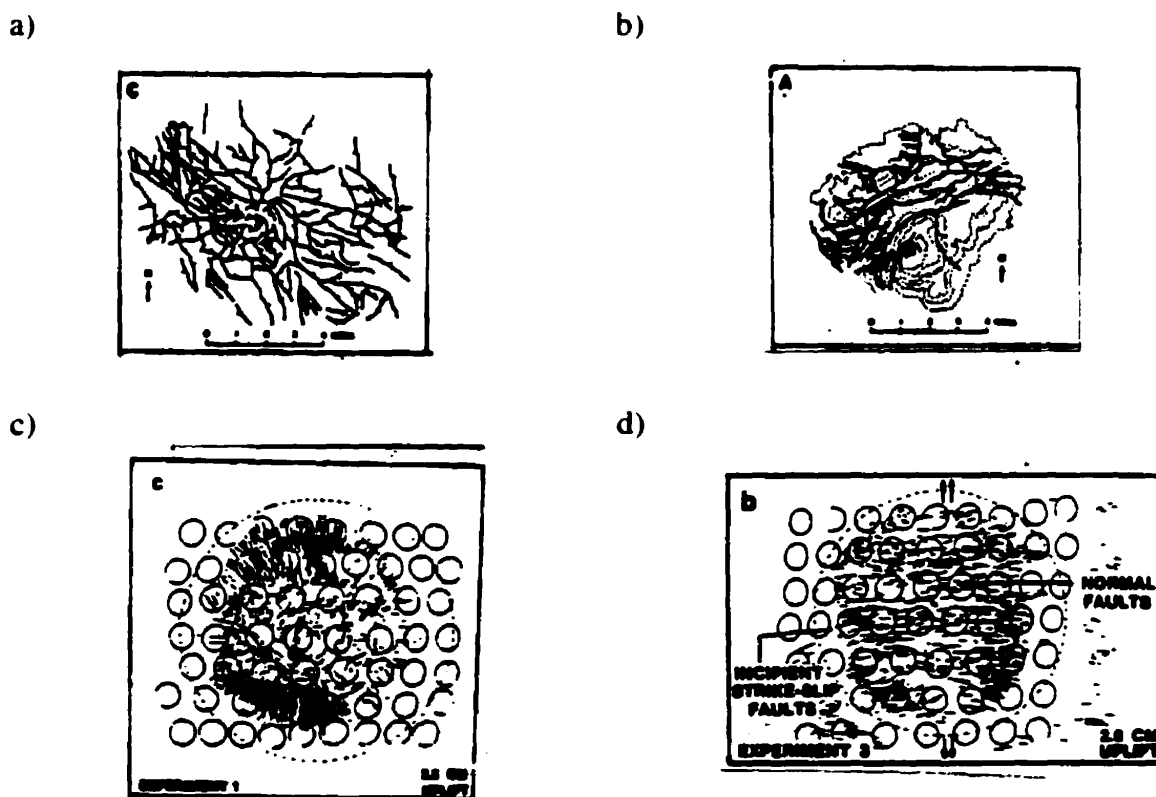


Figure 32. Comparison between experimental doming and resurgence. a) The Timber Mountain resurgent dome (Smith and Bailey, 1968) b) the Valles resurgent dome (Smith and Bailey, 1968) c) Experimental doming without extension and d) experimental doming with extension (Withjack and Scheiner, 1982).

resurgence is because they have become “sealed” or “stitched” by minor intrusions, such as ring dykes and cone sheets. Resurgent doming on the island of Ischia, Italy, has been strongly linked to the regional tectonics of the area where pre-existing normal faults were reactivated during resurgence (Acocella and Funiciello, 1999).

Effusive events often occur after the main period of resurgence and after a period of eruptive quiescence. These effusive events often are seen in the moat area of the caldera between the resurgent dome and the topographic boundary, as at Long Valley and Valles calderas (Fig. 33). The distribution of these moat domes has been interpreted to mark a ring fracture (subsidence controlling faults) (Smith and Bailey, 1968). In theory, domes would be extruded in areas of extension where faults penetrate to the magma chamber, e.g., the peripheral extension outside and concentric to the subsidence-controlling faults (Fig. 34). The main subsidence-controlling faults are likely to be in an area of compression and may be sealed or stitched by minor intrusions. Therefore, the interpretation that post-collapse domes and vents mark the main subsidence-controlling ring fault (Smith and Bailey, 1968) may not always be correct. These domes and vents instead may form in the area peripheral to the main subsidence-controlling fault (Fig. 34). Another preferential location for extrusions is along regional extensional and transtensional fissures (Walker, 1984). Where regional structures intersect the resurgent dome, effusive eruptive vents may form, as at Long Valley caldera. It is perhaps surprising that domes are rarely extruded along faults formed by the resurgent dome: perhaps these do not penetrate sufficiently deep to reach the chamber (Fig. 34).

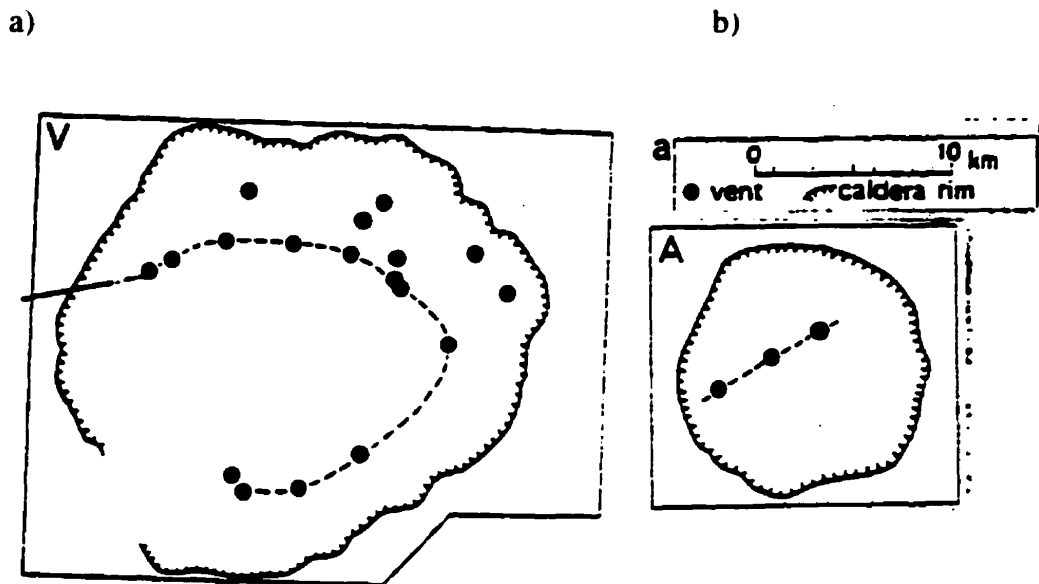


Figure 33 a). Location of post collapse domes at Valles caldera, New Mexico from. b) Location of post collapse domes at caldera, New Mexico (Walker, 1984)

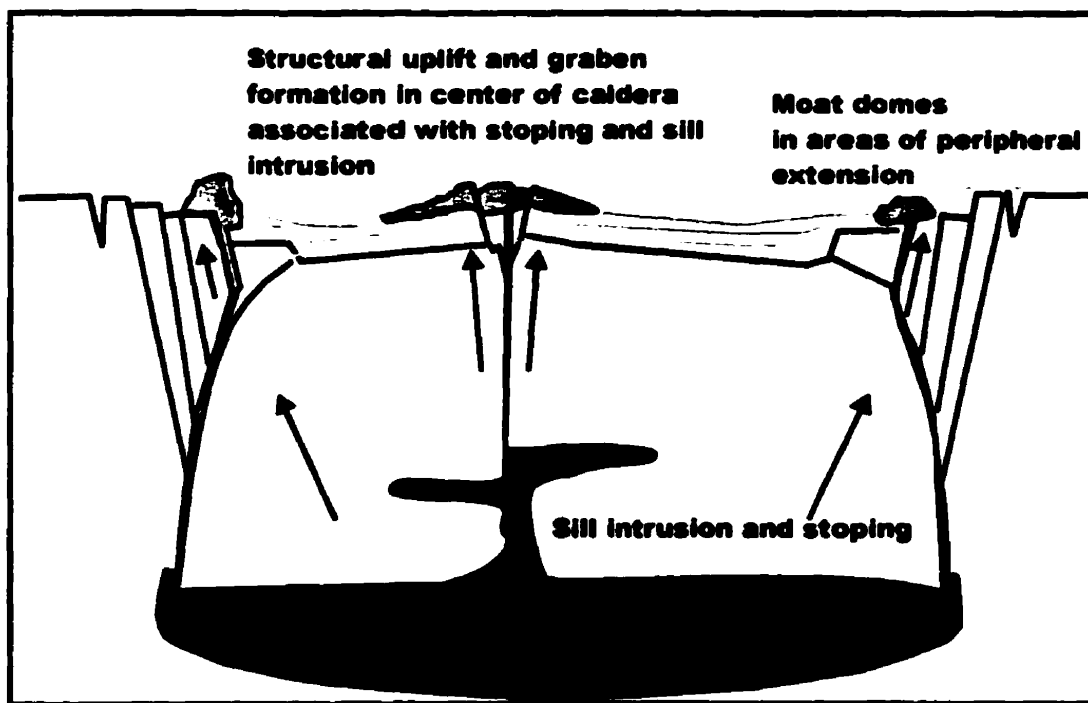


Figure 34. Structural resurgence of the caldera, forming a broad central dome. Magma chamber stoping and shallow intrusion may produce localised uplift and graben formation. The ring faults may also be reactivated during resurgence, this may cause peripheral uplift.

CHAPTER 2

AN EXPERIMENTAL STUDY OF CALDERA FORMATION

General Statement

This experimental study concentrates on only four of the many variables in the caldera process, and investigates the effects of changing these variables on caldera morphology. The four variables chosen are the depth of the magma chamber, pre-existing topography above the magma chamber, chamber pressure and chamber orientation. The depth of the magma chamber was chosen to confirm ideas and mechanisms proposed by Marti et al. (1994) and Roche et al. (2000). The effect of pre-existing topography has not been considered previously at calderas, although Burov and Guillou-Frottier (1999) illustrate the importance of the loading caused by emplacement of intracaldera ignimbrite on deformation of the subsiding block. Calderas often form in regions of high relief. The loading effect of this relief and its influence on principal stress trajectories likely influences surface deformation. The effects of magma chamber pressure have been discussed theoretically (Lipman, 1997; 2000) but require experimental confirmation. Lastly, the orientation of the magma chamber may affect the symmetry of subsidence (Lipman, 1997; 2000). Our study used a scaled three-dimensional physical model to investigate these variables. We place emphasis on the relationship between deformation of the magma chamber and the resultant deformation on the surface (the caldera).

Methodology

Experimental setup

The apparatus comprised a cylinder 0.90 m in diameter and 1 m in height (Fig. 35). The cylinder was filled with unsorted dry sand. Buried within the sand was a 60 cm-diameter rubber bladder filled with water to a maximum capacity of 45 liters. The shape

of the bladder was circular in plan view, with a convex upper and lower surface, so that it had the shape of an oblate or flattened sphere. When the bladder was near its maximum capacity, it deformed elastically maintaining its overall shape. At lower capacities the bladder deformed differently, with the upper surface of the bladder flattening. These different deformation mechanisms represent the elastic behavior of the crust followed by brittle failure. As only 17.7 % of the volume of the bladder was removed, the bladder never became wrinkled.

The bladder could be filled and evacuated from a tube attached centrally to its underside. The evacuation and injection of water into and out of the bladder was controlled and measured by a flowmeter. In the experiments the bladder was evacuated at a constant flow rate of $1600 \text{ cm}^3 \text{ min}^{-1}$ over a period of 5 minutes, resulting in evacuation of 8000 cm^3 , representing 17.7 % of the total volume. This value is similar to the 10 % chamber evacuation conservatively estimated by compositional gradient studies (Smith, 1979) and produced calderas of realistic proportions.

The depth, volume and orientation of the bladder could be varied, as well as the surface relief. The depth of the bladder was varied between 6.0 and 24 cm. As the width of the magma chamber was constant, changing the depth could be treated as changing the aspect ratio (thickness/width) of the subsiding block. However, the convex nature of the bladder roof prevented these aspect ratios from being compared directly with previous experiments which used flat chamber roofs (e.g., Roche et al., 2000). Aspect ratios in our experiments varied from about 0.10 to 0.40; these values are minimums, as the roof thickness was a minimum depth measured from the surface to the top of the convex bladder. The maximum bladder depth was 10 cm greater at the margins of the bladder, giving maximum aspect ratios of 0.27 to 0.57.

Pre-existing topography was created by building scaled stratocones, ridges and mountain ranges of sand and placing them in different locations and orientations above the bladder. A mass of 1 kg of sand was used to produce a 16 cm-diameter and 6 cm-high stratocone, 1 kg for the 30 cm-long, 13 cm-wide and 4.3 cm-high ridge, and 5.7 kg for a 58 cm-long, 23 cm-wide and 5 cm-high mountain range.

The volume of the bladder before evacuation was measured by weight (1 liter of water = 1 kg) using a simple spring scale. We used two volumes in the experiments, 45 and 40 liters. By changing the volume of the bladder, we changed its internal pressure. The larger volume simulated collapse into an overpressured, closed-system magma chamber, while the smaller volume represented an open-system magma chamber with little overpressure. Pressure within a closed magma chamber will build up and then be released after eruption: this release of pressure may cause elastic contraction of the crust. This effect will not be seen in a more open system.

The bladder could be tilted to simulate a magma chamber which was higher in one area than another, in order to test ideas about asymmetric collapse (Lipman, 1997). The orientation and minimum depth of the bladder was monitored using a dipstick and grid (Fig. 36). This allowed the bladder orientation to be kept constant when the depth, volume or topography was being varied. The same method was used to measure the relief of the caldera and the magma chamber after the collapse. Depths were measured every 5 cm on the x and y axes, except where the topography was complex, in which case depths were measured every 2.5 cm.

Two lasers were positioned at right angles to each other and inclined at an angle of 30.5 degrees from the horizontal to produce lines that formed a cross on the planar

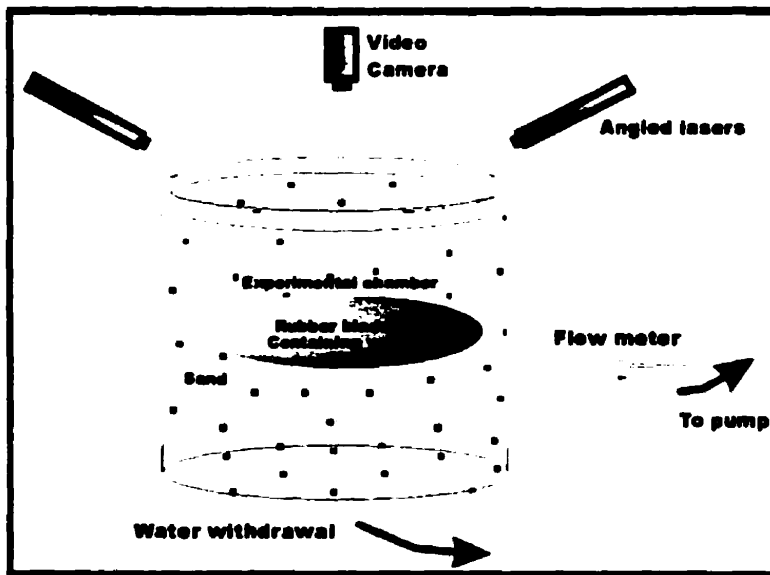


Figure 35. Experimental setup, with camera mounted on ladder above cylinder containing sand.



Figure 36. Verification of surface and magma chamber morphology using a dipstick and grid.

surface of the sand. The lasers were calibrated to measure changes in surface relief during the experiments. A 1 cm change in relief was represented by a lateral displacement of 1.8 cm of the laser line. These displacements therefore could be used to measure temporal changes of surface deformation.

The experiments were recorded by a video camera positioned above the center of the experimental caldera and perpendicular to the surface of the sand. To allow surface features to be highlighted on the video image, low-angle lighting was used to produce fault scarp shadows. This lighting made it difficult to see the laser lines; for this reason, the lighting was turned off every 8 seconds for a duration of 2 seconds, to allow a laser measurement to be recorded on the video image.

Before each experiment, the bladder was refilled, weighed and repositioned within the sand, taking care with the dipstick and grid that the bladder was symmetrically positioned. To achieve repeatable results, care was taken to accurately position the bladder, since it would shift in position in the sand after evacuation and refilling. Before an experiment, the sand would be stirred evenly to remove all structures produced from the previous experiment. Care also was required in maintaining a consistently level and smooth sand surface, as well as maintaining uniform compaction of the sand beneath. The laser lines were calibrated by measuring their displacements on blocks of known thickness. The lighting, timer and evacuation were started simultaneously. The flow rate was monitored continuously during the five-minute evacuation. During the evacuation, detailed observations were made that could not be seen on the video image. The resultant experimental caldera was then sketched, described and measured in cross section and plan view. For selected experiments, volumes of the calderas were calculated by two different techniques for redundancy. The X, Y and Z coordinates of the calderas were used to calculate volumes using the computer program Surfer. These results were

confirmed by gradually filling the caldera with a known volume of sand. The results of the two techniques agreed to within 3 %. Each experiment was repeated three or four times producing similar results. The most representative experiment was then chosen for detailed analysis.

The volume evacuated from the chamber was greater than the volume of the caldera. A volume of 8000 cm³ of water was removed from the bladder in every experiment, while caldera volumes varied from 6140 to 3880 cm³. These large differences result from sand being dilatant during evacuation, causing substantial increases in porosity.

Scaling of variables

For an analogue model to represent reality, certain scaling considerations are required. Both geometric and dynamic similarity is necessary between the model and nature. Ratios are used to help maintain this similarity (Sanford, 1959).

Calderas have diameters varying from more than 50 km down to 2 km (Branney, 1995). The experimental setup could be no larger than 1 m x 1 m x 1 m, due to constraints of the large weight of this volume of sand. For this reason, a 50 cm-diameter experimental caldera represents a 20 km-diameter caldera:

$$\frac{\text{Max. diameter of model}}{\text{Max. diameter of caldera}} = \frac{0.5 \text{ m}}{20,000 \text{ m}} = 2.5 \times 10^{-5}$$

A length ratio (L^*) of 2.5×10^{-5} was therefore used, allowing the analogue model to have a larger size than previous caldera models (Komuro 1984, 1987; Marti et al., 1994; Odonne et al., 1999; Roche et al., 2000). Caldera dimensions, surface topography and bladder depths were scaled using this ratio.

The scaling of crustal rock and magma to experimental materials also was determined. The densities, viscosities and cohesions of the experimental materials needed to be considered. Cohesion was scaled using the stress ratio (σ^*), which is a product of the length ratio (L^*), the gravity ratio (g^*) and the density ratio (ρ^*):

$$\sigma^* = \rho^* g^* L^* = 1.8-2.4 \times 10^{-5}$$

where the density ratio $\rho^* \cong 0.95-0.70$ (uncompacted sand used in experiments 1890 kg m^{-3} , natural rock $2000-2700 \text{ kg/m}^{-3}$) and the gravity ratio $g^* = 1$ (both experimental and natural calderas form under the same gravity conditions).

The cohesion of volcanic rock (equivalent scaling ratio to σ^*) is on the order of 10^7 Pa (10 MPa); this means that the model should have cohesion values of around 100-200 Pa. However, on a larger scale, jointing and fracturing reduce the cohesion of volcanic rock to about 10^6 Pa (Schultz, 1996), so the model should have a cohesion of 10-20 Pa. Although in theory well-sorted dry sand has no cohesion, the sand used in the experiments was poorly sorted and contained moisture absorbed from the air. Attempts were made to measure the sand cohesion using shear box tests, but it was difficult to accurately measure such low cohesion values. As a result, the sand can only be said to have a cohesion of 0-100 Pa, which is appropriate to the scaled cohesion of volcanic rock containing some fractures. As sand and rock are in theory Coulomb materials, varying timescales should not affect the deformation. Some preliminary shear box tests on the sand showed that time may in fact influence the resultant deformation in pure dry sand: this could be a result of compaction.

The time ratio is based on 5 minutes evacuation time, representing eight days for a large caldera to form in nature (Wilson and Hildreth, 1997):

$$\text{Collapse time ratio } t^* \cong \frac{300 \text{ seconds}}{8 \text{ days}} = \frac{300}{691200} = 4.34 \times 10^{-4}$$

Other scaling ratios that may need consideration are viscosity of the magma and velocity of magma evacuation. These will be important if the deformation of the sand is found to be time-dependent. A simple way to define a viscosity ratio was used:

$$\text{Viscosity ratio } (\mu^*) = t^* L^* = 10^{-8}$$

Viscosities in magmas have been calculated to vary over 16 orders of magnitude, from 10^2 Pa s for basalt to in excess of 10^{18} Pa s for anhydrous rhyolite (Hess and Dingwell, 1996); this creates a problem for scaling. A mean value of around 10^8 Pa s indicates a very low viscosity is required for the analogue model. The water in the bladder has a viscosity of less than 1 Pa s, which seems appropriate.

Relevance and Limitations

The experimental calderas that were produced can never accurately reproduce the complex process of caldera formation. However, the experiments do provide insights into the manner by which a block of homogeneous crust may deform when subsiding into a shallow oblate magma chamber. A large proportion of the structures seen at calderas is associated with this process. However, structures produced by the complex processes of magma intrusion and resurgence could not be reproduced in our experiments. Also, many calderas have undergone a complex collapse history, as represented by several caldera cycles and multiple collapse episodes within these cycles. Our experiments represent only a single collapse event. However, many aspects of the structures seen in the experiments still have relevance to these complex systems.

Our experimental model has certain restrictions. Although sand can deform in a brittle manner and has appropriate cohesion values, its granular nature allows granular flow that does not occur in rigid rocks. The granular nature of sand also produces problems of compaction. A subsiding block of sand will expand, increasing its volume and porosity, thereby changing its compaction. In a subsiding caldera, compaction effects are likely to be minor. A further problem with using a granular material is its angle of repose of 30° ; natural rock can remain stable to much higher angles. This implies that fault scarps greater than 30° cannot be created in our experiments, whereas calderas in nature frequently have scarps that are steeper.

There are also some problems with using a water-filled rubber bladder to represent a magma chamber. The rubber bladder containing the water represents a boundary that is not present in nature. This boundary prevents subsiding blocks from descending into the chamber. It also prevents upward intrusion and stoping of the magma between foundering blocks. Scaling restrictions in terms of viscosity support the use of water in the bladder to represent magma. It is also an incompressible fluid, and its physical properties appear appropriate. However, gas bubbles may exist in magma, making it partly compressible.

The recent thermomechanical model developed by Burov and Guillou-Frottier (1999) indicates the importance of intracaldera ignimbrite and the geothermal gradient on the properties of rocks around the chamber. Neither of these factors were considered in our analogue model. There are also some unresolved scaling problems related to the amount of overpressure within the chamber.

Despite these constraints, the experiments produced repeatable results which showed many features that can be observed at calderas. We have carefully constructed

our experimental setup in order to eliminate many of the problems encountered in previous experimental studies, such as inappropriate chamber deformation and viscosities of experimental liquids. We therefore believe that our experimental approach is a good approximation of caldera formation.

Results

The results presented here are a representative selection of the experiments undertaken. Type experiments were chosen to show the range of experiments carried out. Type experiments for different depths, topography, pressure and chamber symmetry are discussed in detail below. Using the video footage of the experiments, temporal surface observations of each type experiment are described. The most important observational trends for each set of experiments are then presented.

Depth

In the depth experiments, the surface was always smooth and horizontal, the bladder volume was kept constant at 45 liters and the bladder was oriented horizontally.

Experiment 7B: depth 6.0 cm (2.5 km).

In this experiment surface deformation began by symmetric sag that formed above the center of the bladder. This sag became more asymmetric, and the first fault was seen at the surface in the southwest after 2 min 43 s (Fig. 37, 3 min). Subsidence was greatest associated with this fault, whereas the remaining subsidence was controlled by sagging. The main fault developed in a curve laterally outward from the area of maximum subsidence. Other small linear faults developed both inside and outside this main fault, which produced a complex fault pattern in the area of maximum subsidence. After 3 min 50 s a second fault also developed in the southwest corner 15 cm outside the

first fault and concentric to it. This fault developed in the same way as the first, developing as a curve growing outward from the southwest corner (Fig. 37, 5 min). It had only a small amount of subsidence associated with it. Both faults remained active until the end of the experiment but never progressed beyond the southwest quadrant. This resulted in a highly asymmetric depression both in cross-section and plan view. At the base of the fault scarp a small terrace developed (Fig. 37, 5 min). Sagging controlled the subsidence in most of the depression and reached a maximum diameter of 80 cm. The main semi-circular inner fault reached a diameter of 24 cm.

Experiment 3B: depth 9.5 cm (3.75 km)

Surface deformation began with a symmetric sag above the center of the bladder. After 1 min 55 s, a 3 cm-diameter horseshoe-shaped fault developed in the center of the sag. Subsidence on this fault was limited (Fig. 38, 3 min). After 2 min 20 s, subsidence shifted, and two faults began to develop simultaneously in the north and in the west: both were initially linear but propagated toward each other. Curved corner faults formed in the north, south and west. On the southwestern margin, two parallel faults formed, and a terrace developed between the two. These faults then joined with the southern corner and the northwestern side and formed a coherent ring structure (Fig. 38, 4 min). After 4 min 30 s, arcuate outer fault structures began to develop in the north, west and southeast located 10-20 cm outside the main fault. This principal structure was not circular in plan view; it instead consisted of four sides with four distinct corners, two faults bounding the southwestern side and its diameter varying from 30 cm to 45 cm. Sagging reached a diameter of 65 cm.

Experiment number	Scaled depth km	bladder depth cm	Bladder Volume Litres	sagging diameter cm	maximum subsidence depth cm	inner fault diameter cm	pre-existing topography style	Caldera Volume Cm	time taken first fault min. s.
7B	2.4	6	45	80	6.8	24		6140	2.43
3B	3.8	9.5	45	65	4.6	53		5600	1.55
33A	4.64	11.6	45	63	6.1	39		4650	2
14B	5.56	13.9	45	67	5.4	25		5510	2.07
11B	6.8	17	45	70	5	17		4630	2
23B	8.72	21.8	45	66	5.9	25		4450	
18A	9.6	24	45	61	4.5	17		3880	3.3
36A	4.48	11.2	45	60	5.9	43	ridge E-W	5610	1.45
38A	4.52	11.3	43.8	70	4.8	43	range N-S	6050	1.3
30A	4.64	11.6	45	55	5.2	43	volcano E	4800	2.05
41A	5.6	14	40	62	4.6	38		6180	1.2
22B	4.16	10.4	45	66	7.2	26			1.5

Table 1. Summary of the experimental results.

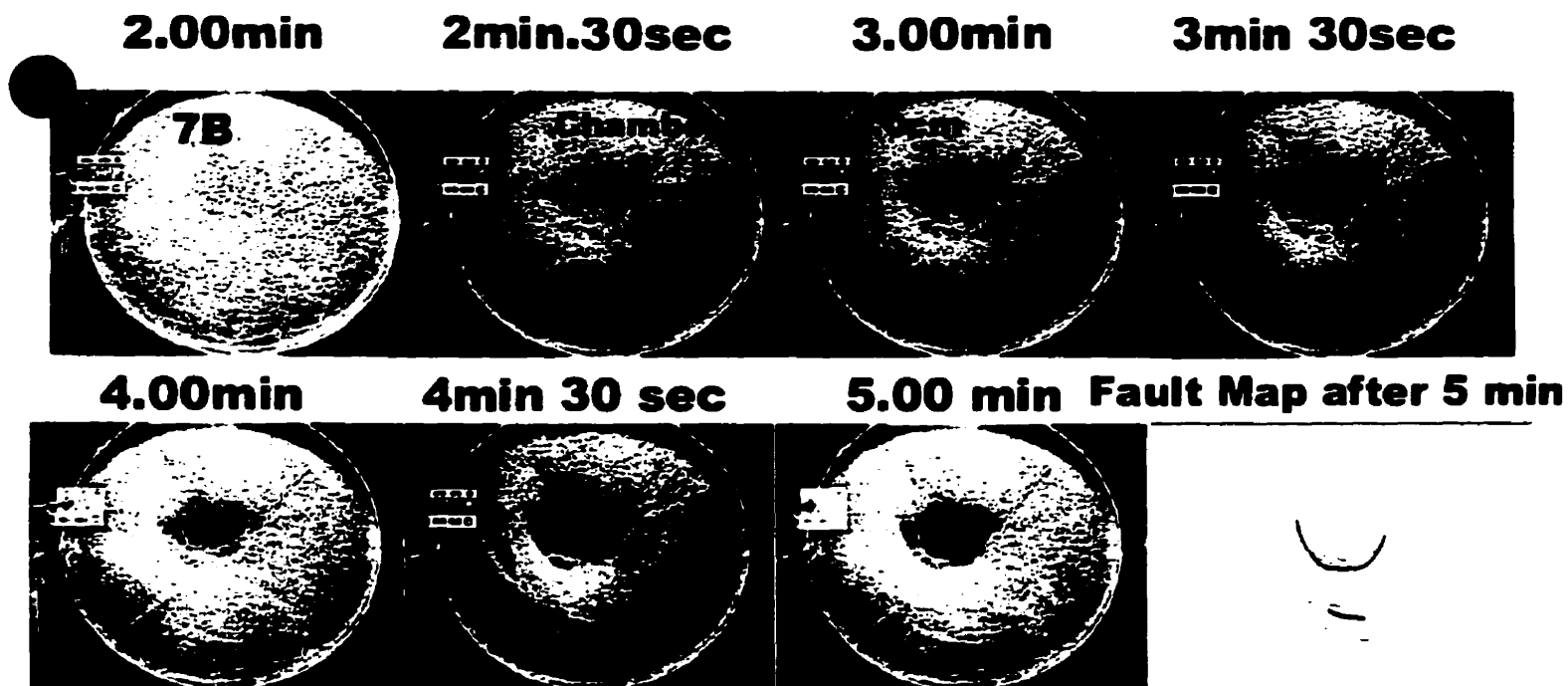


Figure 37. Type experiment for shallow magma chambers (6.0 cm. scaled to 2.5 km), showing temporal evolution of faults at the surface.

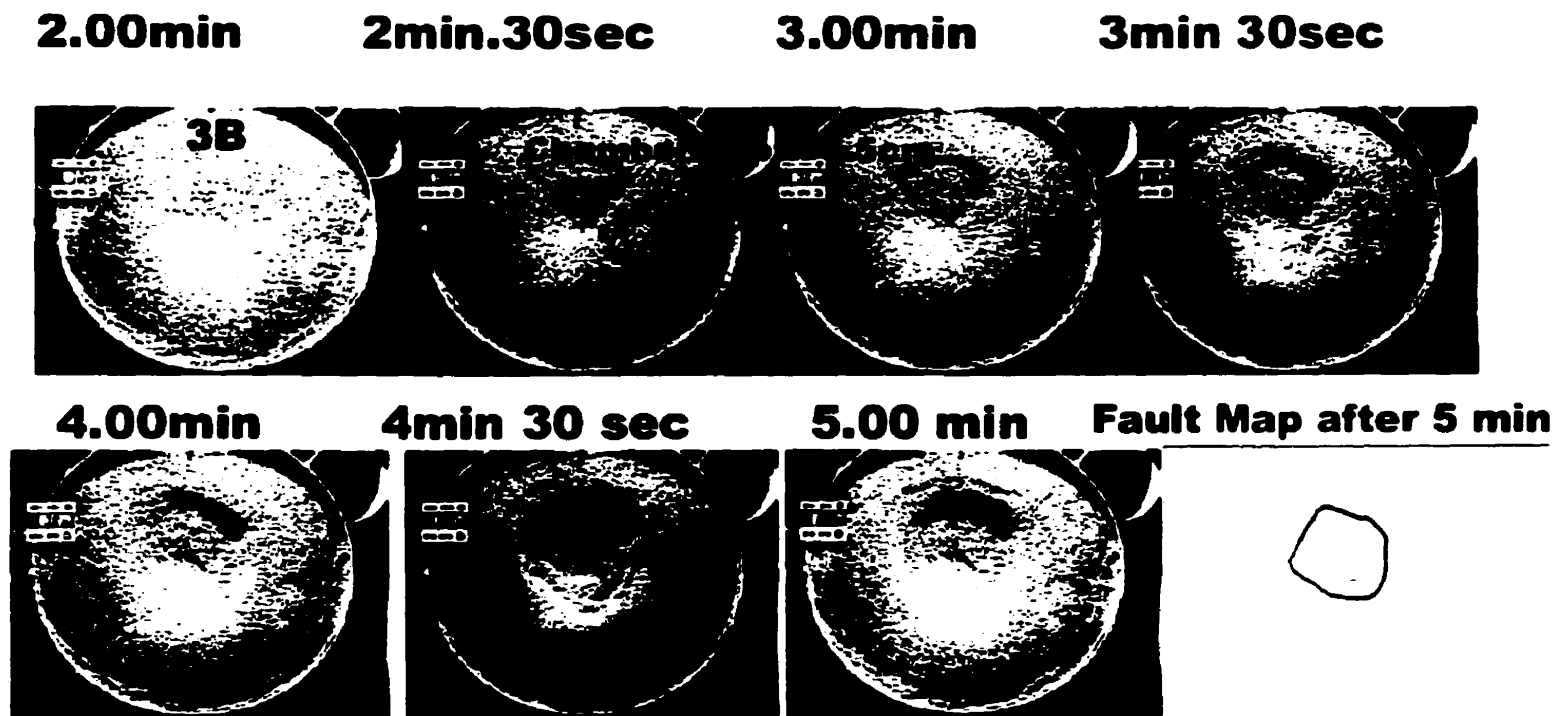


Figure 38. Type experiment for shallow-medium depth magma chambers (9.5 cm scaled 3.8 km). showing temporal evolution of faults at the surface.

Experiment 33A: depth 11.6 cm (4.6 km)

Surface deformation began with a symmetric sag. This sag became asymmetric, and the first fault was seen at the surface after 2 min (Fig. 39). It formed as a series of connecting linear faults which began on the side of greatest subsidence and propagated towards the side of least subsidence (Fig. 39, 3 min). These faults joined up to form an irregular horseshoe-shaped fault which subsided rapidly in the south. In this area, part of the inner fault propagated outward to become part of the outer fault. This outer fault never formed well but could be seen developing in the south where it formed the topographic boundary. Slumping of material was common in the south, and extension related to this slumping could be seen (Fig. 39, 5 min). The inner faults propagated almost the entire distance around the caldera to form a coherent, polygonal-shaped subsiding block which reached a maximum diameter of 39 cm. Sagging continued to control subsidence in the northwest. The diameter of visible sagging reached 63 cm.

Experiment 14B: depth 13.9 cm (5.5 km)

Deformation at the surface began as a symmetric sag. After 2 min 7 s the first faults were seen to form in the north; these were linear and at right angles to each other. Two sets of subsidence-controlling faults quickly developed concentric to one another, both controlling the asymmetric subsidence (Fig. 40, 3 min). One arm of each of these faults propagated south in an arc joining the faults (Fig. 40, 4 min). This formed a semi-coherent, almost rectangular subsiding block. The outermost part of this fault continued to develop in the east and was again linear. This produced an overall rectilinear, spiral-shaped, subsidence-controlling fault with nearly flat terraces between the faults. Initially asymmetric subsidence became symmetric, subsidence shifting from the north to the south. The spiral fault did not form from the center outwards but rather in two sections from the north southward. Outside the main areas of faulting, a circular peripheral outer

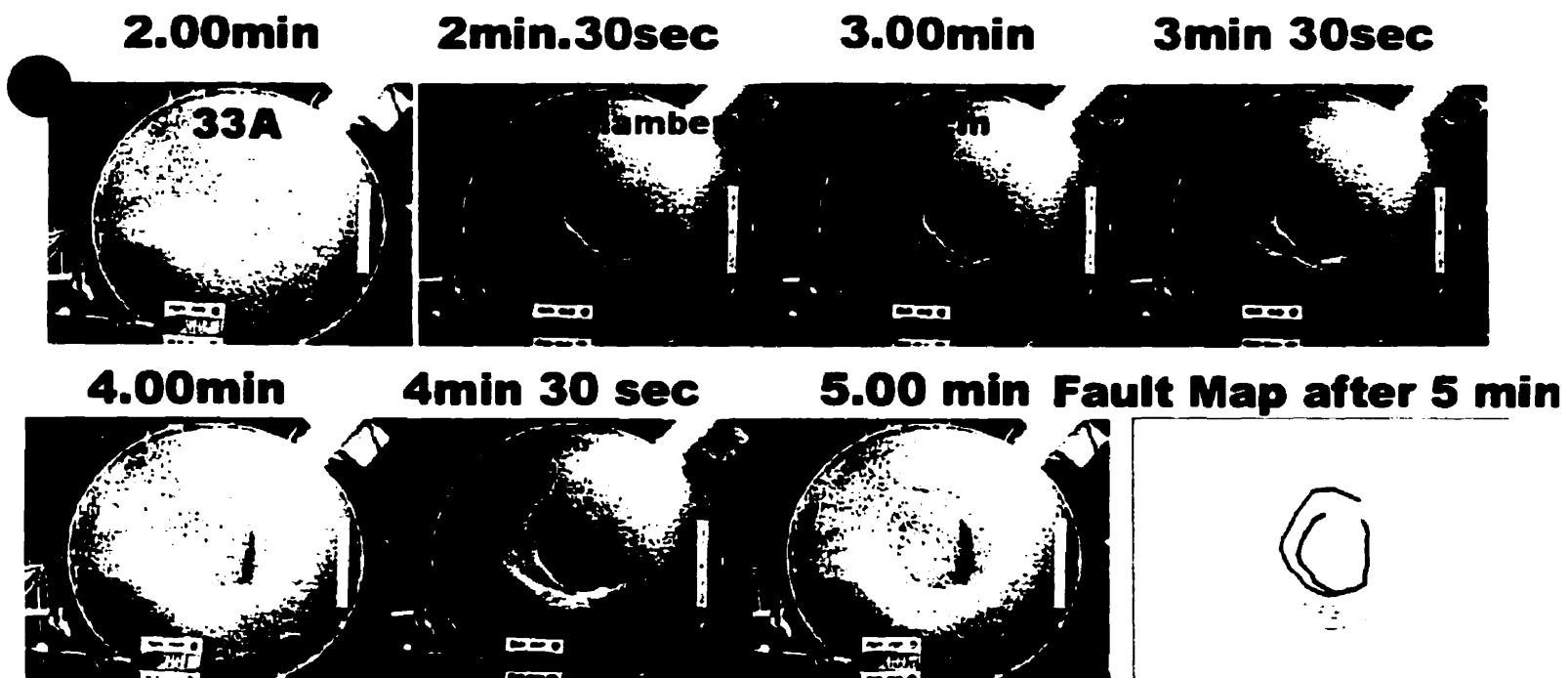


Figure 39. Type experiment for medium depth magma chambers (11.6 cm scaled 4.6 km). showing temporal evolution of faults at the surface.

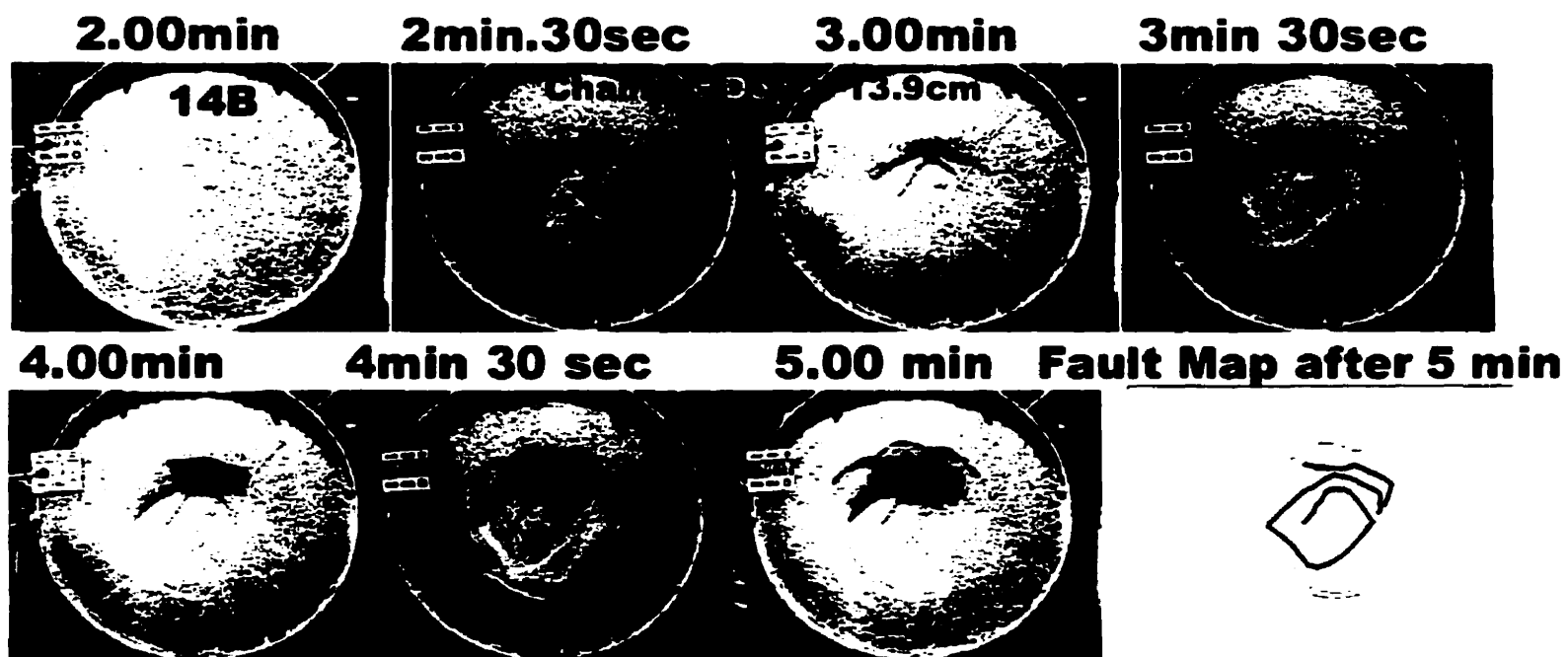


Figure 40. Type experiment for medium depth magma chambers (13.9 cm scaled 5.5 km). showing temporal evolution of faults at the surface.

fault marked the limit of slumping and extension (Fig. 40, 5 min). Sagging was of little importance and extended to a diameter of 67 cm just beyond the limit of slumping.

Experiment 11B: depth 17 cm (6.8 km)

Deformation at the surface began as a symmetric sag. After 2 min a small 10 cm-diameter nearly circular fault formed at the surface. A small central piston began to subside. Subsidence then shifted to just north of this piston, and two linear faults formed at right angles concentric to the central piston (Fig. 41, 2 min 30 s). These joined up with the first-formed faults, enlarging the subsiding block. A linear subsidence-controlling fault propagated outside this new piston, forming a new subsiding block in the northwest (Fig. 41, 3 min 30 s). This again joined up with part of the piston forming a rectilinear subsiding block. Another fault once again propagated outside the subsiding block. This produced a further subsiding block in the north, improving the plan-view symmetry and circularity of the depression (Fig. 41, 4 min 30 s). Just prior to the end of the experiment, another fault-bounded subsiding block formed in the northwest. This depression was clearly fault-controlled, forming as a series of separate subsiding blocks, incrementally enlarging the depression northwards and forming a series of terraces or benches between faults. Subsidence was fairly symmetric but greatest in the south. Beyond the first-formed fault, the south was largely controlled by sagging. A clear outer fault never developed in this experiment. This experiment produced a maximum sagging diameter of 70 cm.

Experiment 18: depth 24 cm (9.6 km)

For the first 2 min 40 s nothing was seen at the surface except a broad symmetric sag. Faults began to form at the edge of the main sag; however, this fault never developed into a ring fault, as there was very little subsidence upon it. Sagging at the surface continued to dominate the subsidence: after 3 min 30 s, two small intersecting arcuate faults formed in the center (Fig. 42, 4 min). Arcuate faults continued to develop in this

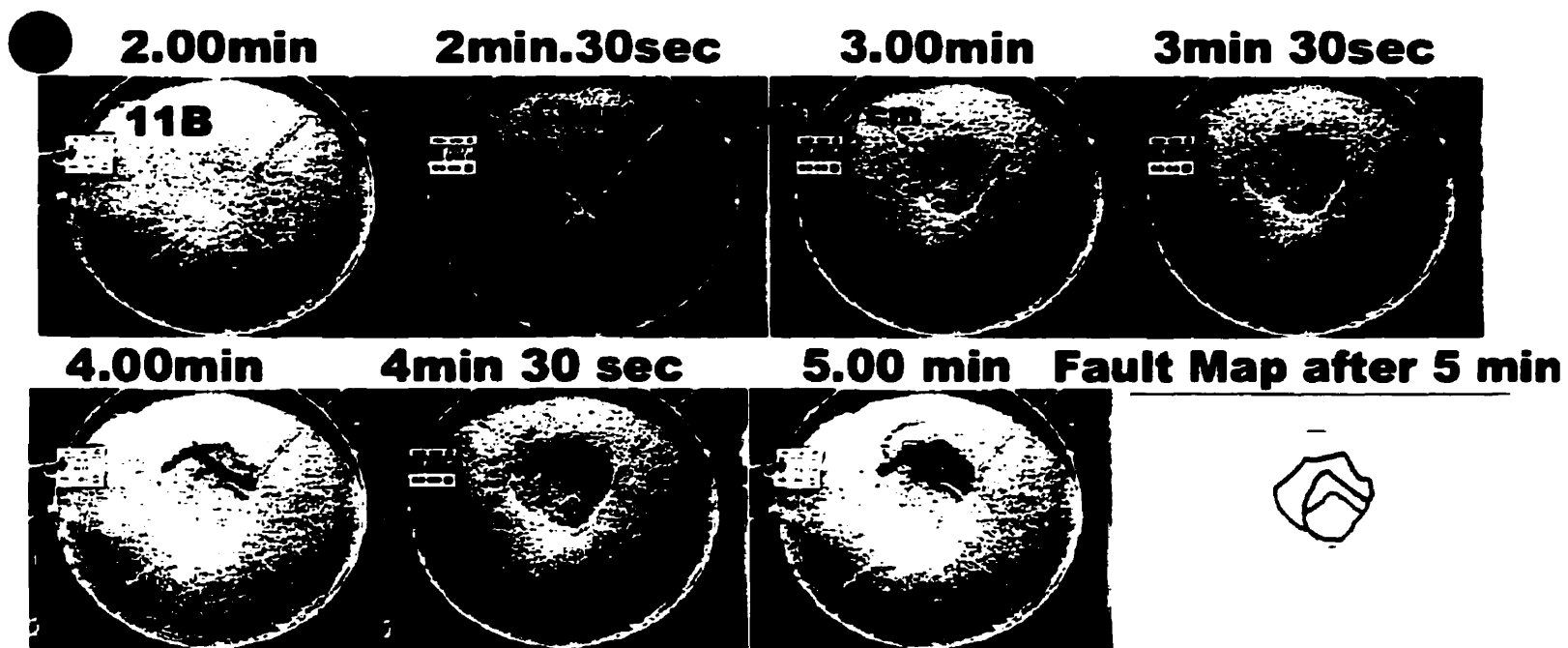


Figure 41. Type experiment for medium-deep depth magma chambers (17cm scaled 6.8 km). showing temporal evolution of faults at the surface.

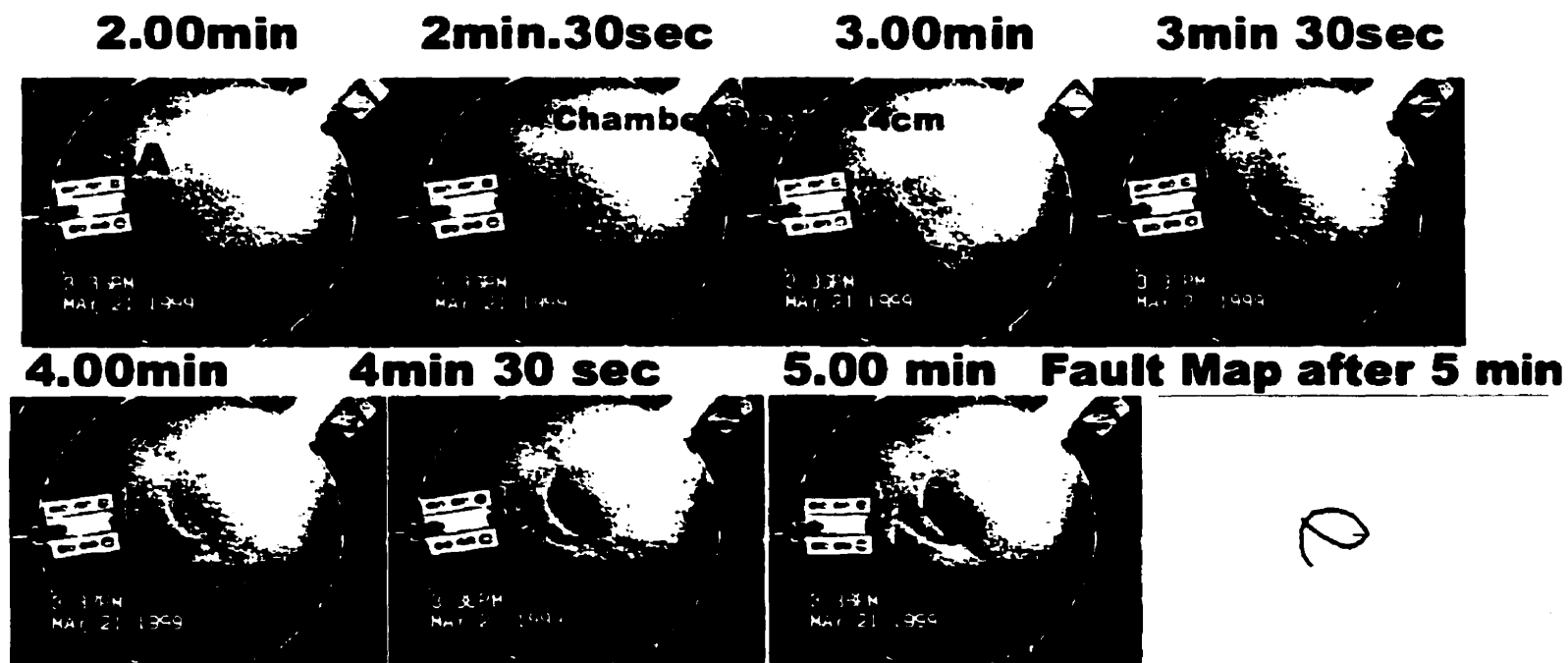


Figure 42. Type experiment for deep magma chambers (24cm scaled 9.6 km). showing temporal evolution of faults at the surface.

central region, joining up and intersecting one another to produce a series of overlapping arcuate faults. These faults formed two fault blocks in the centre of the depression, both highly asymmetric in plan view. The rest of the depression was dominated by sagging with no outer fault developing. Faults were never well-developed in this sagged zone which extended to a maximum diameter of 61 cm.

Summary of observations of depth experiments

As chamber depth increased:

1. The area of faulting decreased, thereby increasing the fault density.
2. The subsiding block became less coherent.
3. Faults became less arcuate, trending toward intersecting linear faults.
4. More terraces formed between faults.
5. The maximum area of sagging decreased.

Topography

In the topography experiments, the depth of the bladder was kept constant at a depth of about 11 cm (4.4 km), which is an intermediate value. The bladder volume was constant at 45 liters, and its orientation was kept horizontal (Table 1).

Experiment 29A: 1 kg sand cone in east

Surface deformation began by sagging. After 2 min 5 s, the first fault formed at the base of the cone, propagating westward and south through the cone's eastern flank (Fig. 43, 3 min). This caused oversteepening of the cone and slumping to occur on the flanks of the cone. A second fault then propagated away from the cone in the north and south, forming a north-south oriented arcuate fault. The inner fault continued to propagate west from the south edge of the cone in a series of linear faults, joining up to form a polygonal subsiding block. The north-south arcuate fault then propagated west

and east, forming an outer concentric ring (Fig. 43, 4 min). Subsidence was most rapid in the east, and two concentric fault scarps formed in the northeast (Fig. 43, 5 min). The outer fault never propagated all the way around to the west, while the inner fault could be seen to propagate beyond the piston in the east and form a cross which was related to a corner of the subsiding polygon (Fig. 43, 5 min). Sagging reached a maximum diameter of 55 cm.

Experiment 36A: 1 kg sand ridge oriented east-west

Surface deformation began with sagging. The first fault appeared after 1 min 45 s; this fault began at the eastern edge of the ridge and propagated west in an arc just north of the ridge to the other end (Fig. 44, 3 min). A second fault formed following the first along the northern margin of the ridge. Another fault also propagated south from the edge of the ridge, then propagated west in a smooth arc. A further fault formed concentric to this in the southeast and southwest. The northern and southern faults met in the west. Subsidence was greatest in the east, and a steep fault scarp formed here with associated slumping. Arcuate faults formed, extending beyond the central block in the north (Fig. 44, 5 min). In the northeast and south, a series of outer faults appears to have formed. Sagging was most important in the north and east and extended to a diameter of 60 cm.

Experiment 38A: 5.7 kg range oriented north-south in the west

Surface deformation began by sagging. The first fault was seen after 1 min 30 s and developed in the north at the eastern edge of the mountain range; it almost instantly propagated south in a smooth curve (Fig. 45, 2 min). Large amounts of slumping could be seen where the fault intersected the range. As subsidence continued, a coherent, nearly circular block subsided. Faults could not be clearly seen within the sand range due to slumping. Continued subsidence formed steep fault scarps in the east, and continued slumping of the sand was observed within the range. An arcuate fault formed in the west

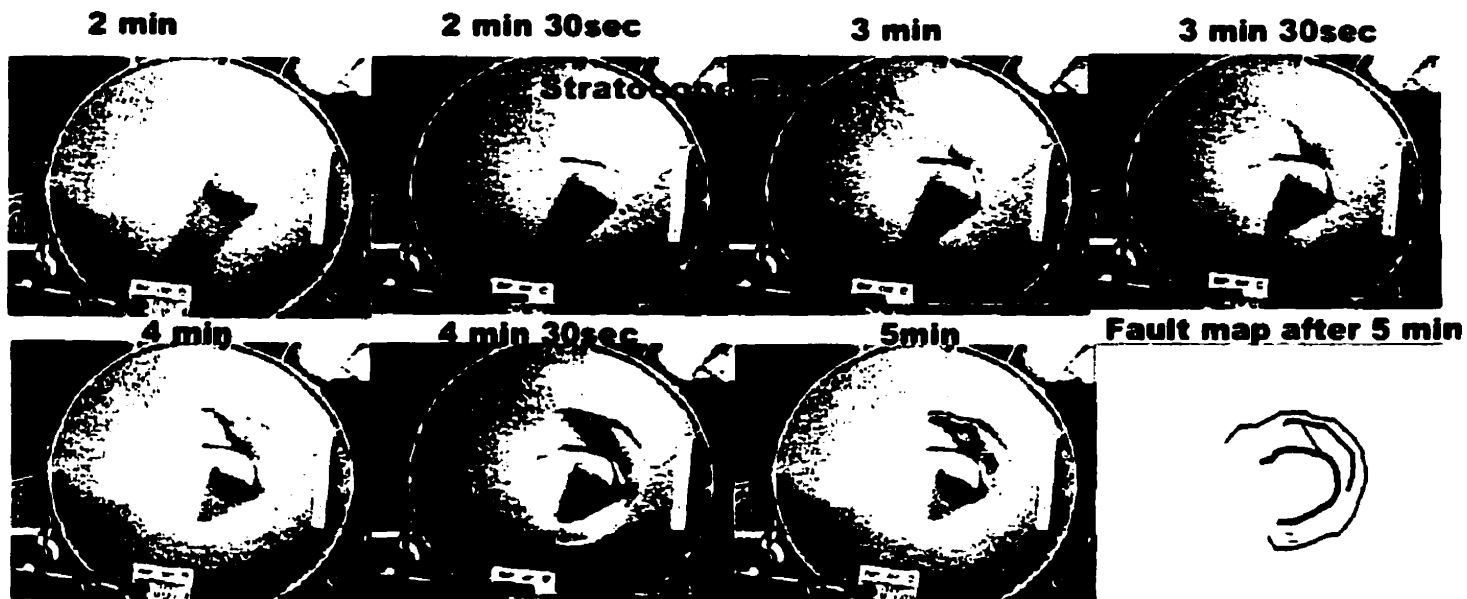


Figure 43. Type experiment for a 1kg stratocone. magma chamber depth (11.6 cm scaled 4.6 km) showing temporal evolution of faults at the surface.

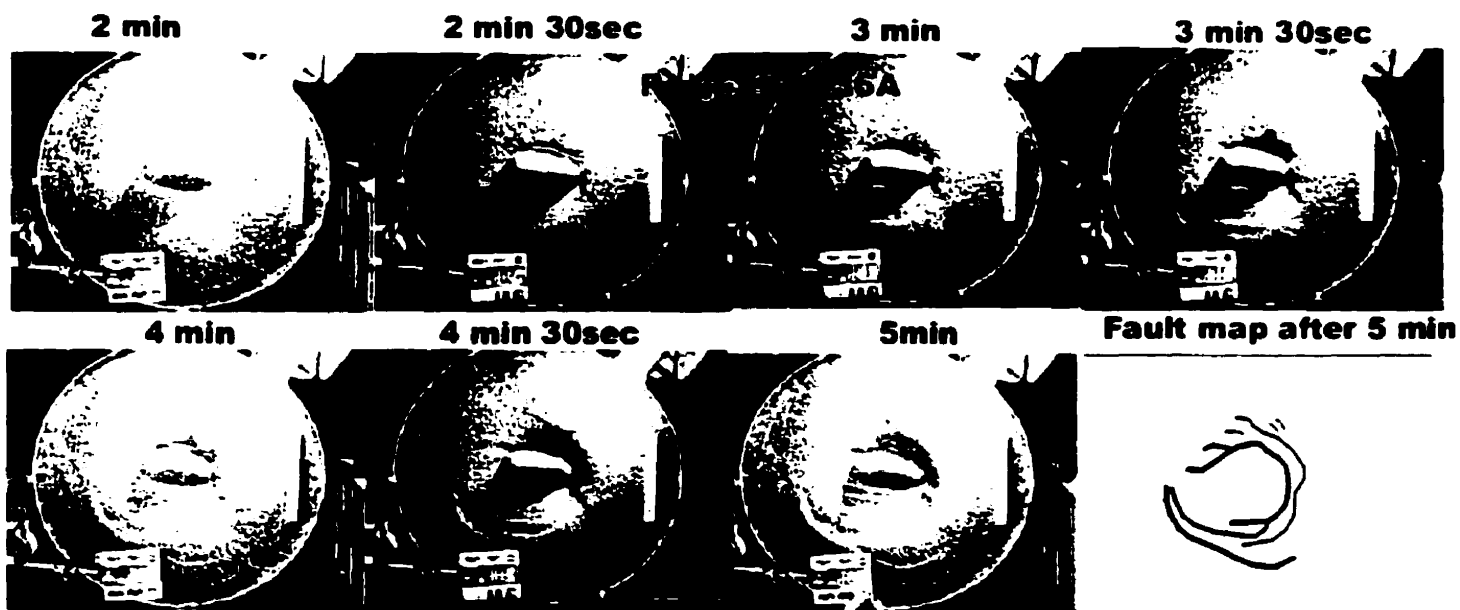


Figure 44. Type experiment for a 1kg sand ridge. magma chamber depth (11.2 cm scaled 4.5km), showing temporal evolution of faults at the surface.

beyond the ridge, then propagating south in a smooth arc. A steep fault scarp could not be seen in the west as it was obscured by the range. This depression was a simple, highly circular depression bounded by a single fault. A concentric fault appeared to have formed in the southwest, although it was difficult to see its relationship to the main fault that was obscured by the range. A full outer fault never developed. Sagging reached a maximum diameter of 70 cm.

Summary of observations of topographic experiments

As a greater mass of topography was added:

1. The ring fault became more coherent with a larger diameter.
2. Faults became smoother and more arcuate.
3. Faults formed earlier at the surface.
4. The maximum diameter of sagging increased.

Pressure

In the pressure experiments, the depth was kept constant at 14 cm (5.6 km), and the relief and the bladder orientation were kept horizontal (Table 1).

Experiment 41A: low-pressure 40 liter bladder

Surface deformation began with a symmetric sag. After only 1 min 20 s, a series of linear faults formed in the south and propagated north in a smooth curve. This formed a nearly circular ring fault with a comparatively large diameter of 38 cm (Fig. 46, 3 min). As this circular block subsided symmetrically, a second concentric fault began to form in the east and west outside the first fault. A linear section of the inner circular fault extended outward in the north and east, forming a terrace bounded by irregular faults. In the west, an arcuate outer fault propagated south and north, forming a circular outer fault (Fig. 46, 4 min). Both the inner and the outer faults continued to subside, and smaller

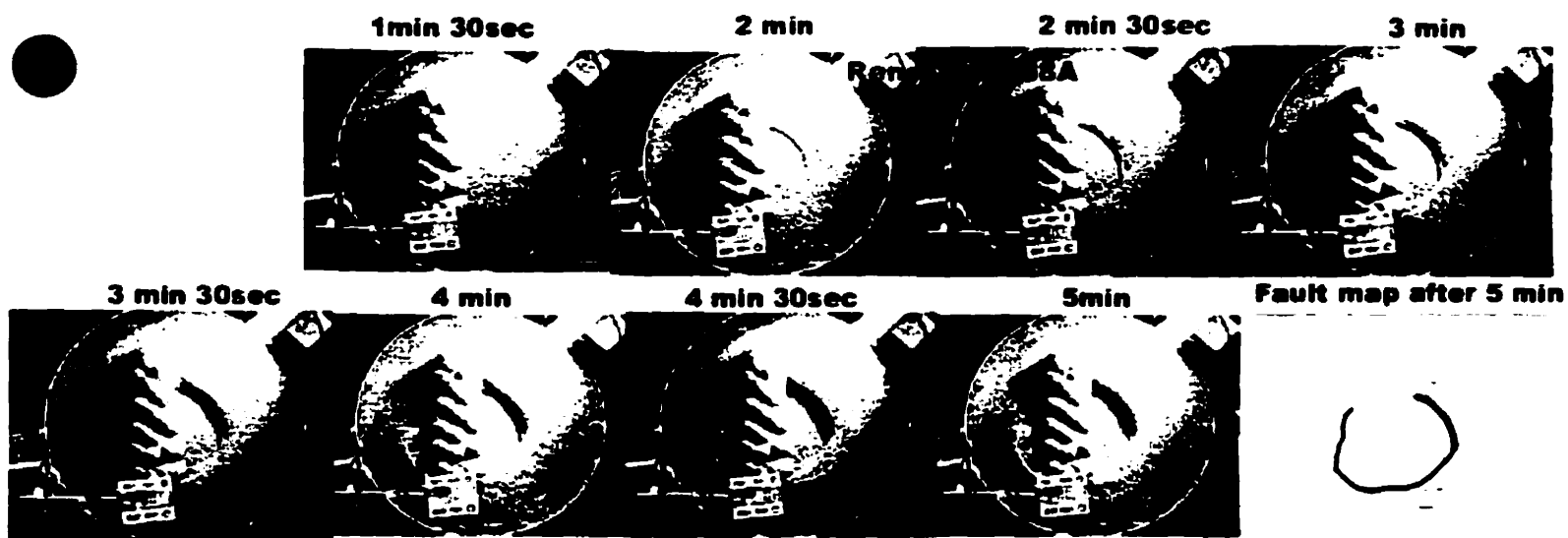


Figure 45. Type experiment for a 5.7 kg sand range, magma chamber depth (11.3 cm scaled 4.5 km), showing temporal evolution of faults at the surface.

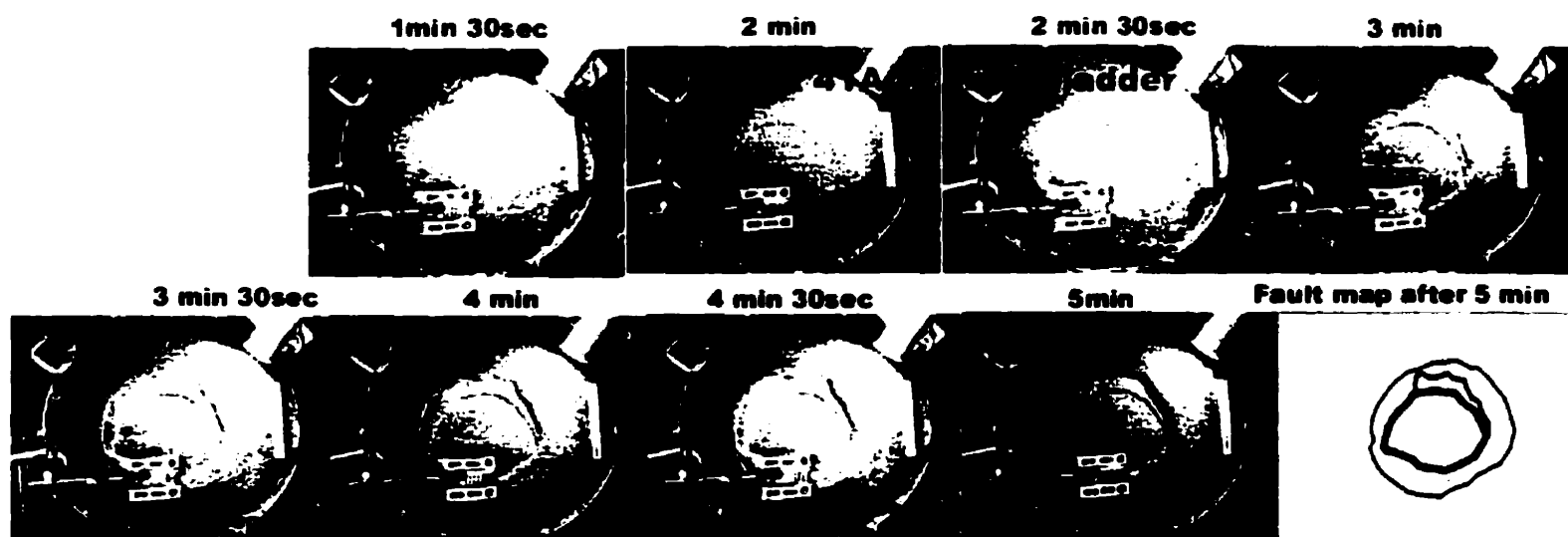


Figure 46. Type experiment for a low pressure 40 liter bladder, chamber depth (14cm scaled 5.6 km), showing temporal evolution of faults at the surface.

extensional fractures developed between the two faults in the south. The subsided block was horizontal, and sagging only extended to 62 cm, being most important in the northeast where the outer circular fault was poorly developed. The central subsiding block appeared to be completely coherent. Subsidence was slightly asymmetric, being greatest in the south where faults first formed.

Summary of low-pressure experiments

Compared to the higher-pressure experiments, the low-pressure experiments showed:

1. The subsiding block had a larger diameter and appeared to be more coherent.
2. Sagging was of smaller diameter.
3. Faults were less linear and formed nearly circular ring structures.

Tilted chamber

In the tilted bladder experiments, the depth was kept constant at 10.4 cm (4.2 km), as measured from the surface to the highest point of the bladder, the surface was always smooth and horizontal, and the bladder volume was constant at 45 liters (Table 1).

Experiment 22B: Tilted bladder elevated in the northeast

Surface deformation began by sagging, which was almost immediately asymmetric, subsiding faster in the north and east (Fig.47, 2 min). After 1 min 50 s a series of poorly-developed faults formed first in the northeast, then in the east and south (Fig. 47, 2 min 30 s). Little subsidence occurred on these faults, and sagging increased rapidly in the west and south, with linear faults forming in these areas. These faults joined up with the earlier-formed faults to form a rectangular northeast–southwest oriented subsiding block (Fig. 47, 3 min). Subsidence became rapid in the south and west.

and a second fault set formed parallel to the original faults, forming terraces, enlarging the area of faulting and maintaining the rectangular shape of the subsiding block (Fig. 47. 4 min). Simultaneously, an arcuate outer fault formed in the southwest which joined with a second arcuate outer fault in the east (Fig. 47. 4 min 30 s). Together, these faults formed a semi-circular outer fault in the south (Fig. 47. 5 min). This outer fault joined with a more linear fault in the north, forming an elongate outer ring oriented northeast-southwest. Subsidence continued to be most rapid in the southwest. A steep fault scarp formed along a linear fault in the northwest in the last minute (Fig. 47. 4 and 5 min): here the outer fault did not develop well. During the last stages of the experiment, a small curved graben developed in the northeast which was oriented northwest-southeast (Fig. 47. fault map, highlighted in blue).

Summary of tilted chamber experiments

Compared to horizontal orientations, tilted chambers showed:

1. Subsidence was greatest where the chamber was deepest.
2. The depressions that formed were elongate perpendicular to the hinge of subsidence.
3. Faults were highly linear, and the subsiding block was often rectangular.
4. Subsidence-controlling faults were initiated on the side of minimum subsidence and propagated in a complex manner.
5. Graben formed related to subsidence hinges.

General observations of experimental calderas

1. Subsidence occurs as a result of both sagging and faulting.
2. A subsidence-controlling inner fault and a later-formed outer fault are usually seen.
3. Multiple concentric subsidence-controlling faults are common.
4. Subsidence-controlling faults are rarely circular ring faults.

5. Polygonal ring faults are common and form by a series of connecting curvilinear faults.
6. Subsidence is almost always asymmetric in cross section.
7. The highest surface dip angles occur between the outermost inner fault and the outer fault.
8. The effects of sagging always extend beyond the outermost fault.

Interpretation of Results

Temporal caldera development in plan view

Although our experimental calderas showed varied morphologies, they also exhibited some important similarities. For all experiments, the surface deformation began with a period of downsagging, which is the inward tilting of the surface caused by downwarping (Fig. 48). A fault then was initiated on the side of maximum downsagging (Fig. 48a). Initial subsidence was often asymmetric: this was caused by part of the caldera being controlled by downsagging and part by faulting. Downwarping tended to distribute the deformation, whereas faulting concentrated it. This is illustrated by the laser line developing a gradual curve for downwarping versus an abrupt displacement for faulting (Fig. 48b).

The initial fault propagated laterally from the side of maximum subsidence (Fig. 49a), sometimes joining up with other simultaneously-developing faults (Fig. 49b). Further faulting developed as subsidence continued: these faults tended to be concentric and outside the first faults. Terraces formed between these concentric inner faults: these terraces showed some inward dip due to initial downwarping (Fig. 48b). Subsidence shifted from the earlier inner faults outward to the later-formed outer faults. This may be

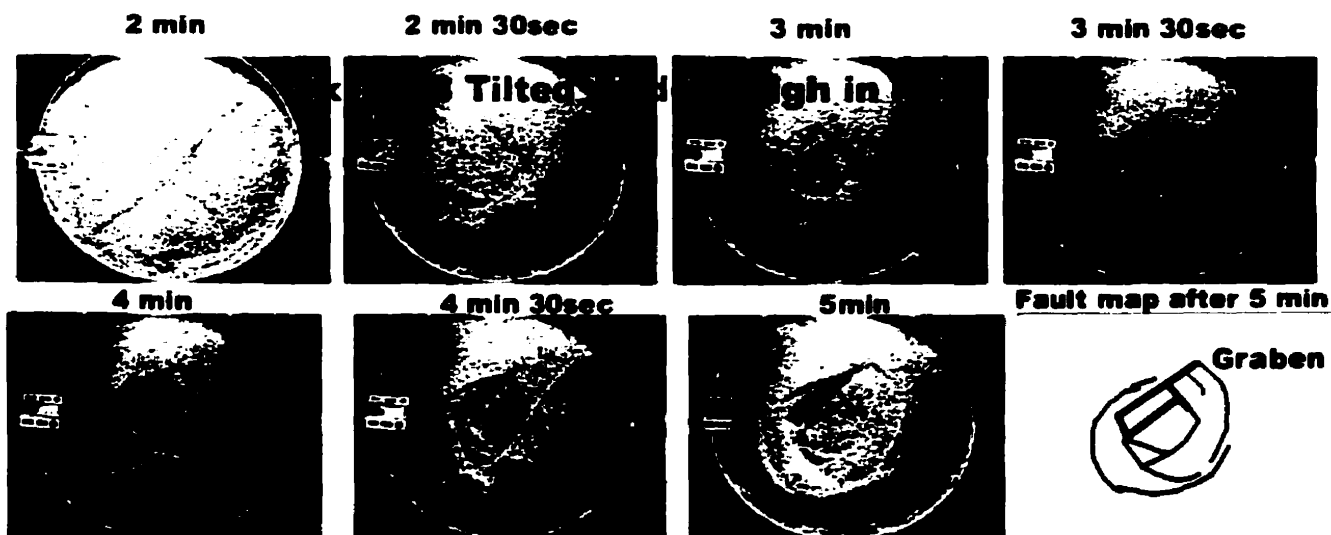


Figure 47. Type Experiment for tilted bladder chamber depth (high in northeast minimum depth 10.4 cm scaled 4.2 km) showing temporal evolution of faults at the surface.

a)

b)

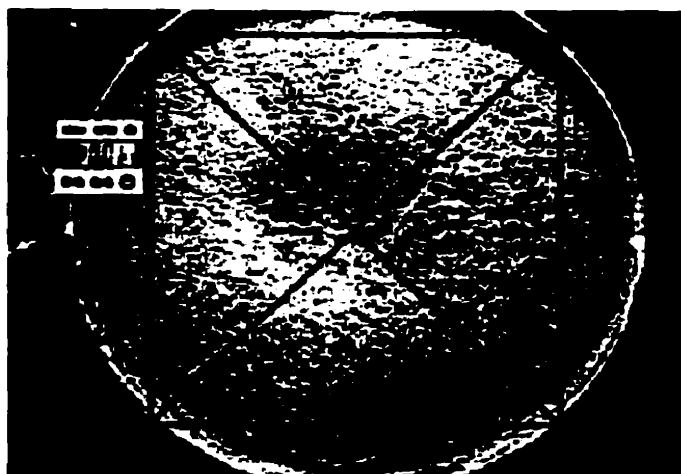


Figure 48. Subsidence controlled by both sagging and faulting. a) Faulting develops first in the south where downsagging is greatest. Downsagging is shown by the change in angle of the red laser line. b) The laser line distinguishes two styles of subsidence: the gradual curve of the laser showing downwarping-controlled downsagging, and the sharp notches in the laser line where faulting controls the subsidence.

a)

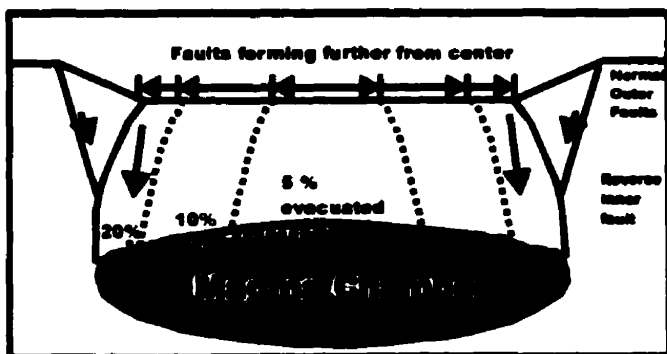


b)



Figure 49. a) Fault propagation laterally from the area of maximum subsidence, indicated by arrows. b) Faults joining up to form polygonal ring faults, but still propagating away from the side of maximum subsidence.

a)



b)

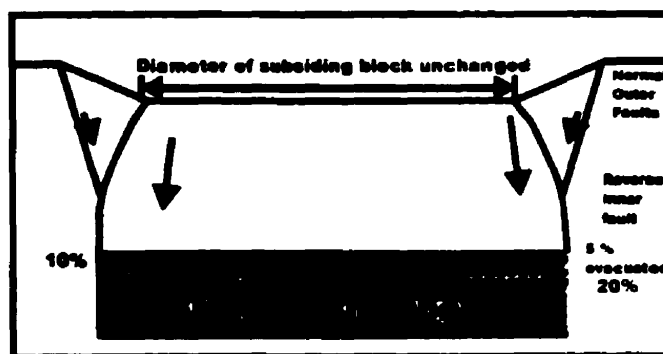


Figure 50. a) Due to the convex nature of the upper surface of the magma chamber, as magma is progressively removed from the chamber, the position of ring faults shifts progressively outward, producing an incrementally-growing caldera. b) A flat-topped chamber will not cause this effect.

caused by the convex nature of the upper surface of the experimental magma chamber (Fig. 50).

The inner subsiding area caused a peripheral area of extension to develop (Branney, 1995; Roche et al., 2000). An outer fault frequently developed in the late stages of subsidence, caused by extension and slumping of the oversteepened fault scarp. In this area of peripheral extension, downwarping-related downsagging may be enhanced by fault-controlled inward tilting of the surface (Fig. 51). In this marginal area of the caldera, downsagging has been shown to be greatest (Branney, 1995). The experiments illustrate this point, showing significantly higher angles of downsagging between outer peripheral faults and inner subsidence-controlling faults than between inner subsidence-controlling faults (Fig. 51). However, these angles could never exceed 30° in the experiments, since this is the angle of repose for sand. Some experiments indicated that the zone of peripheral extension may be represented by multiple normal faults with small displacements (Fig. 52).

Temporal fault development in cross section

Little is known about the temporal development of calderas, as the process has never been observed directly. However, as eruptions are contemporaneous with collapse and pyroclastic flows pond in depressions, good cross-sectional exposure at deeply eroded calderas can reveal relationships between faults, deposit thicknesses and megabreccias. These relationships can be used to infer the temporal development of the caldera.

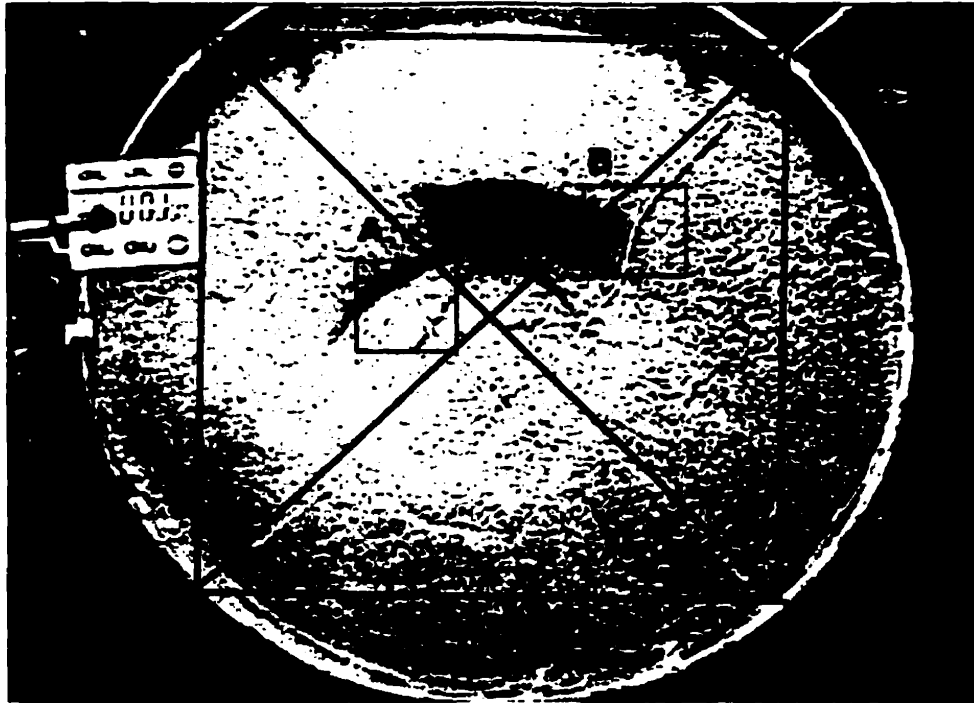


Figure 51. In the blue box marked A in experiment 14B, a terrace is observed between two inner subsidence-controlling faults: this terrace shows very little downsagging. In the green box marked B, comparatively high amounts of downsagging are seen between an inner subsidence-controlling fault and a peripheral extension-related outer fault.

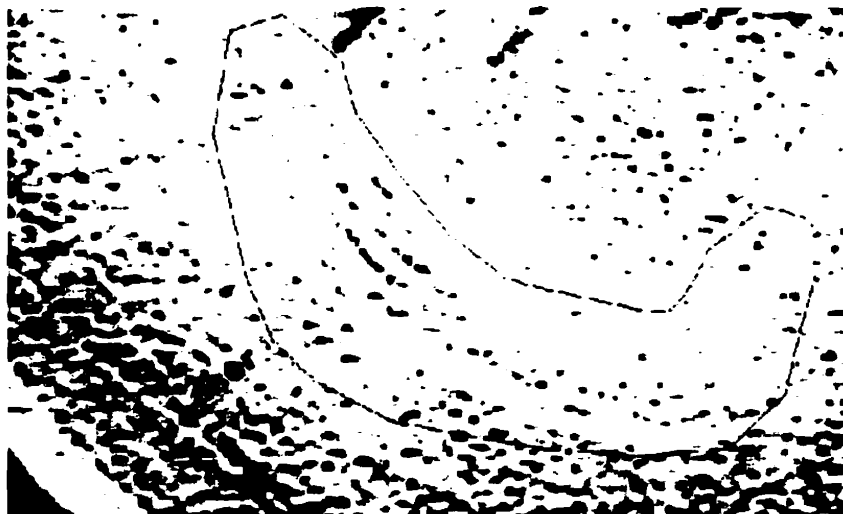


Figure 52. Peripheral extension outside the subsidence-controlling fault in the southwest region of experiment 14B.

In our experiments, the main subsidence-controlling faults were interpreted to be outward dipping from detailed observations of sand movement during our experiments and supported by previous experimental work (Branney, 1995; Odonne et al., 1999; Roche et al., 2000). Sand could be seen moving from the interior of the subsiding block toward the subsidence-controlling fault like a subducting oceanic slab, implying an outward dipping fault. Experimental studies and examination of collapse pits have shown that these subsidence-controlling, outward dipping faults are curved, with shallow dips at the surface which steepen with depth (Sanford, 1959; Branney, 1995; Odonne et al., 1999; Roche et al., 2000) (Fig. 53). This can be explained by tensional failure at shallow levels and shear failure at depth. The curved, outward dipping nature of these faults also is supported by earthquake data from recent activity at Rabaul caldera, Papua New Guinea (Mori and McKee, 1987) and at Mount Pinatubo, Philippines (Mori et al., 1996) (Fig. 13). In experiments at intermediate and slightly greater depths (Fig. 54d, e, f), multiple subsidence-controlling faults existed which were probably dipping outward; this is supported by the experiments of Odonne et al. (1999) which show a horizontal terrace between two outward dipping faults (Fig. 53c).

Downsagging and peripheral extension

Downsagging is the tilting of strata towards the center of the caldera (Branney and Kokelaar, 1999). In our experiments, this is represented by the tilting of the surface towards the center of the caldera, which can occur in three ways. The first is caused by downwarping (Fig. 48a); no faults are used, the subsiding block is simply bent. There is probably some re-arrangement of sand grains during this process, allowing the surface to

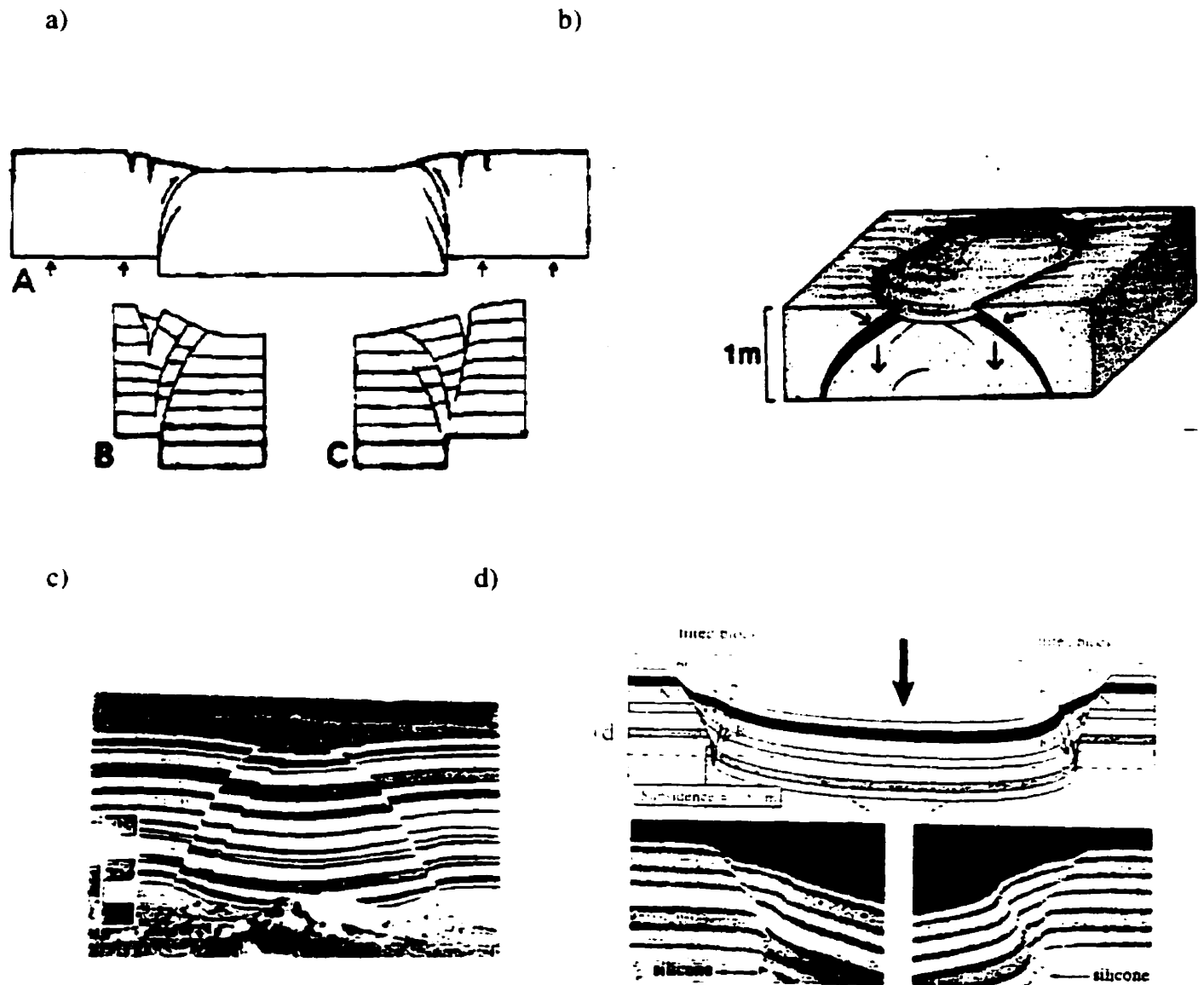


Figure 53. Outward dipping faults which are curved and steepen with depth. a) Experimental models (Sanford, 1959). b) Ice-melt collapse pits (Branney, 1995). c) Experimental models from Odonne et al. (1999); this diagram also shows horizontal terraces between parallel, outward dipping faults. d) Experimental model from Roche et al. (2000); this figure also shows peripheral inward tilting (downsagging) between inner and outer faults.

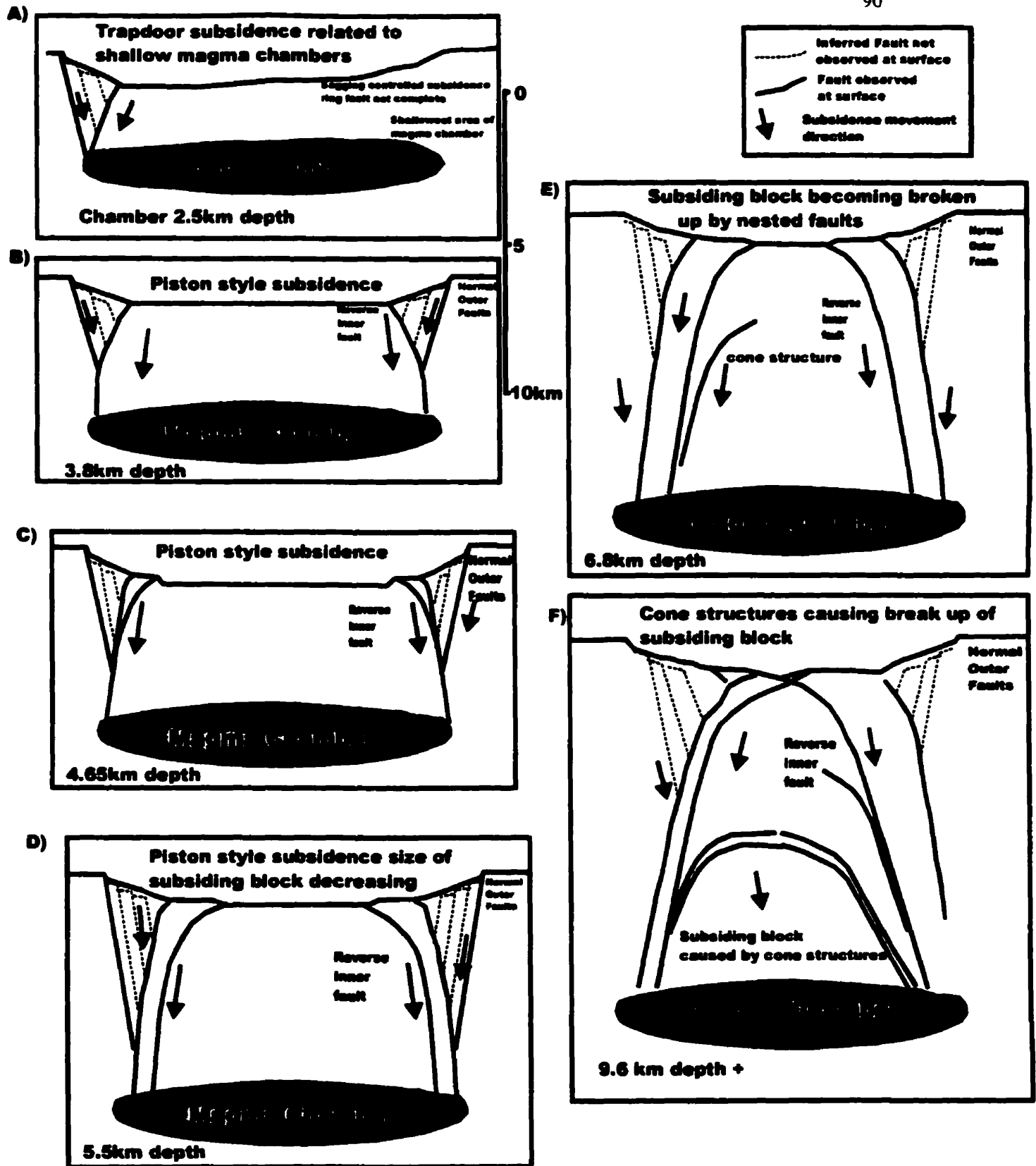


Figure 54. Inferred cross-sectional structure as it varies with depth and aspect ratio of the magma chamber.

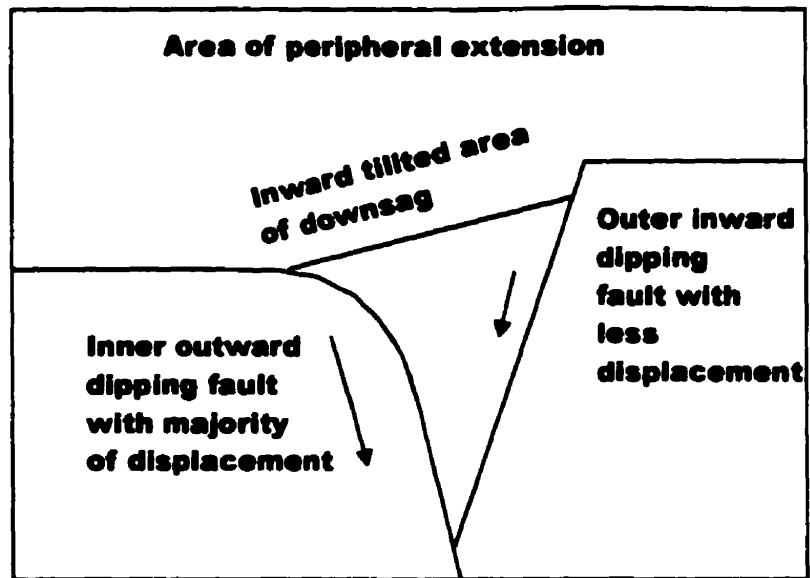


Figure 55. Peripheral downsagging caused by differential displacement on an outward dipping inner fault and an inward dipping outer fault.

bend without faulting. It is this process that occurs at the beginning of each experiment. The second is caused by tilting related to faulting (Branney, 1995); an inner outward dipping fault, representing most of the displacement, and an outer inward dipping fault, with less displacement, are used together to tilt the surface towards the center of the caldera (Fig. 55). This process causes the downsagging shown in box B in Figure 51. The third mechanism does not tilt the strata but instead causes the surface to dip towards the center of the caldera from slumping of the sand. Such a slump on a previously horizontal caldera floor will create a slope which dips towards the center of the caldera (Fig. 56).

The peripheral area outside the main subsidence-controlling faults is extensional (Fig. 52). Thus, the outermost faults are normal faults; this is supported by previous field and experimental work (Branney, 1995; Odonne et al., 1999; Roche et al., 2000) (Fig. 53b, d). The faults form as a result of subsidence on the main inner fault. The scarp produced by the inner fault will grow in height during subsidence but cannot maintain an angle greater than that of repose and therefore will continually collapse. This causes the caldera margin to widen by normal faulting and slumping. In most experiments only one outer fault was seen. However, the area of peripheral extension may represent a series of normal inward dipping faults whose surface expression is concealed by slumping and grain flow (Fig. 52). In the experiments, it was often difficult to interpret which mechanism causes the inward tilting of the surface. Often all three mechanisms occurred together.

Controls on caldera morphology

1) Magma chamber depth

The depth of the magma chamber was scaled to between 2.5 km and 9.6 km. This depth variation caused distinct trends in the resultant caldera morphology. (1) The

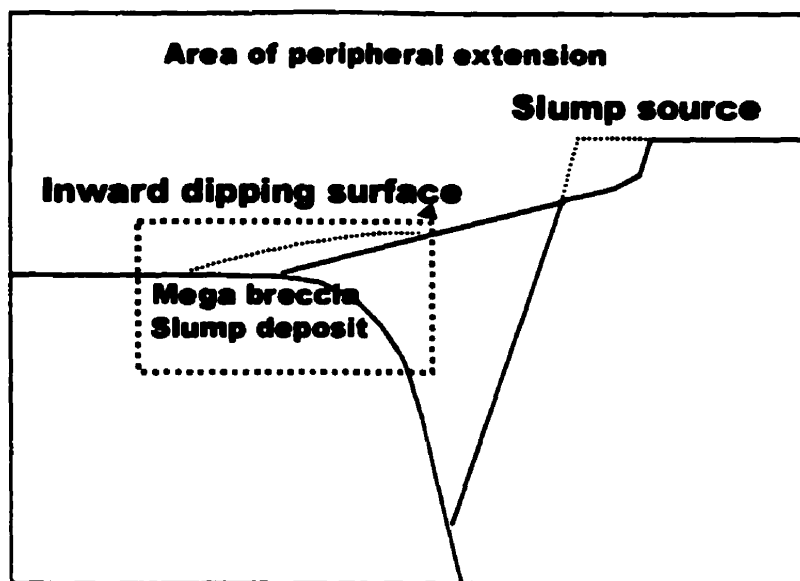


Figure 56. Slumping causing an inward dipping surface. The red square shows how a slump deposit results in a previously horizontal area of the caldera dipping inwards.

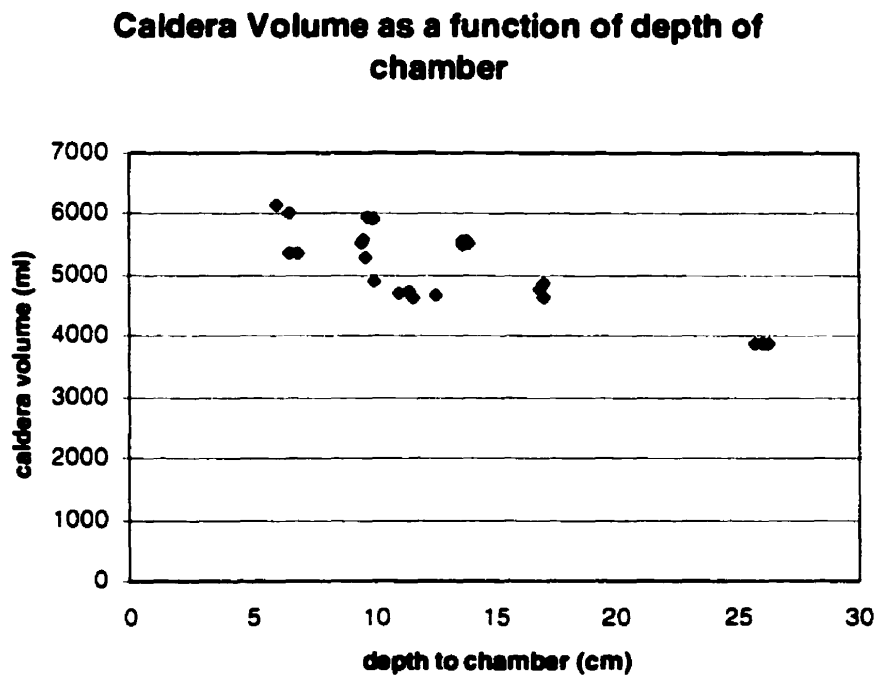


Figure 57. Caldera volume versus chamber depth.

volume and the maximum amount of subsidence in the calderas both decreased as the depth of the chamber was increased (Fig. 57, Table 1). (2) As the magma chambers became deeper, the area of faulting of the resultant calderas decreased (Figs. 58, 59).. (3) Faults became less smooth and arcuate, trending towards irregular intersecting linear faults (Fig. 59). (4) The subsiding block also became less coherent, and nested structures developed (Fig. 59). (5) Terraces formed between faults (Figs. 54, 59).

By increasing the depth of the magma chamber, the aspect ratio (thickness to width) of the collapsing roof also increased. It is the aspect ratio of the subsiding block which is critical in controlling the style of collapse (Roche et al., 2000). Therefore, our observations and interpretations regarding the effect of chamber depth apply equally to the aspect ratio.

Shallow chambers which scaled to 2.5 km produced asymmetric subsidence in cross section and a trapdoor-style collapse, one side of the caldera being controlled entirely by downwarping and the other side mainly by faulting (Fig. 54 a). Medium-depth chambers scaled to 3.8-4.6 km produced a piston style collapse with well-developed inner and outer ring faults (Fig. 54b, c). Deeper magma chambers scaled to 5.5-6.8 km depth produced a concentric, step-down style of faulting, resulting in breakup of the subsiding block (Fig. 54d, e). The deepest magma chambers scaled to 9.5 km showed a more chaotic style of faulting (Fig. 54f).

The area of faulting decreased as depth increased (Fig. 58). This is strong support that the subsidence-controlling faults were dipping outward (Fig. 60). The deeper experiments may have formed outward dipping faults which intersect upward before reaching the surface, producing cone structures (Fig. 54e). Some subsidence may have

Maximum radius of caldera faulting as a function of chamber depth

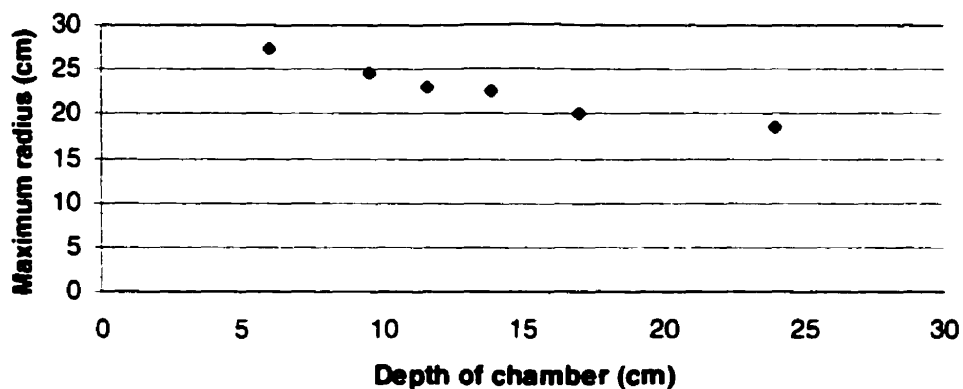


Figure 58. Maximum radius of faulting versus chamber depth.

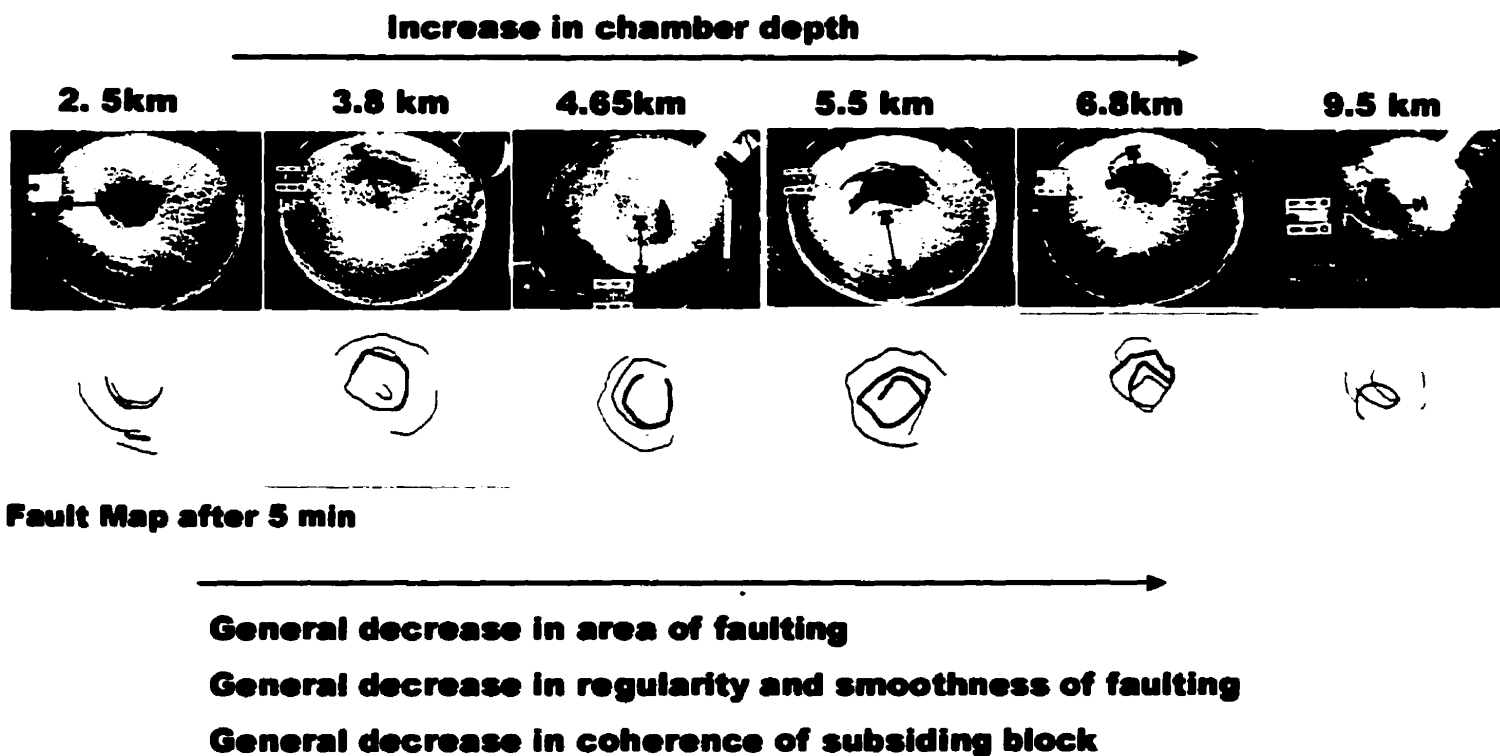


Figure 59. Summary of experimental caldera styles for different chamber depths.

occurred along these structures; this also was observed in previous experimental models (Roche et al., 2000).

Initial asymmetry was seen in most experiments. For a shallow chamber, this asymmetry was maintained throughout the experiment. In these shallow experiments, the principal stress trajectory σ_1 was probably insufficient to cause faulting on both sides of the chamber. With deeper chambers, a large mass of sand above the chamber may have induced faults to form on both sides of the caldera. A deeper chamber increases the lithostatic pressure, so increasing σ_1 . Increasing the value of σ_1 causes its stress trajectories to concentrate, promoting faulting (Fig. 61). This observation is supported by the experiments involving topography, as discussed below.

As the chamber increased to a scaled depth of 6.8 km, faults at the surface appeared less arcuate and more linear. A curved fault surface at deep levels may propagate upwards more efficiently if it becomes progressively more planar at higher levels. This causes faults associated with deeper chambers to appear more linear at the surface.

In a general manner, more complex fault patterns developed above deeper chambers. In these experiments, faulting occurred within a smaller area. Therefore, the local stress systems associated with propagating fault tips interacted to a greater degree, causing faults to change orientation, despite the overall stress trajectories being similar (Fig. 61). Multiple concentric faults formed terraces above deeper magma chambers. Horizontal terraces will develop best when these two faults are parallel in cross-section (Fig. 53c). By contrast, a terrace that develops between a curved, outward dipping fault and a linear fault may promote block rotation, causing down-sagging (Figs. 53d, 55).

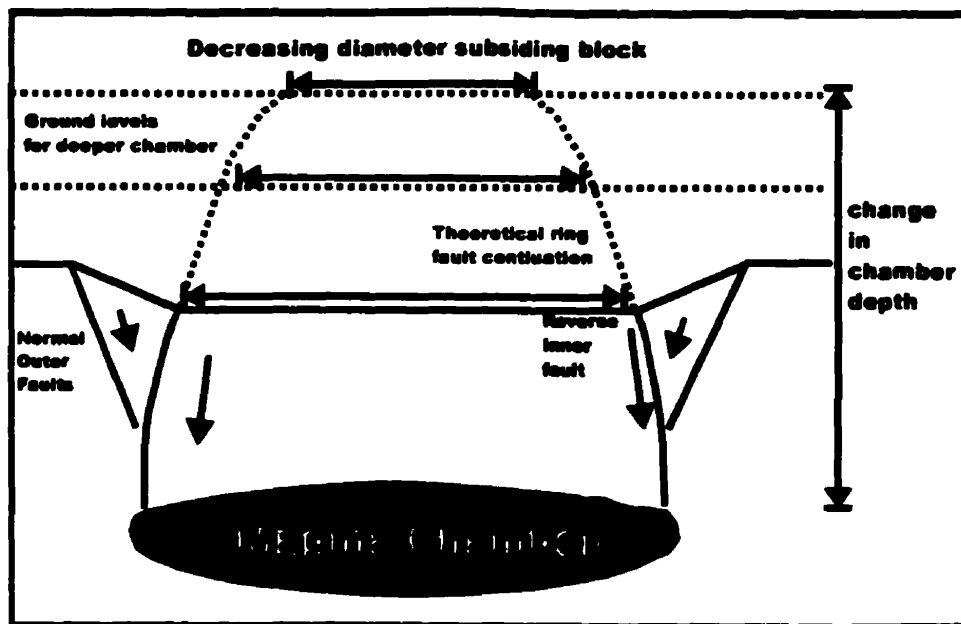


Figure 60. The diameter of faulting decreases with depth due to the outward dipping nature of the subsidence-controlling faults.

a)

b)

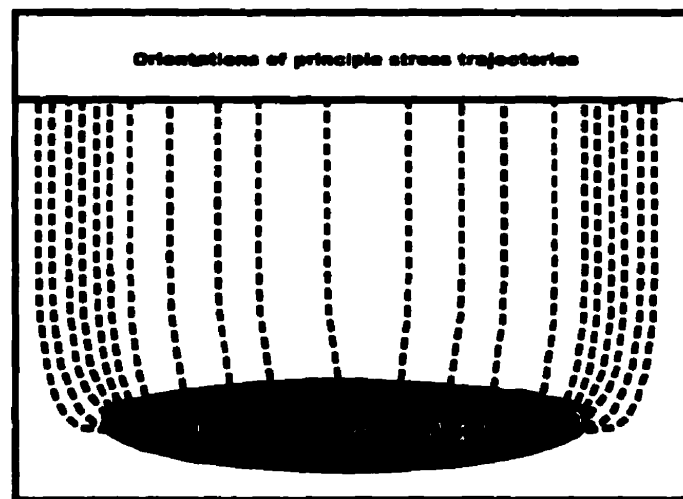
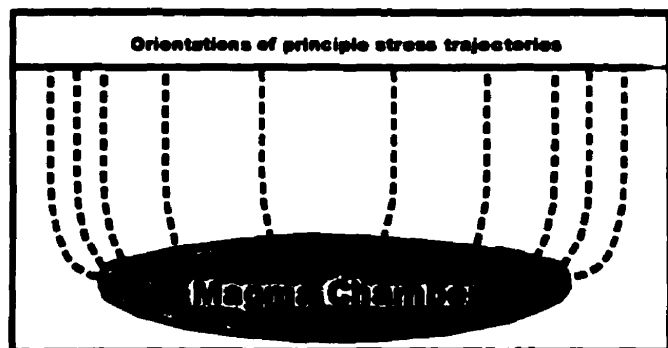


Figure 61. a) The principal stress trajectories associated with a shallow magma chamber. These stress trajectories run orthogonal to the free surfaces, which are the convex chamber roof and the horizontal surface. b) The principal stress trajectories associated with a deep chamber. The increased depth of the chamber does not significantly alter the orientations of the trajectories. However, the increased lithostatic load causes these stress trajectories to be concentrated. The closer the spacing of the trajectories, the more likely faulting is to occur.

Caldera volumes decreased as the depth of the magma chamber increased (Fig. 57). This is due to an increasing volume of sand between the chamber and the surface. The more sand available for dilation, the larger the volume change. The dilation of the sand also was promoted by increased faulting, further reducing the volume of the caldera.

A general decrease in the amount of maximum subsidence with chamber depth was observed (Table 1); this may be caused by the dilatant nature of sand. However, a general increase in cross-sectional symmetry also occurred with depth. The large subsidence values observed above shallow chambers may be the product of trapdoor-style collapse which focused subsidence on one side of the caldera. This produced an anomalously high maximum subsidence value in this area.

2) Pre-existing topography

A change in style and mass of topography from stratocone through ridge to mountain range promoted a piston-style collapse (Fig. 62). (1) The subsiding block became more coherent and larger (Fig. 62). (2) Subsidence became more symmetric in cross section (Fig. 63). (3) Faults became smoother and more arcuate (Fig. 62). (4) Faults formed earlier at the surface (Table 1). (5) The volume of the resultant caldera increased (Fig. 64). (6) Sagging was less important.

The addition of topography increased the lithostatic load without significantly changing the depth of the chamber, thereby maintaining the diameter of the caldera (Fig. 65). The increased lithostatic load caused faults to form more efficiently and earlier, since σ_1 was increased; this allowed smoother, more coherent faults to form. The simplest, most coherent ring faults were seen in the experiments with the highest additional mass, i.e., the mountain range.

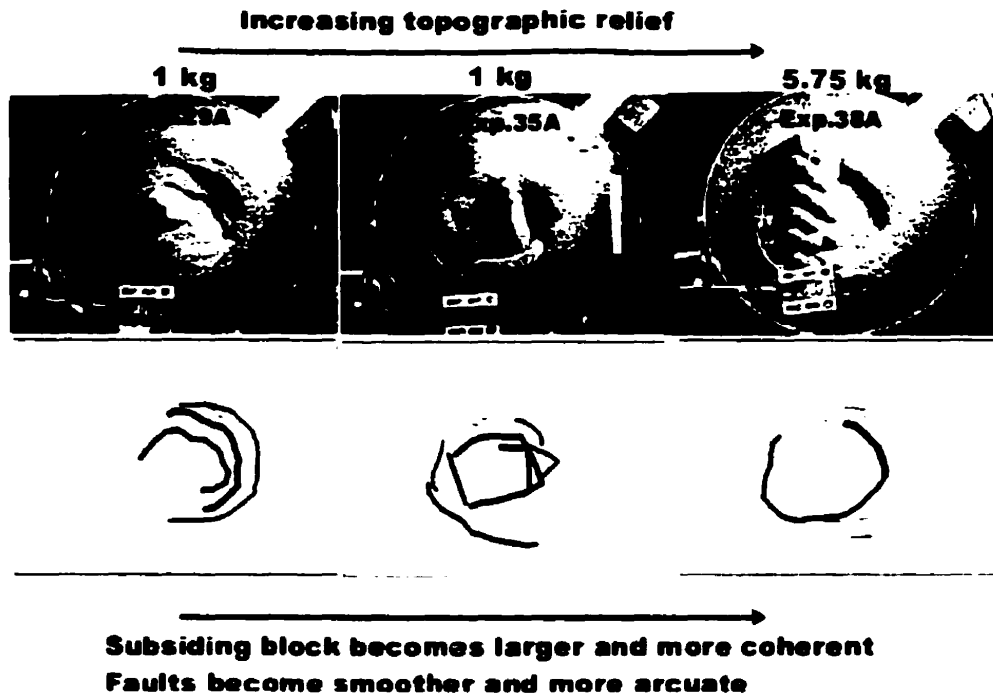


Figure 62. Summary of experimental caldera styles for different masses and styles of pre-existing topography.

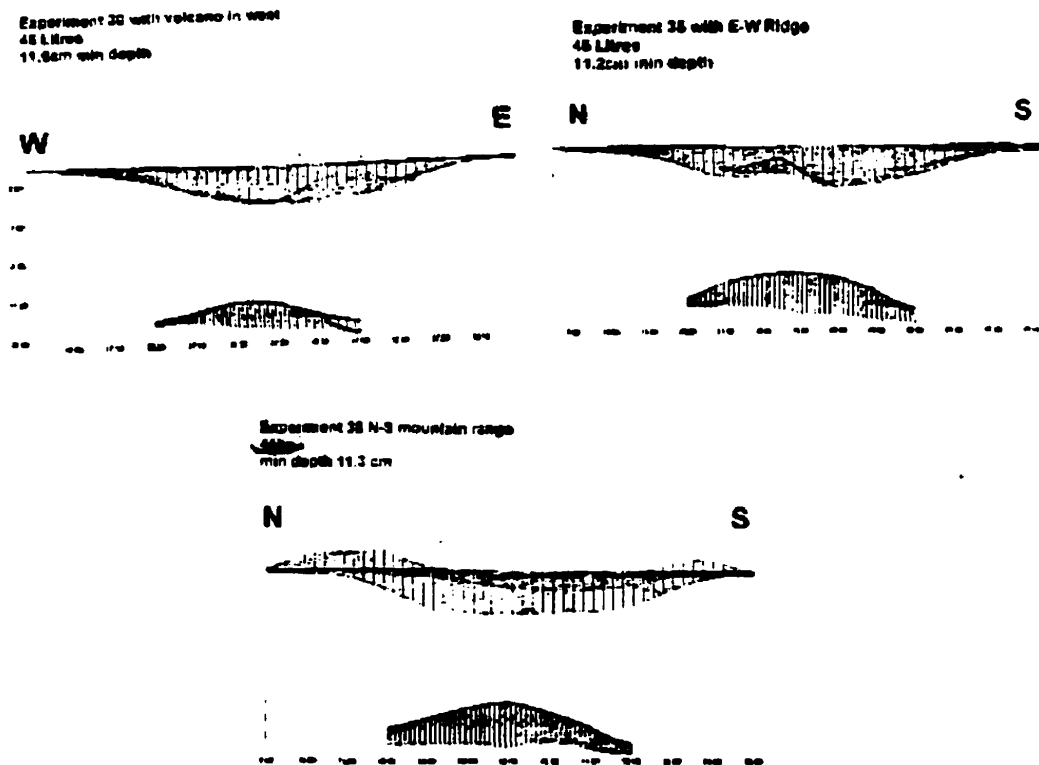


Figure 63. Cross-sectional changes in symmetry as a function of topography.

Relationship between the volume of the caldera and the pre-existing topography

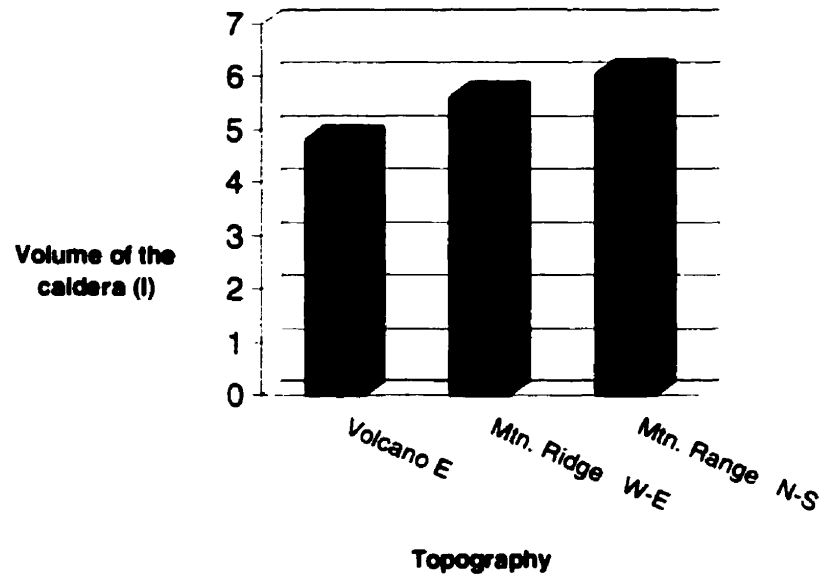


Figure 64. Caldera volume versus changes in topography.

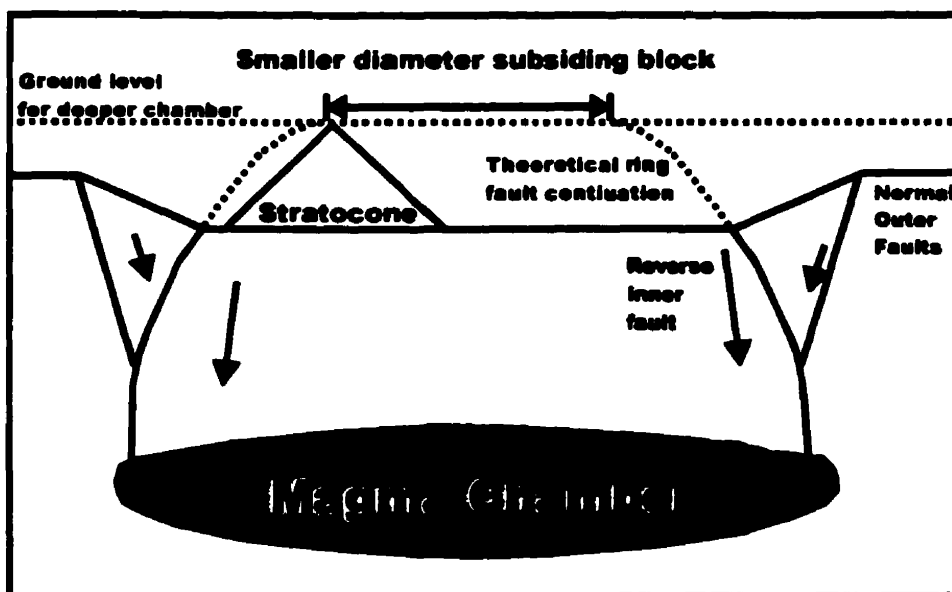


Figure 65. Additional topography increases the lithostatic load without increasing the depth of the chamber, therefore maintaining the diameter of the caldera.

First experiment no topography

Different orientations

Influence of stratocone prior to collapse



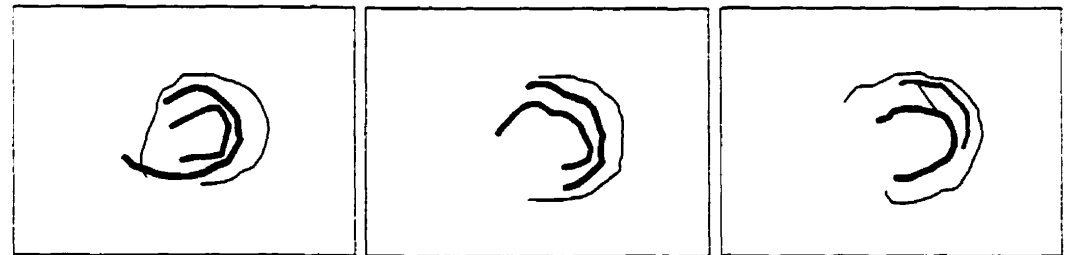
Influence of ridge prior to collapse



Influence of mountain range prior to collapse



Influence of stratocone prior to collapse



Influence of ridge prior to collapse



Influence of mountain range prior to collapse



Figure 66. Changing the position and the orientation of the topography has little effect on the final caldera morphology.

Changes in the position and orientation of the topography prior to collapse did not dramatically affect the plan view or cross-sectional symmetry of the caldera (Fig. 66). However, the position of the topography did control the location of the first fault at the surface. This fault frequently was associated with the base of the topography (Figs. 43-45). This observation has interesting implications in terms of ring fault evolution and particularly vent evolution during subsidence.

A general observation was that large amounts of slumping of the sand occurred throughout the experiments. Due to the enhanced relief, any cross-sectional asymmetry created during subsidence will promote slope failure, without the need to create new fault scarps. As asymmetric subsidence caused the caldera floor to tilt, the oversteepened topographic slopes became unstable, causing failure (Fig. 67).

3) Magma Chamber Pressure

By lowering the pressure in the magma chamber, piston-type calderas were promoted in the following manner. (1) The subsiding block was more coherent and had a larger diameter (Fig. 68). (2) Sagging became less important. (3) Subsidence was more symmetric in cross section. (4) Faults formed earlier at the surface (Table 1). (5) The subsidence-controlling fault formed as one coherent ring, rather than as a polygonal structure (Fig. 68). (6) The volumes of the resultant calderas increased (Fig. 69).

These differences are the result of a change in deformation style of the magma chamber at lower pressures. The magma chamber no longer contracted elastically like a balloon but instead flattened, allowing a more piston-like symmetric subsidence of the chamber roof. This change in deformation style explains most of the differences mentioned above. The low-pressure experiments had higher caldera volumes (Fig. 69).

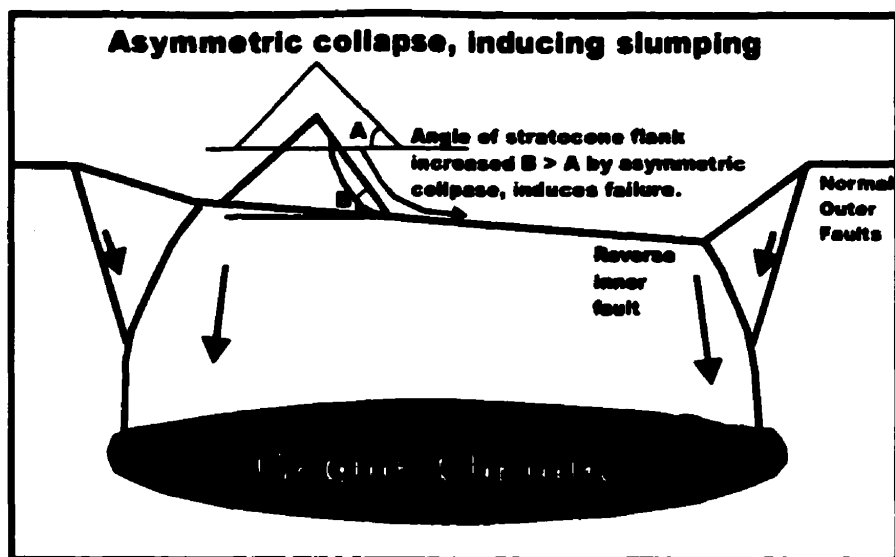
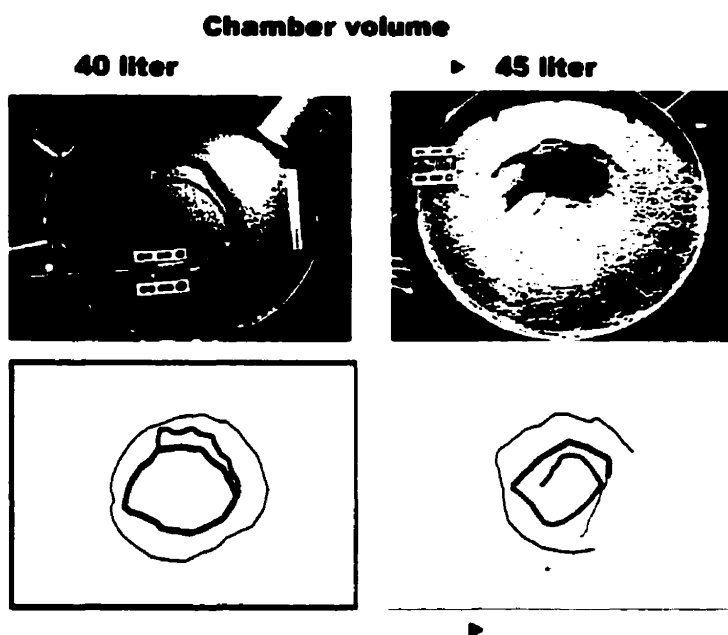


Figure 67. Topography promotes slumping; only a small amount of collapse asymmetry is required to cause failure.



Subsiding block becomes less coherent and has a smaller diameter
Faults are become increasingly linear

Figure 68. Summary of experimental caldera styles for chambers of different volume.

Relationship between the volume of the chamber and the volume of the resultant caldera

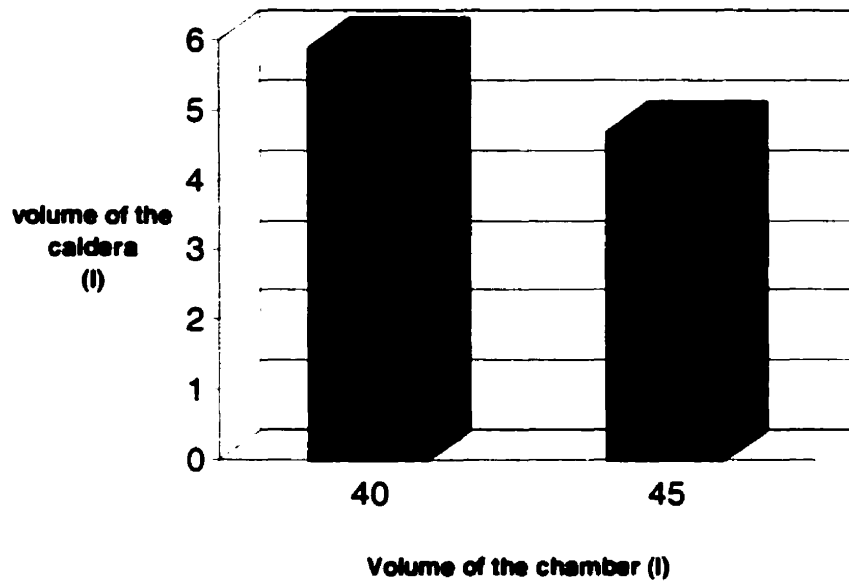


Figure 69. Caldera volume versus chamber pressure (40 liters = low pressure, 45 liters = high pressure).

and sagging was less pronounced. This implies that the sagging phase caused sand to dilate, reducing the caldera volumes in the higher-pressure experiments. In the low-pressure experiments, the sand dilated less; as a result, faults formed earlier, and caldera volumes were greater. At these low pressures, the subsidence mechanism was more akin to the experiments performed by Roche et al. (2000). Such experiments are relevant to collapse into an underpressured chamber related to a more open magmatic system.

4) Tilted magma chamber

Cross-sectional asymmetry can be caused by collapse into a tilted chamber. Tilting the magma chamber caused the following phenomena. (1) Calderas became asymmetric in cross-section. (2) Subsidence was greatest above the deepest part of the chamber (Fig. 70). (3) Elongate calderas formed perpendicular to the subsidence hinge (Fig. 71). (4) A greater number of linear inner faults formed in these calderas, and subsiding blocks were often rectangular (Fig. 71). (5) Graben formed related to the subsidence hinge (Fig. 71).

It has been suggested previously that the deepest area of a caldera may be situated above the shallowest part of the magma chamber (Lipman, 1997) (Fig. 70b). In this model, the level of the magma in the chamber decreases as a function of gravity, with the shallowest area collapsing first. This area is also the site of maximum subsidence. This model could explain only the initial stages of collapse in our experiments. Subsidence began above the shallowest part of the chamber. However, in the later stages of our experiments, subsidence was greatest on the deepest side of the chamber, in contrast to the model proposed by Lipman. This may be due to the large difference in lithostatic load which existed above the tilted chamber. The hinge above the shallow part of the chamber caused rotation of the subsiding block, forcing magma to flow laterally within the

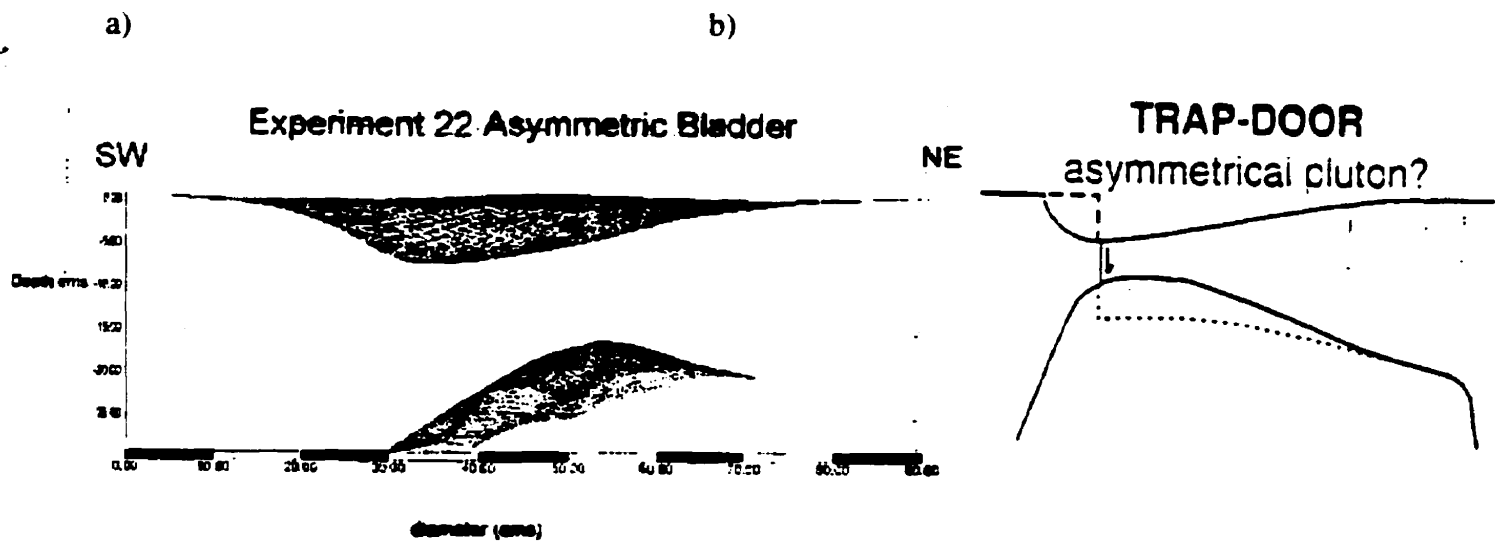


Figure 70. a) For experiment 22, subsidence in cross-section is greatest where the chamber is deepest. b) In Lipman's (1997) conceptual model, subsidence is greatest where the chamber is shallowest.

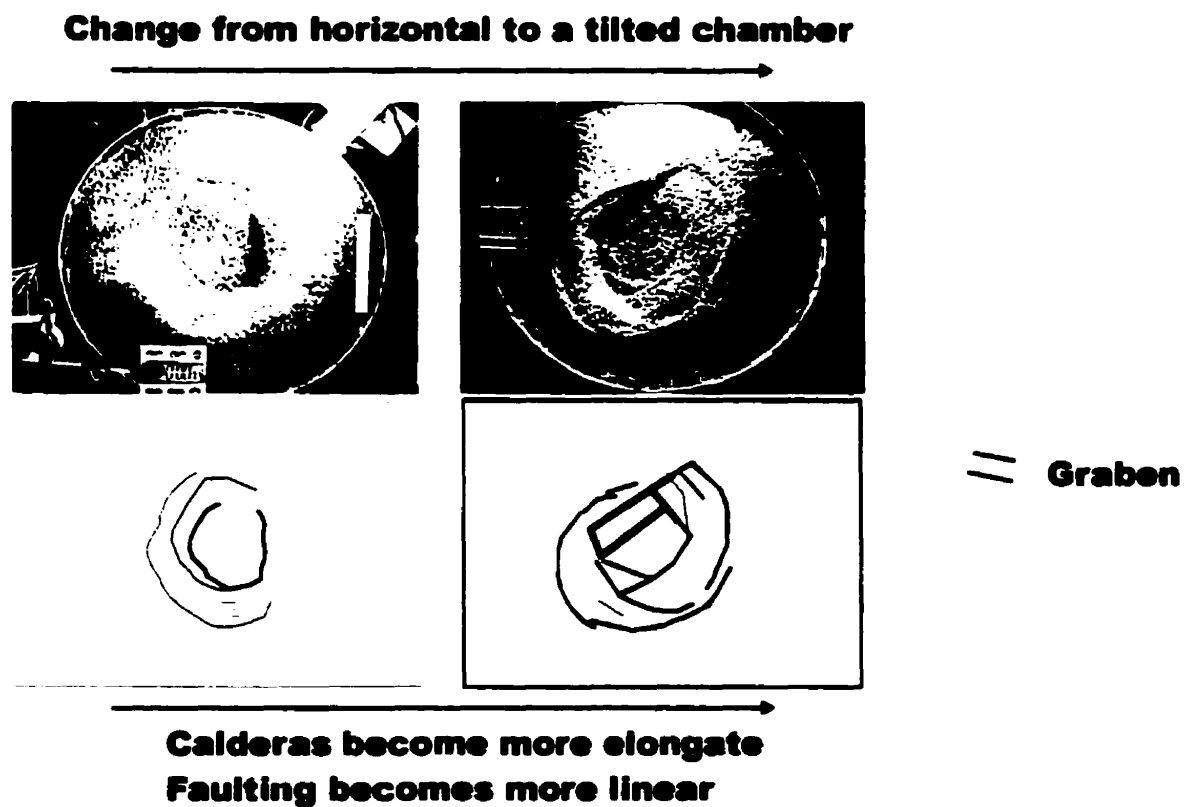


Figure 71. Summary of experimental caldera styles for a horizontal magma chamber and for a tilted chamber.

a)

b)

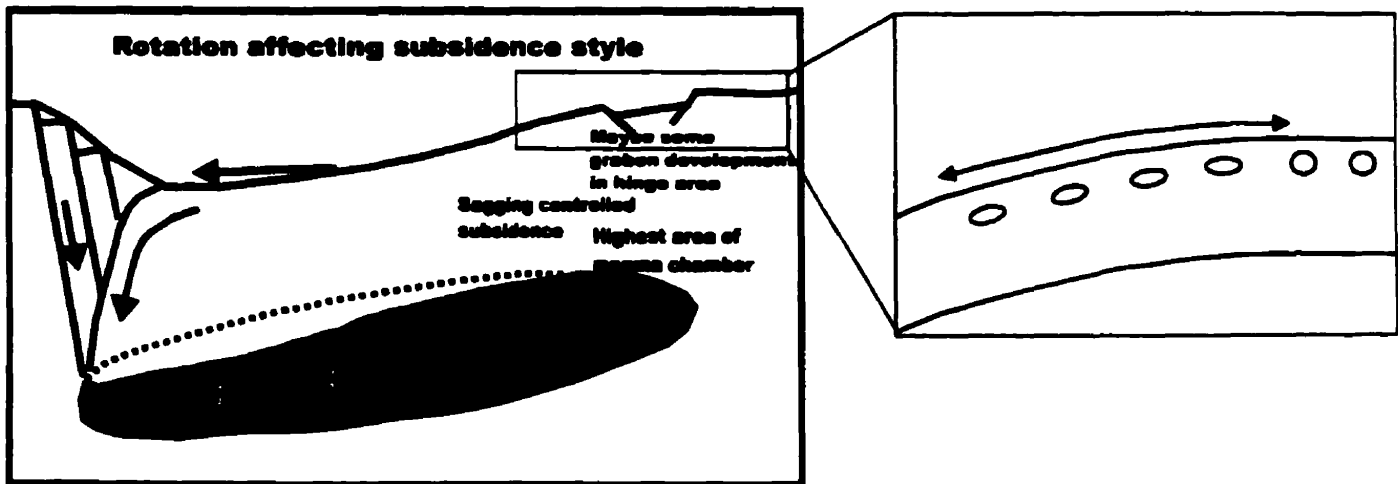


Figure 72. a) The way in which the magma chamber deforms is affected by the subsiding block, causing lateral movement of magma within the chamber. The inverted listric nature of the subsidence-controlling faults promotes lateral motion at the surface, as observed during the experiments. b) Graben development is a product of extrados-type extension in the hinge area of the caldera, similar to the extension seen on the upper surfaces of anticlinal folds.

chamber (Fig. 72). Graben development in the hinge area was related to extrados-type extension caused by bending of the crust (Fig. 72).

Discussion

The nature and origin of caldera faults

Caldera faults are frequently thought of as simple ring structures which are vertical or inward dipping (Smith and Bailey, 1968; Lipman, 1984). More recent studies have shown that this ring structure also may be outward dipping (Mori and McKee, 1987; Ekstrom, 1994; Branney, 1995; Roche et al., 2000). Many models also have been proposed for subsidence unrelated to ring faults (Walker, 1984; Lipman, 1997; 2000). In this section we demonstrate that simple piston-like ring faults rarely develop, and that the subsidence-controlling faults form in a number of ways and orientations for different reasons. The term "ring fault" may therefore not be suitable for many subsidence-controlling faults at calderas.

Homogeneous experimental conditions generally promote subsidence of a coherent block. Under such conditions, circular ring faults have been produced (Roche et al., 2000). However, the results from our experiments show that circular ring faults rarely form; the ring fault is frequently polygonal and constructed from connecting linear or sub-arcuate faults (Figs. 38-40). Such structures commonly are seen at eroded ring complexes associated with calderas, such as the Ossipee cauldron, New Hampshire, U.S.A, the Sande cauldron, Oslo region, Norway, the Liruei ring complex, Nigeria, and the Ishizuchi cauldron, southwestern Japan (Fig. 73). In these polygonal structures, corners form where faults join. Where faults join, one fault may extend outside the ring structure (Fig. 40); alternatively, faults may be seen to cross (Fig. 74). These corners are preferred eruption conduits, as they represent fracture intersections and concentrations.

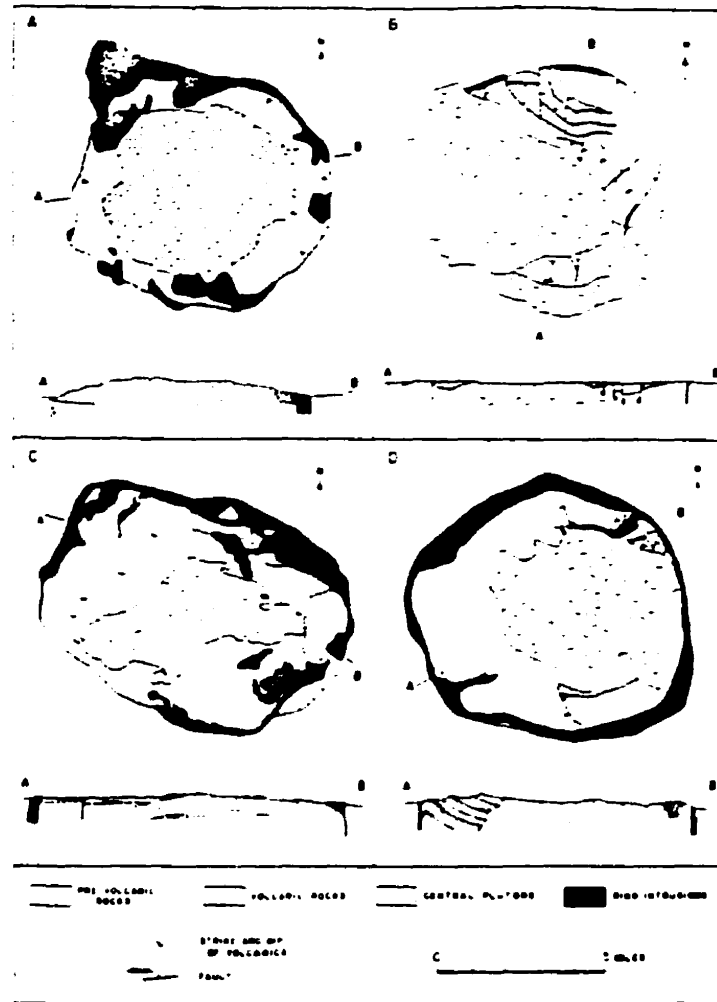


Figure 73 a) Sande cauldron, Oslo region, Norway (Ofte Dahl, 1953). b) Anlnsjo cauldron, Oslo region, Norway c) Liruei ring complex, Nigeria (Jacobson et al., 1958). d) Ossipee cauldron, New Hampshire (Kingsley, 1931).



Figure 74. Crossing faults in experiment 23B.

The dip direction of caldera faults has been an important point of debate over the last decade (Lipman 1984, 1997, 2000; Branney, 1995; Gudmundsson, 1998; Roche et al., 2000). In the absence of significant amounts of extension, the geometry of a collapse structure appears to be controlled by outward dipping inner faults associated with peripheral inward dipping faults (Branney, 1995; Odonne et al., 1999; Roche et al., 2000) (Fig. 53). This geometry is supported by our experiments as discussed above. In several of our experiments, the inner fault propagates outward, becoming part of the outer fault (Fig. 40). This implies that these faults have the ability to change from outward dipping to inward dipping.

In experiments where subsidence is asymmetric, our observations indicate that the subsidence-controlling fault may be inward dipping on one side of the caldera and outward dipping on the other. This was also observed in previous studies of collapse into a half cylinder (Roche et al., 2000). This is also seen at Ishizuchi caldera (Yoshida, 1984). This type of subsidence has interesting implications for oblique slip on caldera faults (Fig. 75). Oblique slip motions have been noted at Kumano caldera, southwest Honshu, Japan (Miura, 1999). In our experiments with a tilted magma chamber, full graben structures could be seen to form at the hinges of subsidence (Figs. 71, 72). Graben also are seen in areas of peripheral extension at Scafell caldera, Lake District, England (Branney, 1995).

In our experiments, the main subsidence-controlling fault exhibits a small diameter compared to that of the topographic boundary of the caldera. At Crater Lake caldera, Oregon, the ring fault, as inferred from subaqueous domes, phreatic craters, hydrothermal vents and high heat flow, also has a small diameter relative to the topographic boundary (Nelson et al., 1994). However, in our experimental calderas, the faults are observed inward of their true position at the surface. This is due to large

amounts of slumping associated with outward dipping reverse fault scarps: slumping will make the faults appear closer to the center of the depression than they actually are (Fig. 76).

These subsidence-controlling faults clearly can be seen in our experimental calderas; however, at real calderas pyroclastic deposits bury these faults. Faults will propagate up through these pyroclastic sequences and collapse breccias as they are emplaced, making these structures a type of growth fault, with progressively less displacement at higher stratigraphic levels. Indeed, the last pyroclastics to be deposited within the caldera may have no displacement upon them, and faults will not be seen at the surface (Fig. 77).

Nested subsidence-controlling faults are also a common feature of our experimental calderas (Figs. 40, 41) and at real calderas, e.g., Guayabo caldera, Costa Rica (Hallinan, 1993). These faults are presumed to result from multiple collapse events. However, our observations reveal that such structures form during one collapse event, and multiple collapse episodes are not required. In our experiments, these nested structures formed by progressive outward growth of concentric faults, and the same process has been inferred at Guayabo caldera (Hallinan, 1993).

The caldera faults formed first in areas of maximum initial downsagging. Once major faults form, they may act as conduits for eruption. Therefore, fault development should control vent evolution during collapse. In reality, however, an eruption conduit must exist prior to this stage in order to cause initial evacuation of magma and downsagging. The general pattern of fault formation in our experiments was lateral propagation around both sides of the caldera from the area of maximum subsidence (Fig.

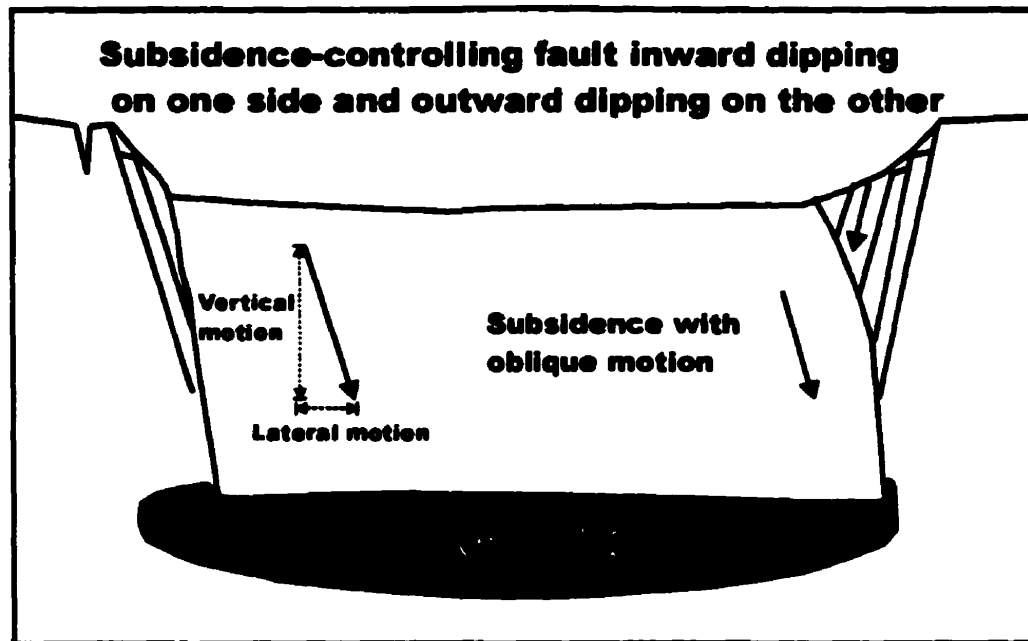


Figure 75. Subsidence on a ring fault that dips inward on one side and outward on the other produces oblique slip motions.

Slumping causes surface
expression of ring fault
to appear here.

It is actually here

Difference

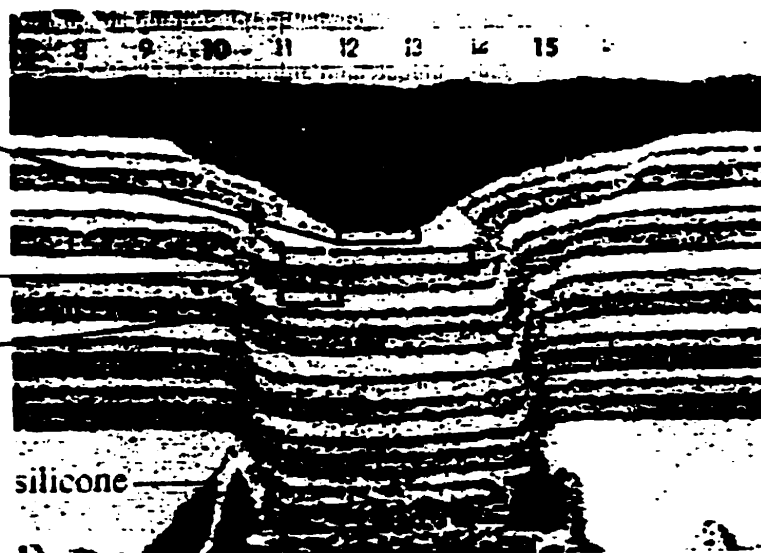


Figure 76. The surface expression of subsidence-controlling faults is inward of their actual position. From Roche et al. (2000).

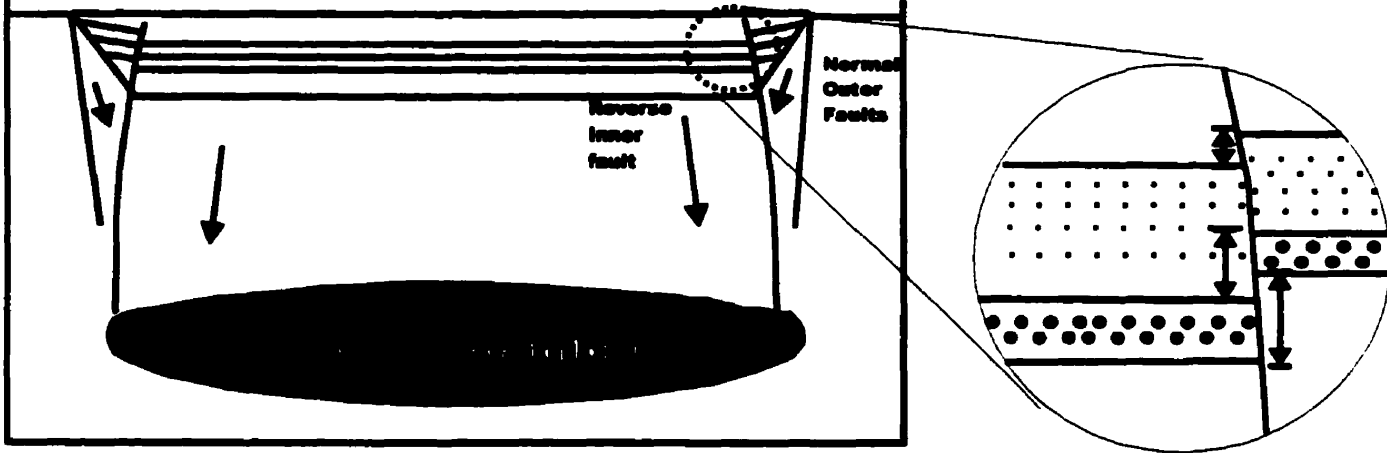


Figure 77. As deposition and faulting is synchronous and as ignimbrites pond in depressions, thickness variations will occur across subsidence-controlling faults. This will result in progressively less displacement upon the faults upward in the sequence, as seen for growth faults in subsiding sedimentary basins.

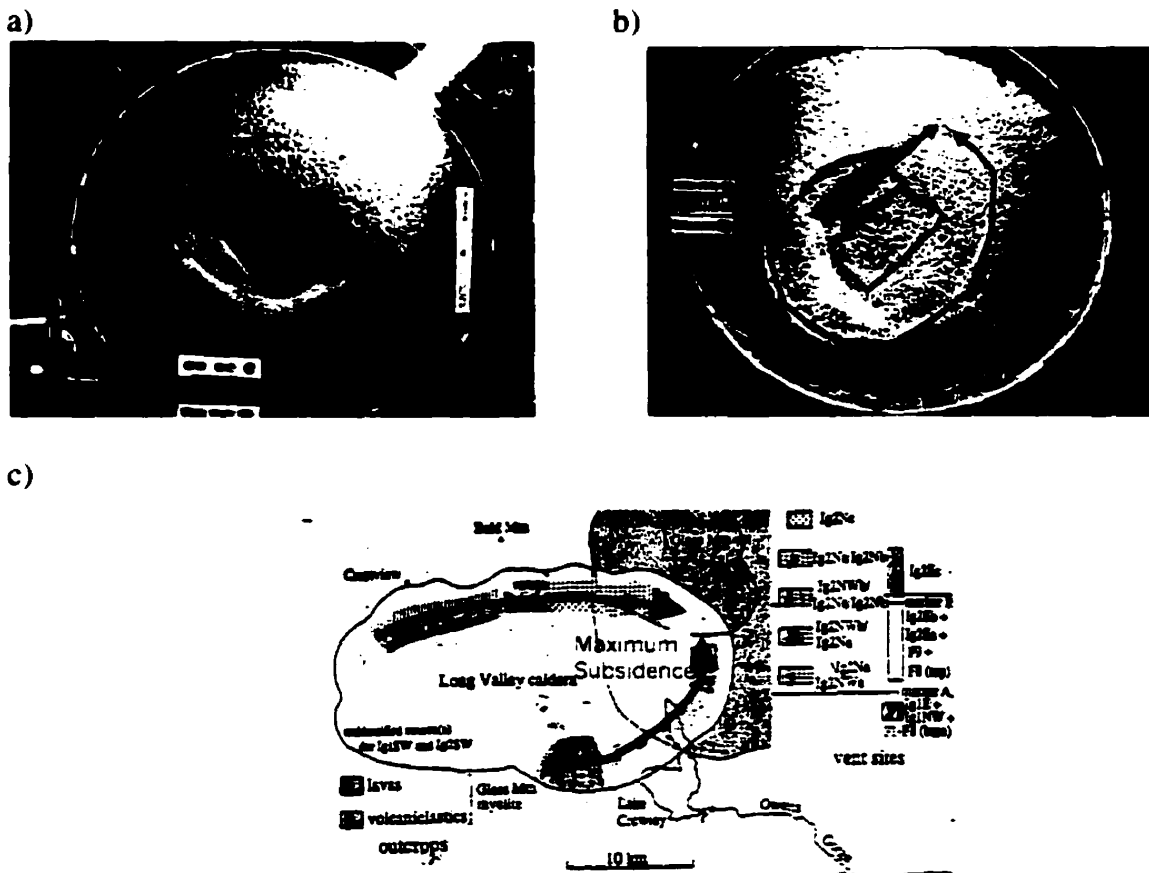


Figure 78. a) Experiment 33A showing lateral fault propagation from the area of maximum subsidence. b) Experiment 22B showing initial faults formed in the area of minimum subsidence. c) Vent evolution at Long Valley caldera, California, showing propagation of the ring fault towards the area of maximum subsidence (Wilson and Hildreth, 1997).

78a, b). This implies that new eruptive vents will form following the same general pattern. However, the vent evolution pattern inferred at Long Valley caldera, California, was a series of vents on a ring fault which migrated toward the area of maximum subsidence (Wilson and Hildreth, 1997) (Fig. 78c). Therefore, the Long Valley caldera example does not appear to be consistent with the majority of our experimental data. It should be noted that our experiments with a tilted magma chamber showed the location of initial faulting and subsidence was on the opposite side to the area of maximum subsidence (Fig. 78b).

Downsagging

Downsagging at calderas has been recognized by backtilting of originally horizontal ignimbrite sheets (Walker, 1984; Branney, 1995). In our experiments, downsagging caused by downwarping can be seen to be significant after small amounts of evacuation (Fig. 48). The amount of downsagging from downwarping at real calderas may be less (O. Roche, personal communication, 1999), as the rigid crust is less susceptible to bending than sand which has the ability to rearrange its grains. Nevertheless, this initial period of downsagging can be recognized at calderas by the gradual thickening of the early intracaldera ignimbrite deposits towards the center of the caldera. These first units pond in the depression which is controlled not by faults but rather by the inward tilting of beds. The initiation of the main subsidence-controlling fault may be associated with early downsagging and maximum thicknesses of first-erupted ignimbrite. The increased lithostatic pressure from the ponded ignimbrite may promote initiation of the main fault.

Peripheral downsagging will occur in the late stages of caldera development and is related to the extensional area outside the main subsidence-controlling fault (Branney, 1995). In our experiments, this is seen by surface dip angles in the area of peripheral extension (Fig. 51). In this area downsagging is greatest, as the surface is tilted to high angles by faulting. Scafell and Snowdon calderas, show this type of downsagging: beds are tilted up to 50° (Branney and Kokelaar, 1999).

Inward dipping stratigraphy also is promoted inside the caldera by slumping. In our experiments, slump deposits represent megabreccia and mesobreccia deposits that form from slope failure of caldera walls. During collapse, the meso- and megabreccia deposits create slopes which dip towards the center of the caldera (Fig. 79). Subsequent pyroclastics deposited on top of these paleoslopes therefore will dip towards the centre of the caldera (Fig. 79).

In our experiments, the effects of downsagging could be seen well beyond the topographic margin of the caldera (Fig. 80a). However, inward tilting of beds in this area is small and may be due to downwarping. The effects of downsagging also can be seen outside the topographic margin of Taupo caldera complex, New Zealand (Cole et al., 1998) (Fig. 80b).

The nature of subsidence can be illustrated by gravity maps of calderas. A strong gravity gradient usually marks a single subsidence-controlling fault or closely-spaced faults, whereas a gentle gravity gradient indicates a sagging-controlled basin or a series of concentric faults with small displacements (Fig. 81).

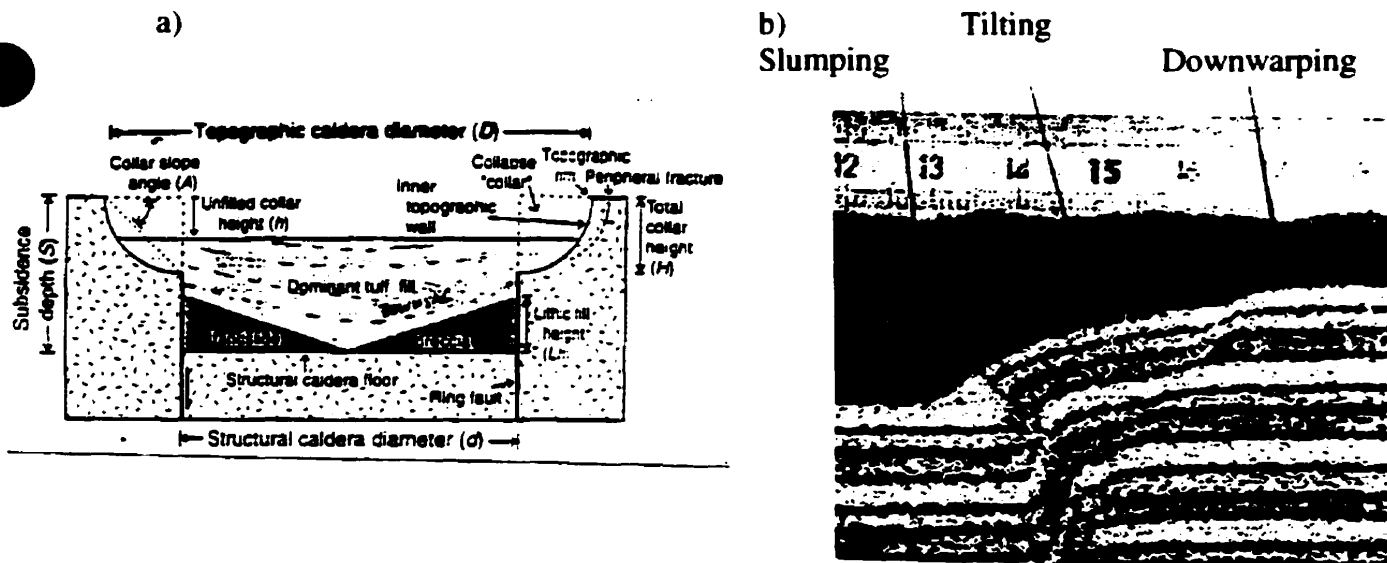


Figure 79. a) Megabreccias causing inward dipping caldera-fill deposits (Lipman, 1997).
b) Downsagging in experiments from Roche et al. (2000).

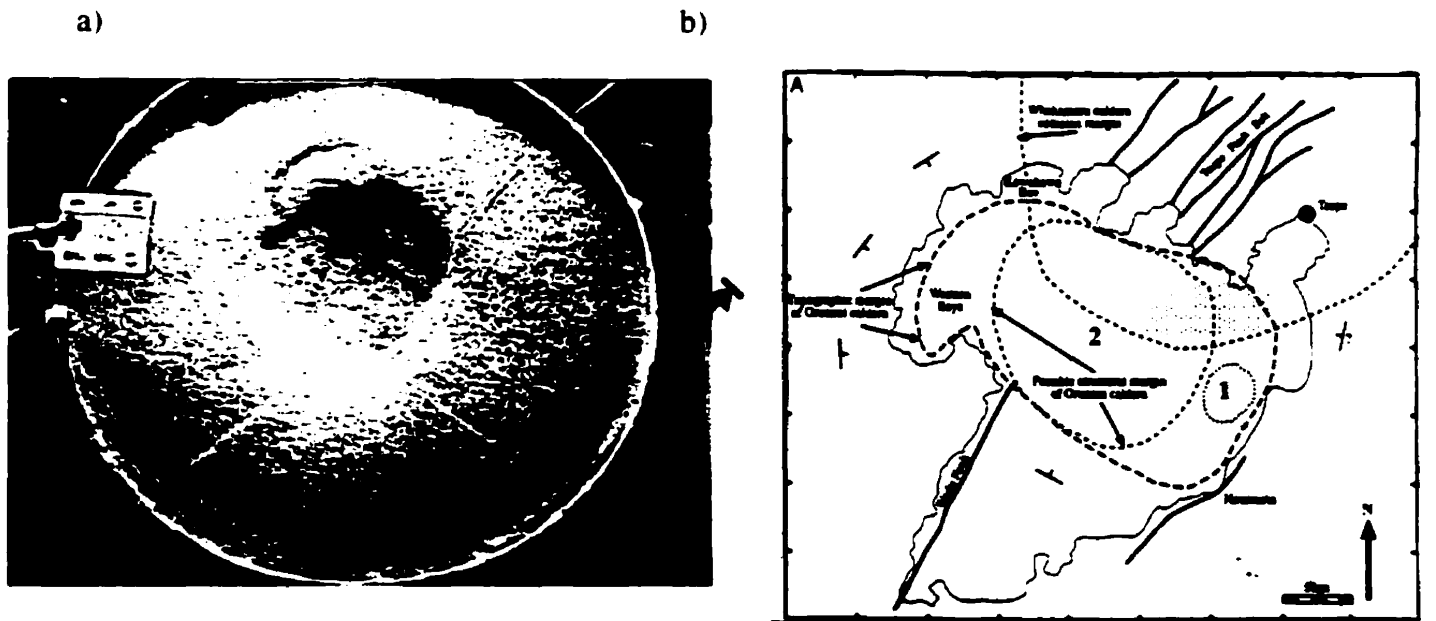


Figure 80. The displacement of the red laser line indicates the effects of downsagging. a) In experiment 11B, the effects of downsagging extend beyond the topographic boundary of the caldera by an amount equal to the diameter of the fault-bounded part of the caldera. b) Inward dips extending well beyond the topographic margin of Taupo caldera, New Zealand (Cole et al., 1998).

Resurgence

After each collapse experiment, the bladder was refilled, representing resurgence as in the classic magma chamber replenishment model (Smith and Bailey, 1968). However, this resurgence produced peripheral uplift, while the central piston, although uplifted, remained largely undeformed (Fig. 82). This style of uplift supports our inferred fault orientations by producing "push-up" structures at the margins of the central block. This style of resurgent uplift has not been recorded at any actual resurgent caldera. For this reason, these experiments were not pursued further. However, the observations imply that (1) the resurgence mechanism is not being represented accurately by refilling of the chamber; (2) resurgent calderas have disrupted floors, rather than a coherent piston, and the central faulted areas can be reactivated; (3) the importance of regional extension, which has been recognized at resurgent domes (J. Stix, personal communication, 1999), produces new rifts and encourages magma chamber stoping.

Implications for styles of caldera collapse

Based on our experiments, piston-style calderas form preferentially from collapse into (1) chambers between 4 and 5 km (medium aspect ratios); (2) open-system magma chambers where large overpressures have not developed; (3) symmetrically-oriented magma chambers; and (4) chambers above which significant surface relief existed prior to collapse.

Trapdoor-style calderas can form as a result of collapse into (1) shallow magma chambers (low aspect ratios). This experimental observation is supported by interpretations of Kumano caldera, southwest Honshu, Japan, where a 2 km deep magma chamber was associated with trapdoor-style collapse (Miura, 1999). Trapdoor calderas

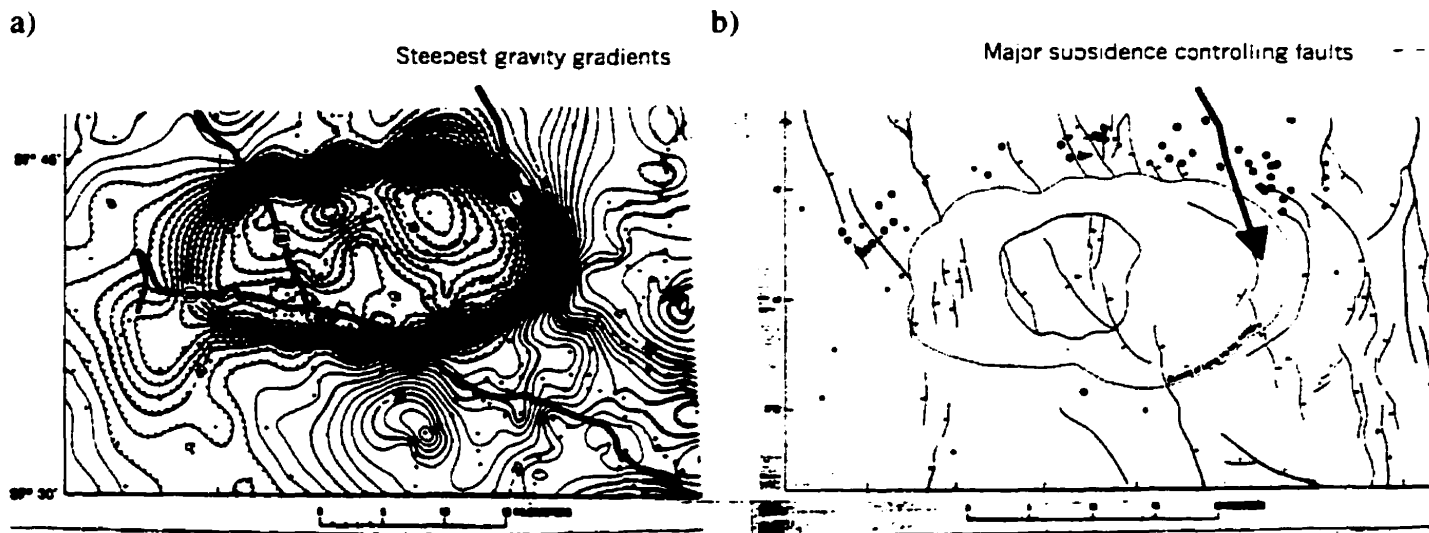


Figure 81. a) Gravity map of Long Valley caldera, California (Jachens and Roberts, 1985), where the steepest gravity gradients are in the east. b) Surface fault map of Long Valley: the major subsidence-controlling faults also occur in the east (Bailey, 1989).

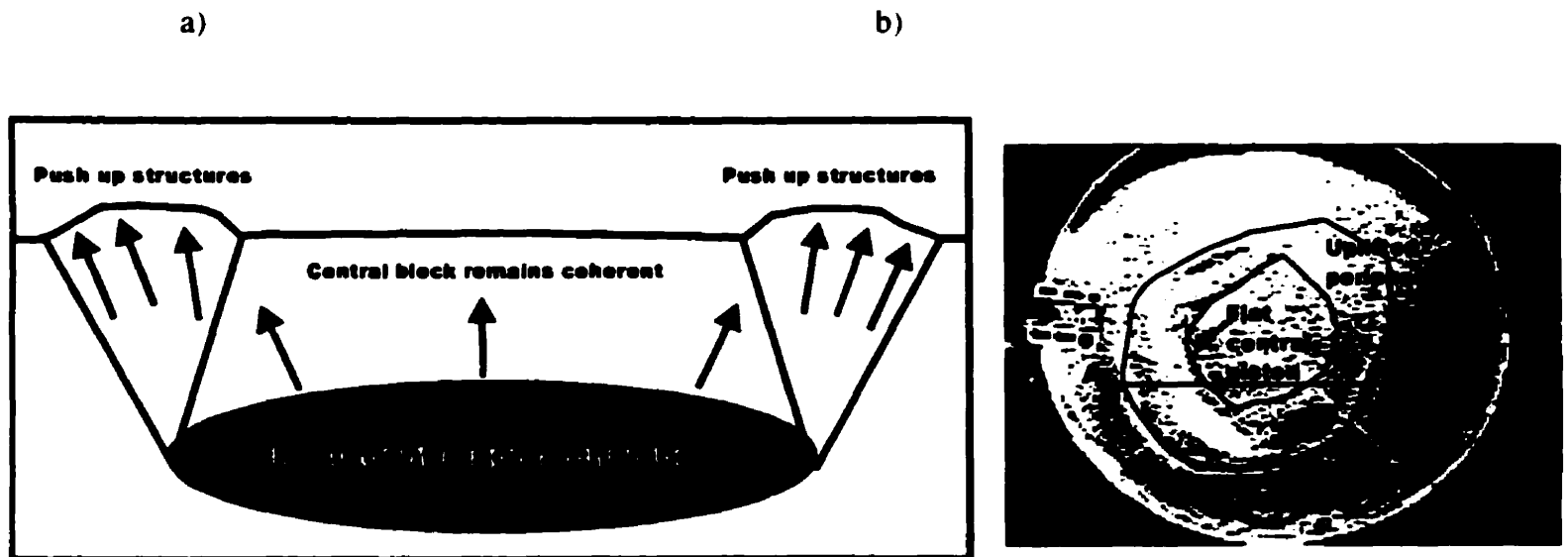


Figure 82. Resurgence "push ups". a) Theoretical cross-sections. b) Plan view in experiment 22B.

also are favored by (2) magma chambers with asymmetric upper surfaces and (3) small-volume caldera-forming eruptions from large chambers. This is illustrated by the early stages of our experiments where subsidence is often asymmetric: faults are restricted to one side of the caldera until the final two minutes of the experiment when more than 10% of the chamber has been erupted (Figs. 37-39).

Concentric step-down calderas are promoted by (1) chambers which are closed systems and are thus strongly overpressured prior to eruption, collapse promoting faulting within the subsiding block; (2) little pre-existing relief; and (3) chambers between 5 and 7 km deep (medium-high aspect ratios). By contrast, chaotic-style calderas are promoted by chambers deeper than 7 km (high aspect ratios).

Conclusions

The observations from our experiments attempt to illustrate some important structural details that could occur during caldera collapse. The experiments also show that piston-style collapse occurs only under certain conditions, and that many other collapse geometries may be common. These details help provide useful information when mapping young calderas where the internal structure is hidden. Structural details of faulting relationships and fault interactions also may provide information concerning hydrothermal pathways. Understanding controls on these pathways is very useful to the mining industry, as volcanogenic massive sulfide and epithermal mineralization may be controlled by these structures within calderas. Hydrothermal pathways also have economic interest for the geothermal power industry. Our observations show that the structural style of faulting varies considerably between the different caldera types. This may be one reason why hydrothermal activity is not always restricted to the area of the ring fault.

The major conclusions from this set of experimental results are the following. (1) Trapdoor-style calderas form as a result of both sagging and faulting, with faults usually propagating laterally from the area of maximum subsidence. (2) Concentric annular faults form from progressive outward growth of the caldera and may be the result of the convex nature of the magma chamber roof. (3) The aspect ratio of the subsiding block affects the collapse style of the caldera. (4) Pre-existing topography controls the position of fault initiation at the surface, promotes early fault initiation and piston style calderas, but does not affect the cross-sectional symmetry of the caldera. (5) Ring structures may be more complicated than previously thought, showing linear portions and crossing faults which produce a complex polygonal form. (6) Tilted and overpressured magma chambers also control the collapse style of the caldera.

Improvements and Future Research

Due to the success of the experiments discussed in this thesis, future experiments are planned. These experiments will investigate caldera formation in different geological environments. Experiments will be performed to investigate the effects of precursory tumescence, pre-existing faults, and active external stress systems on the collapse process and the resultant caldera morphology.

Before these experiments can be done, some improvements and modifications to the experimental approach and apparatus are necessary. The basic model will be improved by developing a magma chamber with varying rheological properties, as is believed to be the case in nature. Previous experiments have presumed time-independent sand deformation. This may not be the case, and the rheology of the system may

dramatically affect the pattern of fracture development and thus the resultant experimental calderas. By improving the scaling of viscosities of both the magma and the wallrocks, the details of the resultant deformation should be more realistic. The timescales of tumescence, tectonic movement, evacuation and resurgence also must be scaled accurately if the deformation of the sand is found to be time-dependent.

The magma chamber will consist of water and silicone of different viscosities. Water will represent hot magma and will be contained in a thick silicone jacket rather than the rubber bladder previously used. The silicone jacket will represent the highly viscous crystal mush that may represent a large proportion of the magma chamber, particularly at its base and margins (Marsh, 2000). A data acquisition board and peripherals will allow the pressure within the chamber to be monitored continuously and scaled correctly, since results from this thesis showed that magma chamber pressure was an important control on the caldera morphology.

In addition to the viscosity variability in the area immediately around the magma chamber, the crustal block above the magma chamber also may have significant rheological differences (Burov and Guillou-Frottier, 1999). These rheological differences are shown by the ductile-to-brittle transition, which can be represented in the model by introducing a lower layer of mixed sand and clay representing a more ductile layer related to the magma chamber, and an overlying layer of pure sand representing a more brittle surface layer. Both layers will obey the appropriate scaling considerations.

A further improvement to the basic model will be the addition of material to the subsiding block: this material will represent the emplacement of ignimbrite sheets within the caldera as it is subsiding. Volumes, rates, and densities will be calculated according to the scaling considerations and the water evacuation rate from the chamber. The mass of this material may have an important effect on the caldera forming process and fault formation at the surface (Burov and Guillou-Frottier, 1999).

For each group of experiments, we will perform several using layered sands. Sections of these sands will be sampled after the experiment in order to reveal the internal caldera structure of the model. The layering of the sand is time-consuming, and for this reason only selected experiments will be chosen for sectioning.

The first set of experiments will use both the shallow magma chamber and a deep, large-scale tumescent source to create precursory doming prior to collapse. Firstly, the effect of precursory tumescence related to the main shallow chamber will be investigated. Before collapse is initiated, a dome will be created by the addition of water to the shallow chamber. Secondly, the effect of precursory tumescence related to a deeper source will be investigated. A large deep inflatable chamber will be introduced below the pre-inflated shallow chamber. This lower chamber will be gradually inflated prior to collapse.

The second set of experiments will involve pre-existing faults: specifically, the effects of these faults on the collapse process in the absence of an external stress field will be investigated. Firstly, the effect on collapse style of single faults, their dip

directions and spatial location will be investigated. Isolated linear faults, whose dip directions are vertical, steeply inward or steeply outward dipping, will be introduced in various locations above magma chamber; collapse then will be initiated. Secondly, the effect on collapse style of parallel and cross-cutting multiple faults will be investigated. In contrast to the experiments involving isolated faults, initially a series of parallel linear faults also will be introduced, the spacing of which will be varied, in order to examine the effects of fault density on the collapse process. Further experiments will involve multiple cross-cutting faults.

The third set of experiments will use mobile walls to create an external stress field that is active prior to or during collapse. Firstly, the effect of extension and precursory rifting on collapse style will be investigated. Mobile walls will allow the production of an active rift prior to and during collapse. Caldera collapse will be initiated at various stages during the rifting process, e.g., during early stages of rifting (narrow rifts) as opposed to mature, wider rifts. Secondly, the effect of precursory pull-apart basins on collapse style will be investigated. Mobile walls and strike slip motion between basal plates will allow the formation of an active pull-apart basin prior to and during collapse. Similar to the rifting experiments, caldera collapse will be initiated at various stages during the development of the pull-apart basin.

The fourth set of experiments will investigate the effects of resurgence on the caldera structure. Firstly, the effect of regional detumescence on collapse style will be

investigated. The lower tumescent source, as previously described above, will be deflated to observe the effects at the surface. Secondly, the effect on collapse style of re-inflation of the main magma chamber will be investigated. The main magma chamber will be refilled after collapse of the caldera. This refilling could represent a simple replenishment of magma or a volume increase in the chamber caused by magma input and/or vesiculation. Thirdly, the effect of sill intrusion above the chamber on collapse style will be investigated. A series of small, sill-like chambers will be introduced and inflated above the main chamber, and their effect at the surface will be observed. Fourthly, the effect of resurgent doming on the different caldera types will be investigated. These experiments will be performed on the different caldera types created in previous experiments. This approach will help to isolate the effects of caldera structure on the style of resurgent doming.

REFERENCES

- Acocella, V., and R. Funiciello, The interaction between regional and local tectonics during resurgent doming: the case of the island Ischia, Italy, *J. Volcanol. Geotherm. Res.*, 88, 109-123, 1999.
- Anderson, E.M., The dynamics of the formation of cone-sheets, ring dykes and cauldron subsidences, *Proc. R. Soc. Edinburgh*, 56, 128-157, 1936.
- Aramaki, S., Formation of the Aira caldera, southern Kyushu, ~22000 years ago, *J. Geophys. Res.*, 89, 8485-8501, 1984.
- Bacon, C., Eruptive history of Mount Mazama and Crater lake caldera, Cascade range, U.S.A. *J. Volcanol. Geotherm. Res.*, 18, 57-115, 1983.
- Bailey R. A., Geological map of the Long Valley caldera, Mono-Inyo craters volcanic chain, and vicinity, Eastern California. Miscellaneous Investigations Series, Department of the Interior, U.S. Geological Survey, Map 1-933, 1989.
- Bailey R. A., G. B. Dalrymple, and M. A. Lanphere, Volcanism, structure, and geochronology of Long Valley caldera, California. *J. Geophys. Res.*, 81, 725-744, 1976.
- Barberi, F., F. Innocenti, P. Landi, U. Rossi, M. Saita, R. Santacroce, and I.M. Villa. The evolution of Latera caldera (Central Italy) in the light of subsurface data. *Bull. Volcanol.*, 47-1, 125-141, 1984.
- Bower, S., and A. Woods, Control of magma volatile content and chamber depth on the mass erupted during explosive volcanic eruptions, *J. Geophys. Res.*, 102, 10, 273-10,290, 1997.
- Branney, M.J., and P. Kokelaar, Volcanotectonic faulting, soft state deformation, and rheomorphism of tuffs during development of a piecemeal caldera, English Lake District, *Geol. Soc. Am. Bull.*, 106, 507-530, 1994.
- Branney, M.J., Downsag and extension at calderas. New perspectives on collapse geometries from ice melt, mining and volcanic subsidence, *Bull. Volcanol.*, 57, 303-318, 1995.
- Branney M.J., and P. Kokelaar, Inside silicic calderas. Interactions of caldera development, tectonism and hydrovolcanism, Field Guidebook of the I.A.V.C.E.I. Commission on Explosive Volcanism field workshop, 7-18 July 1999, 152 pp 6 colour plates.
- Burov E.B. and L. Guillou-Frotier, Thermomechanical behaviour of large ash flow calderas. *J. of Geophys. Res.*, 104, 23,081- 23,109, 1999

- Chesner, C.A., and W.I. Rose. Stratigraphy of the Toba Tuffs and the evolution of the Toba Caldera Complex, Sumatra, Indonesia. *Bull. Volcanol.*, 53, 343-356, 1991.
- Clough, C.T., H.B. Maufe, and E.R. Bailey. The cauldron subsidence of Glencoe and the associated igneous phenomena. *Q. J. Geol. Soc. London*, 65, 611-678, 1909.
- Cole, J.W., S.J.A. Brown, R.M. Burt, S.W. Beresford, and C.J.N. Wilson. Lithic types in ignimbrites as a guide to the evolution of a caldera complex, Taupo volcanic centre, New Zealand. *J. Volcanol. Geotherm. Res.*, 80, 217-237, 1998.
- Chadwick, W.W., and K.A. Howard. The pattern of circumferential and radial eruptive fissure on the volcanoes of Fernandina and Isabela islands, Galapagos. *Bull. Volcanol.*, 53, 259-275, 1991.
- Chadwick Jr, W.W., and J.H. Dieterich. Mechanical modeling of circumferential and radial dike intrusion on Galapagos volcanoes. *J. Volcanol. Geotherm. Res.*, 66, 37-52, 1995.
- Christiansen, R.L.. Yellowstone magmatic evolution: Its bearing on understanding large-volume explosive volcanism. *Studies in Geophysics/Explosive volcanism: Inception, Evolution, and Hazards*. Washington D.C, National Academic Press, 84-95, 1984.
- Druitt, T., and R.S.J. Sparks. On the formation of calderas during ignimbrite eruptions. *Nature*, 310, 679-681, 1984.
- Ekstrom, G., Anomalous earthquakes on volcano ring-fault structures. *Earth Planet. Sci. Lett.*, 128, 707-712, 1994.
- Elston, W.E., Mid-Tertiary ash flow tuff cauldrons, southwestern New Mexico. *J. Geophys. Res.*, 89, 8733-8750, 1984.
- Fouqué, F.. Santorin et ses Eruptions. Paris, Masson, 440 pp., 1879.
- Francis, P., Caldera complexes and complex calderas, Volcanoes a Planetary Perspective. Oxford, Oxford University Press, 291-321, 1993.
- Fridrich, C.J., R.P. Smith, E.D. DeWitt, and E.H. McKee. Structural, eruptive, and intrusive evolution of Grizzly Peak caldera, Sawatch range, Colorado. *Geol. Soc. Am. Bull.*, 103, 1160-1170, 1991.
- Geist, D., K.A. Howard, A.M. Jellinek, and S. Rayder. The volcanic history of Volcan Alcedo, Galapagos Archipelago: A case study of rhyolitic ocean volcanism. *Bull. Volcanol.*, 56, 243-260, 1994.
- Gudmundsson, A., Formation of collapse calderas. *Geology*, 16, 808-810, 1988.

Gudmundsson, A., J. Martí, and E. Taroni. Stress field generating ring faults in volcanoes. *Geophys. Res. Lett.*, 24, 1559-1562, 1997.

Gudmundsson, A.. Formation and development of normal fault calderas and the initiation of large explosive eruptions, *Bull. Volcanol.*, 60, 160-170, 1998.

Hallinan, S.. Non-chaotic collapse at funnel caldera: Gravity study of the ring fractures of the Guayabo caldera, Costa Rica. *Geology*, 21, 367-370, 1993.

Hallinan, S., and G. Brown. Incremental collapse and stratocone growth within a funnel shaped caldera, Guayabo, Costa Rica. *J. Volcanol. Geotherm. Res.*, 67:101-122, 1995.

Hess, K.U., and D.B. Dingwell. Viscosities of hydrous leucogranitic melts: A non-Arrhenian model. *Am. Mineral.*, 81, 1297-1300, 1996.

Jachens, R.C., and W. Roberts. Temporal and areal gravity investigations at Long Valley caldera, California. *J. Geophys. Res.*, 90, 11 210-11 218, 1985.

Jacobson, R.R.E., W.N. MacLeod, R. Black. Ring complexes in the Younger Granite province of northern Nigeria. *Geol. Soc. London Mem.* 1, 72p, 1958.

Jaupart, C., and C. Allegre. Gas content, eruption rate and instabilities of eruption regime in silicic volcanoes. *Earth Planet. Sci. Lett.* 102, 413-429, 1990.

Kamata, H.. Shishimuta caldera, the buried zone of the Yabakei pyroclastic flow in the Hoho volcanic zone, Japan. *Bull. Volcanol.*, 51, 41-50, 1989.

Komuro, H., Y. Fujita, and K. Kodama. Numerical and experimental models on the formation of collapse basins during the Green Tuff Orogenesis of Japan. *Bull. Volcanol.*, 47, 649-666, 1984.

Komuro H.. Experiment on cauldron formation: A polygonal cauldron and ring fractures. *J. Volcanol. Geotherm. Res.*, 31, 131-149, 1987.

Kennedy, B., J. Stix, J. Vallance, and Y. Lavallée. Controls on caldera structure and morphology results from experimental simulations. EOS, Trans. Am. Geophys. Union, 46, F1121.

Lagabrielle Y. and Garel E., Extensional faulting and caldera collapse in the axial region of fast spreading ridges: analogue modeling. Submitted to *J. Geophys. Res.*, 2000.

Lipman, P.W., The roots of ash flow calderas in western North America: windows into the tops of granitic batholiths, *J. Geophys. Res.*, 89, 8801-8841, 1984.

Lipman, P.W., Subsidence of ash flow calderas: Relation to caldera size and magma chamber geometry, *Bull. Volcanol.*, 59, 198-218, 1997.

- Lipman, P.W., Calderas. In: H. Sigurdsson, B. Houghton, S. McNutt, H. Rymer, and J. Stix (Editors), *Encyclopedia of volcanoes*. San Diego, Academic Press pp. 643-662, 2000.
- Marsh, B., On the mechanics of caldera resurgence. *J. Geophys. Res.*, 89, 8245- 8241, 1984.
- Marsh, B., 2000 Magma Chambers. In: H. Sigurdsson, B. Houghton, S. McNutt, H. Rymer, and J. Stix (Editors), *Encyclopedia of volcanoes*. San Diego, Academic Press pp. 191-206, 2000.
- Marti, J., G.J. Albay, L.T. Redshaw, and R.S.J. Sparks, Experimental study of collapse calderas. *J. Geol. Soc. London*, 151, 919-929, 1994.
- Massol, H., and C. Jaupart. The generation of gas overpressure in volcanic eruptions. *Earth and Planetary Science Lett.*, 166, 57-70, 1999.
- McConnell V.S., C. K. Shearer, J.C. Eichelberger, M. J. Keskinen, P.W. Layer, and J. J. Papike. Rhyolite intrusions in the intracaldera Bishop Tuff, Long Valley Caldera, California. *J. Volcanol. Geotherm. Res.*, 67, 41-60, 1995.
- McLeod, P., The role of magma buoyancy in caldera forming eruptions. *Geophys. Res. Lett.*, 26, 2299-2302, 1999.
- Merle, O., and A. Borgia. Scaled Experiments of volcanic spreading. *J. Geophys. Res.*, 101, 805- 817, 1996.
- Miura, D., and M. Tamai, Intracaldera structure and megabreccias at Dorobu caldera, northwestern Honshu, Japan. *J. Volcanol. Geotherm. Res.*, 80, 195-215, 1997.
- Miura, D., Arcuate pyroclastic conduits, ring faults, and coherent floor at Kumano caldera, southwest Honshu, Japan. *J. Volcanol. Geotherm. Res.*, 92, 271-294, 1999.
- Moore, I., and P. Kokelaar, Tectonically controlled piecemeal caldera collapse, at Glencoe volcano, Scotland, *Geol. Soc. Am. Bull.*, 110, 1448-1466, 1998.
- Mori, J., and C. McKee, Outward-dipping ring-fault structure at Rabaul caldera as shown by earthquake locations. *Science*, 235, 193-194, 1987.
- Mori, J., R. A. White, D. H. Harlow, P. Okubo, J. A. Power, R. P. Hoblitt, E. P. Laguerta, A. Lanuza, and B. C. Batistuta, Volcanic earthquakes following the 1991 climactic eruption of Mt. Pinatubo: Strong seismicity during a waning eruption. *Fire and Mud: Eruptions and Lahars of Mt. Pinatubo, Philippines*. Seattle, University of Washington Press, 339-350, 1996.

- Munro, D.C., and S.K. Rowland, Caldera morphology in the western Galápagos and implications for volcano eruptive behavior and mechanism of caldera formation. *J. Volcanol. Geotherm. Res.*, 72, 85-100, 1995.
- Nelson, C.H., C.R. Bacon, S.W. Robinson, D.P. Adam, J.P. Bradbury, J.H. Barber, Jr., D. Schwartz, and G. Vagenas, The volcanic, sedimentologic, and paleolimnologic history of the Crater Lake caldera floor, Oregon: Evidence for small caldera evolution, *Geol. Soc. Am. Bull.*, 106, 684-704, 1994.
- Nielson, D.L., and J.B. Hulen, Internal geology and evolution of the Redondo dome, Valles caldera, New Mexico. *J. Geophys. Res.*, 89, 8695-8711, 1984.
- Odonne, F., I. Ménard, G.J. Massonnat, and J.-P. Rolando, Abnormal reverse faulting above a depleting reservoir. *Geology*, 27, 111-114, 1999.
- Oftedahl, C., Cauldrons of the Permian Oslo rift. *J. Volcanol. Geotherm. Res.*, 3, 343-371, 1978.
- Roche, O., T.H. Druitt, and O. Merle, Experimental study of caldera formation. *J. Geophys. Res.*, 105, 395-416, 2000.
- Sandford, A.L., Analytical and experimental study of simple geologic structures. *Geol. Soc. Am. Bull.*, 70, 19-52, 1959.
- Sawada, Y., Subterranean structure of collapse caldera associated with andesitic and dacitic eruptions: Structural evolution of the Miocene Kakeya cauldron, southwest Japan. *Bull. Volcanol.*, 47, 551-568, 1984.
- Scandone, R., Chaotic collapse of calderas. *J. Volcanol. Geotherm. Res.*, 42, 285-302, 1990.
- Schirnack, C., P. Van der Bogaard, and H. Schmincke, Cone sheet formation and intrusive growth of an oceanic island- The Miocene Tejada complex on Gran Canaria (Canary Islands). *Geology*, 27, 207-210, 1999.
- Schultz, R.A., Relative scale and the strength and deformability of rock masses. *J. Struct. Geol.*, 18, 1139-1149, 1996.
- Self, S., and P.W. Lipman, Large ignimbrites and caldera-forming eruptions, IAVCEI working group on explosive volcanism and its products. Field workshop (11WA) in Jemez Mountains, New Mexico, and San Juan Mountains, Colorado. 128, 1989.
- Skilling, I.P., Incremental caldera collapse of Suswa volcano, Gregory Rift Valley, Kenya. *J. Geol. Soc. London*, 150, 885-896, 1993.

- Simkin, T., and K.A. Howard, Caldera collapse in the Galapagos Islands, 1968. *Science*, 169, 429-437, 1970.
- Smith, R.L., Ash flow magmatism. *Geol. Soc. Am., Spec. Pap.* 180, 5-27, 1979.
- Smith, R.L., and R.A. Bailey. Resurgent cauldrons. *Geol. Soc. Am. Mem.*, 116, 83-104, 1968.
- Spera, F.J., and J.A. Crisp. Eruption volume, periodicity, and caldera area: Relationships and inferences on the development on compositional zoning in silicic magma chambers. *J. Volcanol. Geotherm. Res.*, 11, 169-187, 1981.
- Takahashi, M., Anatomy of a middle Miocene Valles-type caldera cluster: Geology of the Okeueyama volcano-plutonic complex, southwest Japan. *J. Volcanol. Geotherm. Res.*, 29, 33-70, 1986.
- Tait S., C. Jaupart, and S. Vergnolle. Pressure, gas content and eruption periodicity of a shallow crystallizing magma chamber. *Earth Planet. Sci. Lett.* 92, 107-123, 1989.
- Ventura, G., Tectonics, structural evolution and caldera formation on Vulcano Island (Aeolian Archipelago, southern Tyrrhenian Sea). *J. Volcanol. Geotherm. Res.*, 60, 207-224, 1994.
- Walker, G.P.L., Downsag calderas, ring faults, caldera sizes and incremental caldera growth. *J. Geophys. Res.*, 89, 8407-8416, 1984.
- Walker, G.P.L., Three Hawaiian calderas: an origin through loading by shallow intrusions?. *J. Geophys. Res.*, 93, 14 773-14 784, 1988.
- Watson, E.B., Diffusion in volatile-bearing magmas. *Rev. in Mineral.*, vol. 30, 371-411, 1994.
- Westrich, H.R., and T.M. Gerlach, Magmatic gas source for the stratospheric SO₂ cloud from the June 15, 1991, eruption of Mount Pinatubo, *Geology*, 20, 867-870, 1992.
- Williams, H., Calderas and their origin. *Bull.* 25, pp.239-346. Dep. Of Geol. Sci., Univ. of Calif., Berkley, 1941.
- Wilson, C.J.N., and W. Hildreth. The Bishop Tuff: New insights from eruptive stratigraphy. *J. Geol.*, 105, 407-439, 1997.
- Withjack, M.O., and Scheiner, C., Fault patterns associated with domes-An experimental and analytical study. *Am. Assoc. Petrol. Geol. Bull.*, 66, 302-316, 1982.
- Yokoyama, I., and S. De la Cruz-Reyna, Comments on "Chaotic collapse of calderas" by R. Scandone. *J. Volcanol. Geotherm. Res.*, 47, 349-357, 1991.



Yoshida, T.. Tertiary Ishizuki, cauldron, southwestern Japan arc: formation by ring fracture subsidence, *J. Geophys. Res.*, 89, 8502-8510, 1984.